DYNAMIC MODEL-BASED ESTIMATION STRATEGIES FOR FAULT DIAGNOSIS

DYNAMIC MODEL-BASED ESTIMATION STRATEGIES FOR FAULT DIAGNOSIS

By AHSAN SAEEDZADEH, M.A.Sc, B.Sc.

A Thesis Submitted to the School of Graduate Studies in Partial Fulfilment of the Requirements for the Degree of Doctor of Philosophy

McMaster University

McMaster University, DOCTOR OF PHILOSOPHY (2023), Hamilton, Ontario (Mechanical Engineering)

TITLE:	Dynamic Model-based Estimation Strategies for Fault Diagnosis
AUTHOR:	Ahsan Saeedzadeh, M.A.Sc, B.Sc. (Amirkabir University of Technology)
SUPERVISORS:	Dr. Saeid Habibi and Dr. Marjan Alavi
NUMBER OF PAGES:	xxvii, 190

Lay Abstract

In everyday life, from doctors diagnosing illnesses to mechanics inspecting cars, we encounter the need for fault detection and diagnosis (FDD). Advances in technology, like powerful computers and sensors, are making it possible to automate fault diagnosis processes and take corrective actions in real-time when something goes wrong. The first step in fault detection and diagnosis is to precisely identify system faults, ensuring they can be properly separated from normal variations caused by uncertainties, disruptions, and measurement errors.

This thesis explores model-based approaches, which utilizes prior knowledge about how a normal system behaves, to detect abnormalities or faults in the system. New algorithms are introduced to enhance the efficiency and flexibility of this process. Additionally, a new strategy is proposed for extracting information from a robust filter, when used for identifying faults in the system.

Abstract

Fault Detection and Diagnosis (FDD) constitutes an essential aspect of modern life, with far-reaching implications spanning various domains such as healthcare, maintenance of industrial machinery, and cybersecurity. A comprehensive approach to FDD entails addressing facets related to detection, invariance, isolation, identification, and supervision. In FDD, there are two main perspectives: model-based and data-driven approaches. This thesis centers on model-based methodologies, particularly within the context of control and industrial applications. It introduces novel estimation strategies aimed at enhancing computational efficiency, addressing fault discretization, and considering robustness in fault detection strategies.

In cases where the system's behavior can vary over time, particularly in contexts like fault detection, presenting multiple scenarios is essential for accurately describing the system. This forms the underlying principle in Multiple Model Adaptive Estimation (MMAE) like well-established Interacting Multiple Model (IMM) strategy. In this research, an exploration of an efficient version of the IMM framework, named Updated IMM (UIMM), is conducted. UIMM is applied for the identification of irreversible faults, such as leakage and friction faults, within an Electro-Hydraulic Actuator (EHA). It reduces computational complexity and enhances fault detection and isolation, which is very important in real-time applications such as Fault-Tolerant Control Systems (FTCS). Employing robust estimation strategies such as the Smooth Variable Structure Filter (SVSF) in the filter bank of this algorithm will significantly enhance its performance, particularly in the presence of system uncertainties. To relax the irreversible assumption used in UIMM algorithm and thereby expanding its

application to a broader range of problems, the thesis introduces the Moving Window Interacting Multiple Model (MWIMM) algorithm. MWIMM enhances efficiency by focusing on a subset of possible models, making it particularly valuable for fault intensity and Remaining Useful Life (RUL) estimation.

Additionally, this thesis delves into exploring chattering signals generated by the SVSF filter as potential indicators of system faults. Chattering, arising from model mismatch or faults, is analyzed for spectral content, enabling the identification of anomalies. The efficacy of this framework is verified through case studies, including the detection and measurement of leakage and friction faults in an Electro-Hydraulic Actuator (EHA).

Keywords: Model-based Fault Detection and Diagnosis, State Estimation, Adaptive Filtering, Variable Structure Filter, Information Extraction, Spectral Analysis.

Acknowledgements

I would like to thank my supervisors, Dr. Saeid Habibi and Dr. Marjan Alavi for giving me this opportunity and supporting me during this educational journey. I would also like to convey my gratitude to the members of my supervisory committee, Dr. Gary Bone and Dr. Babak Nahid-Mobarakeh, for their feedback.

I extend my thanks to the School of Graduate Studies and the Department of Mechanical Engineering at McMaster University, as well as the Natural Science and Engineering Research Council of Canada (NSERC), for their financial support.

I also like to thank my colleagues and fellow graduate students at the Centre for Mechatronic and Hybrid Technologies (CMHT). I am particularly grateful to Dr. Peyman Setoodeh for his constructive feedback and enriching discussions, which have improved my research.

Lastly, my deepest gratitude is reserved for my family and friends for their constant support and encouragement. I remain grateful for their continued support, which sustains me not only through this academic journey but throughout my life.

Co-Authorship

This thesis has been prepared in accordance with the regulations for a sandwich thesis format or as a compilation of research papers stipulated by the faculty of graduate studies at McMaster University. This thesis has been written based on four papers as follows.

Paper I:

Saeedzadeh, Ahsan, Saeid Habibi, and Marjan Alavi. ***"A Model-Based FDD Approach for an EHA Using Updated Interactive Multiple Model SVSF."*** *Published in Fluid Power Systems Technology Conference. Vol. 85239. ASME, 2021.*

Ahsan Saeedzadeh conducted the literature review, devised the algorithm, developed the codes and the simulation, analyzed the results, and wrote this paper.

Dr. Habibi and Dr. Alavi provided research guidance and edited the paper.

Paper II:

Ahsan Saeedzadeh, Saeid Habibi, Marjan Alavi, Peyman Setoodeh. "***A Robust Model-Based Strategy for Real-Time Fault Detection and Diagnosis in an Electro-Hydraulic Actuator Using Updated Interactive Multiple Model Smooth Variable Structure Filter***." Published in *Journal of Dynamic Systems, Measurement, and Control, 2023 1;145(10).* DOI: 10.1115/1.4063206.

Ahsan Saeedzadeh conducted the literature review, devised the algorithm, developed the codes and the simulation, analyzed the results, and wrote this paper.

Dr. Habibi, Dr. Alavi, and Dr. Setoodeh provided research guidance and edited the paper.

Paper III:

Ahsan Saeedzadeh, Peyman Setoodeh, Marjan Alavi, Saeid Habibi. "***Information Extraction Using Spectral Analysis of the Chattering of the Smooth Variable Structure Filter***." *Published in IEEE Access, 2023.* DOI: 10.1109/ACCESS.2023.3318476

Ahsan Saeedzadeh conducted the literature review, devised the algorithm, developed the codes and the simulation, analyzed the results, and wrote this paper.

Dr. Setoodeh, Dr. Habibi, and Dr. Alavi provided research guidance and edited the paper.

Paper IV:

Ahsan Saeedzadeh, Peyman Setoodeh, Marjan Alavi, Saeid Habibi. "***Adaptive Estimation Using Interacting Multiple Model with Moving Window.***"

Ahsan Saeedzadeh conducted the literature review, devised the algorithm, developed the codes and the simulation, analyzed the results, and wrote this paper.

Dr. Setoodeh, Dr. Habibi, and Dr. Alavi provided research guidance and edited the paper.

Permission to Use

In presenting this thesis in partial fulfillment of the requirements for a Postgraduate degree from McMaster University, I agree that the Libraries of this University may make it freely available for inspection. I further agree that the permission for copying this thesis in any manner, in whole or in part for scholarly purposes, may be granted by the professors who supervised my thesis work or, in their absence, by the Head of the Department or the Faculty Dean in which my thesis work was conducted. It is understood that any copying or publication or use of this thesis or parts thereof for financial gain shall not be allowed without my written permission. It is also understood that due recognition shall be given to me and McMaster University in any scholarly use which may be made of any material in my thesis. Requests for permission to copy or to make other use of material in this thesis, in whole or part, should be addressed to:

Head of the Department of Mechanical Engineering

McMaster University

Faculty of Engineering

1280 Main Street West

Hamilton, Ontario L8S 4L6

Canada

Table of Contents

List of Figures

List of Tables

List of Nomenclature

$\boldsymbol{A}$	Linear system matrix
$\widehat{\boldsymbol{A}}$	Nominal linear system matrix
A_c	Section area between cylinder and rod
a	Viscous friction coefficient
$\boldsymbol{B}$	Input matrix
$\widehat{\boldsymbol{B}}$	Nominal input matrix
b	Input gain
$\boldsymbol{C}$	Linear measurement matrix
$\widehat{\boldsymbol{C}}$	Nominal linear measurement matrix
$\boldsymbol{chattering}$	SVSF chattering vector
$\boldsymbol{D}$	Linear feedthrough matrix
D_p	Pump displacement
$\boldsymbol{d}$	Unknown inputs (or disturbances)
$\boldsymbol{E}$	Disturbance gain matrix
$\boldsymbol{e}$	Error Vector
$\boldsymbol{e_z}$	Measured error Vector
$\boldsymbol{F}$	Fault gain matrix
F_f	EHA actuator friction
F_s	Sampling frequency
$\boldsymbol{I}$	Identity matrix
$\boldsymbol{J}$	Cost function vector
$\boldsymbol{K}$	SVSF filter gain
k	Step value

$\boldsymbol{L}$	Matrix of observer gains
$\mathrm{L_p}$	EHA pump internal leakage coefficient
$\mathrm{L_{in}}$	EHA internal leakage coefficients in the cylinder
$\mathrm{L_{out}}$	EHA external leakage coefficients in the cylinder
$\boldsymbol{M}$	Defined matrix to find the chattering power spectrum threshold
M	EHA load mass
$M_{FL[i]}$	Model associate with fault level i
$M_{RUL[i]}$	Model associate with degradation level i
N	Total number of samples
$\boldsymbol{P}$	States error covariance matrix
$\mathrm{P_a}$	EHA pump outlet pressure
$\mathrm{P_b}$	EHA pump inlet pressure
p_{ij}	Mode transition matrix
$\boldsymbol{p}$	Parity vector
$\boldsymbol{Q}$	Process noise covariance matrix
$\mathrm{Q_a}$	EHA pump outlet flowrates
Q_b	EHA pump inlet flowrates
$\mathrm{Q_1}$	EHA flowrate into cylinder chamber
Q_2	EHA flowrate out of cylinder chamber
$\boldsymbol{R}$	Measurement noise covariance matrix
$\boldsymbol{r}$	Residual vector
r	Number of the model used in MMAE algorithm
$\boldsymbol{S}$	Innovation covariance matrix

T_s	Sampling time
T_u	Updating time of the MWIMM algorithm
t	Time
$\mathbb{R}^n$	n-dimensional real space
$\boldsymbol{u}$	Input vector
V_0	EHA actuator control volume for each side when placed in its reference central position
$\boldsymbol{v}$	Process noise vector
$\boldsymbol{W}$	Kalman filter gain
$\boldsymbol{W_o}$	Weighting matrix of the residuals
$\boldsymbol{w}$	Measurement noise vector
$\boldsymbol{x}$	State vector
$\boldsymbol{y}$	Output vector
$\boldsymbol{z}$	Measurement vector
z	Represents the z-transform
$\boldsymbol{\beta}$	SVSF A priori existence boundary
β_e	Effective bulk modulus
γ	SVSF convergence rate
σ	Standard deviation
ζ	Damping ratio
$\boldsymbol{\Lambda}$	Defined matrix to find the chattering power spectrum threshold
$\boldsymbol{\theta}$	System parameter vector
θ_i	Represents the central value of the i^{th} bin of parameter θ

$\boldsymbol{\mu}$	Mode probability vector
$\mu_{i\|j}$	Mixing probabilities
Λ_j	Likelihood function
ω	Frequency in Hz
ω_{p}	EHA pump speed
ω_n	Discreate Fourier frequency at n$^{\mathrm{th}}$ Hz
ω_0	Natural frequency of the system
$\boldsymbol{\psi}$	Smoothing boundary layer
$\boldsymbol{\mathcal{S}_\Gamma}$	SVSF chattering power spectrum threshold
$\boldsymbol{\psi_{VBL}}$	Variable boundary layer
$\boldsymbol{\psi_{lim}}$	Fixed boundary layer limit
$\boldsymbol{\mathcal{O}}$	Observability matrix
$\boldsymbol{\Delta}$	Denotes additive uncertainty
$\hat{}$	Denotes estimated value
$k+1\|k$	A priori (before the fact) value
$k+1\|k+1$	A posteriori (after the fact) value
$\intercal$	Transpose of matrix
A^+	Pseudo-inverse of matrix A
$\mathcal{N}(\mu,\Sigma)$	Normal distribution with μ mean, and Σ covariance
$\mathcal{N}_c(\mu,\Sigma)$	Complex normal distribution with μ mean, and Σ covariance
χ_2^2	Chi-squared distribution
$diag(A)$	Creation of a vector with diagonal elements of some matrix
$\|a\|_{abs}$	Absolute value of parameter a
$\lfloor\cdot\rfloor$	Floor function

$\odot$	Schur operation
$sgn(\cdot)$	Sign function
$sat(\cdot, \boldsymbol{\psi})$	Saturation function with boundary limit of $\boldsymbol{\psi}$
$\sup(\cdot)$	Supremum function
$max(\cdot)$	Maximum function
$dL_f^n h(\cdot)$	nth order Lie derivative of the measurement function h with respect to the system model f
$\mathbb{E}[\cdot]$	Expected value function
$\Pr(\cdot)$	Probability function
$\mathcal{F}(\cdot)$	Fourier transform
$V^{(N)}(\omega_n)$	Discrete Fourier transform of noise signal v at nth frequency
$\mathcal{S}_v^{(N)}(\omega_n)$	Power spectrum of signal v at nth frequency.
$\Re\{\cdot\}$	Real part of a complex number
$\Im\{\cdot\}$	Imaginary part of a complex number

Abbreviations

CUSUM	Cumulative Sum
EHA	Electro-Hydraulic Actuator
EKF	Extended Kalman Filter
DFT	Discrete Fourier Transform
FDD	Fault Detection Diagnosis
FFT	Fast Fourier Transform
FTCS	Fault-Tolerant Control System
GLR	Generalized Likelihood Ratio
GPB1	General Pseudo-Bayesian first order
GPB2	General Pseudo-Bayesian second order
IMM	Interacting Multiple Model
IFAC	International Federation of Automatic Control
KF	Kalman Filter
LTI	Linear Time Invariant
MLE	Maximum Likelihood Estimate
MMEA	Multiple Model Adaptive Estimation
MMP	Multiple Model Pruning
MWIMM	Moving Window Interacting Multiple Model
PD	Proportional-Derivative controller
PDE	Partial Differential Equations
PDF	Probability Density Functions
PF	Particle Filter
RLS	Recursive Least Square

RUL	Remaining Useful Life
SAEKF	State Augmented Extended Kalman Filter
SPRT	Sequential Probability Ratio Test
STFT	Short Time Fourier Transform
SVSF	Smooth Variable Structure Filter
SVSF-VBL	Smooth Variable Structure Filter with Variable Boundary Layer
UIMM	Updated Interacting Multiple Model
UIO	Unknown Input Observer
UKF	Unscented Kalman Filters
VSF	Variable Structure Filter

1. Introduction

Fault Detection and Diagnosis (FDD) is an integral part of our daily lives, from medical practitioners diagnosing patients to mechanics inspecting car engines, all seeking to address this matter to some extent. According to industrial statistics, approximately 70% of industrial accidents are attributed to human errors, leading to notable economic, safety, and environmental consequences [1]. The continuous advancement of technology, characterized by high-speed computational power and a diverse range of sensors for system behavior measurement, opens up significant opportunities for automating the FDD process and enables real-time automated corrective actions to maintain system performance post-fault occurrence. The initial step in the FDD process involves accurately defining the faults within the system to effectively distinguish them from other acceptable changes that may arise due to uncertainties, disturbances, and measurement noise under normal conditions. This thesis focuses on FDD within the context of control and industrial applications, thereby most of the definitions and terminologies are borrowed from the International Federation of Automatic Control (IFAC) technical committees.

An effective diagnostic approach should be capable of addressing the following aspects:

- **Detection:** Determine whether faults are observable based on the available measurements.
- **Invariance:** Distinguish between faults and other variations in observations caused by uncertainties, disturbances, or measurement noise, to prevent false alarms.

- **Isolation:** Determine the specific type of fault, its location, and the time of occurrence.
- **Identification:** Determine the magnitude and dynamic behavior of the faults.

A meaningful fault detection process needs both detection and invariance, whereas the isolation and identification further enhance the efficacy of the diagnostic approach.

In the literature, fault detection and diagnosis are perceived from two different perspectives: the model-based approach, which relies on prior knowledge describing the system's behavior, and the data-driven approach, which seeks to extract patterns or model directly from data when an effective model cannot be generated or does not exist. This thesis is focused on model-based approaches, where innovative estimation strategies are explored to enhance the performance of the diagnosis process. The thesis introduces new algorithms aimed at improving computational efficiency and relaxing fault discretization in adaptive estimation methods. Additionally, it proposes a fault detection strategy by extracting information from a system using a robust filter, using its robustness to accurately estimate states even after a fault occurs. This chapter starts with a presentation of the problem statement, followed by an exploration of the relevant literature. Subsequently, it delves into the distinctive contributions and novel aspects of the research. The final section outlines the thesis structure and organization.

1.1. Problem Statement

Fault detection plays a crucial role in control and industrial applications, given its ability to maintain system integrity, optimize performance, and ensure safety.

According to the IFAC technical committees, a fault is defined as "an unpermitted deviation of at least one characteristic property or parameter of the system from the acceptable/usual/standard condition". Fault detection allows for the early identification of abnormalities, such as sensor or actuator faults, process malfunctions, or parameter variations. By promptly detecting and diagnosing faults, control systems can initiate appropriate corrective actions, thereby minimizing the impact on system performance and preventing catastrophic failures. Industrial applications heavily rely on fault detection to uphold the reliability and efficiency of complex processes and machineries. By timely identifying faults in industrial equipment, unexpected shutdowns can be prevented, downtime can be reduced, and maintenance schedules can be optimized. Incorporation of robust fault detection strategies in control and industrial applications leads to significant enhancements in system performance, productivity, and overall operational effectiveness.

The issue of fault management has various levels, which are outlined below using widely recognized terminology employed by IFAC technical committees [2], [3]:

- **Fault detection:** This level involves determining the presence of faults in a system and identifying the time of detection. It can be represented in binary form, such as a simple label indicating fault/no-fault, or based on a scoring system.
- **Fault isolation:** At this level, the objective is to determine the specific type of fault, its location, and the time of detection. Fault isolation follows fault detection and aims to narrow down the potential causes of the detected fault.

- **Fault identification:** In this stage, the focus shifts to determining the magnitude and time-varying behavior of a fault. It follows fault isolation and provides additional information about the characteristics and dynamics of the detected fault.
- **Fault diagnosis:** Fault diagnosis encompasses the comprehensive determination of the type, magnitude, location, and time of detection of a fault. It includes the processes of fault detection, isolation, and identification.
- **Monitoring:** This level involves the continuous, real-time task of observing and recording information about the conditions of a physical system. The aim is to recognize and indicate any anomalies or deviations in the system's behavior.
- **Supervision:** Supervision entails actively monitoring a physical system and taking appropriate actions to maintain its operation in the event of faults. It involves implementing strategies to mitigate the impact of faults and ensure the overall functioning and stability of the system. Fault Tolerable Control Systems (FTCS) can be considered part of this level.

These distinct levels of fault management provide a structured framework for addressing fault-related challenges in various domains.

The fault diagnosis process typically involves a sequence of fundamental stages aimed at transforming measurement or observation data into practical insights. The initial step involves collecting data from sensors or observations within the system which serves as the foundation for subsequent analysis. The next step, which varies based on the chosen diagnosis method, involves either feature extraction (in data-

based approaches) or residual generation (in model-based approaches). This step entails extracting relevant features from the data or residuals by comparing the data to a prior model. These features or residuals capture the characteristics or deviations that indicate the presence of faults. Following this, decision-making techniques are employed to interpret the extracted features or residuals and make informed judgments about the occurrence of faults. Algorithms or models are utilized in this step to analyze the data and determine the likelihood or severity of a fault. Finally, fault classification is performed, where the identified faults are categorized into specific fault types or classes. The flowchart illustrating these steps is presented in Figure 1-1.

It is important to note that these steps are not always performed independently; they are often combined or interconnected. For example, feature extraction and decision-making techniques can be integrated, or fault classification can be incorporated into the decision-making process. Such combinations typically yield a more comprehensive and efficient fault diagnosis process, enabling accurate identification and effective mitigation of faults, or reducing computational requirements.

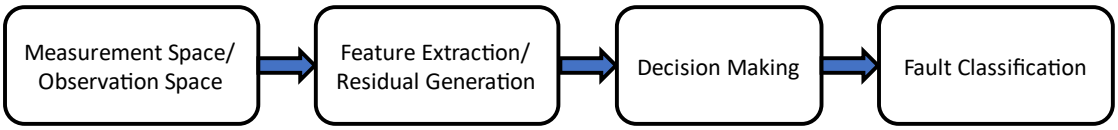

Figure 1-1. The fault diagnosis steps flowchart.

Fault diagnosis poses several challenges that need to be addressed for effective and reliable fault detection and identification. One crucial challenge is maintaining an invariance relation or minimizing false alarms. Robustness plays a key role here,

as the algorithm's performance should remain unaffected by noise, disturbances, and uncertainties in the system model. Another challenge is ensuring high detectability, which involves the sensitivity of the algorithm in detecting faults. It is essential to design diagnostic techniques that can accurately detect faults, even in the presence of various system conditions and operational scenarios. Identifiability is another challenge, focusing on the ability to decouple and differentiate between multiple faults occurring simultaneously. Fault diagnosis algorithms should aim to provide distinct and reliable information about individual faults. The diagnostic response time, or mean detection delay, is another critical factor to consider. Timely fault detection and response are crucial for minimizing the impact of faults on system performance and avoiding potential hazards. Moreover, addressing storage and computation requirements is vital. The fault diagnosis system should compromise between the amount of data storage necessary for fault analysis and the computational resources needed for efficient and real-time fault diagnosis. Overcoming these challenges is essential for developing robust fault diagnosis methodologies that deliver accurate, timely, and efficient fault detection and identification.

This thesis is centered around model-based approaches for fault diagnosis, presenting innovative estimation strategies to enhance the diagnostic process. The research primarily focuses on utilizing estimation techniques rooted in stochastic filter-based methods, specifically the Kalman Filter (KF), to effectively handle process and measurement noise. Robust filtering techniques, such as the Smooth Variable Structure Filters (SVSF) [4], developed using variable structure theory, are also employed to address uncertainties encountered during fault diagnosis. A key contribution of this thesis is the introduction of a computationally efficient version

of Multiple Model Adaptive Estimation (MMEA). This approach combines residual generation, decision-making, and classification steps to create an efficient diagnostic process. To demonstrate the real-time application of this strategy, a Fault-Tolerant Control System (FTCS) is developed. Furthermore, the thesis extends the application of this approach by introducing a more general algorithm that can be applied to estimating the Remaining Useful Life (RUL) and parameter estimation in a broader context. Additionally, the thesis explores the potential of extracting information from robust SVSF filters for use in the diagnostic process. By addressing these topics, the thesis aims to contribute to advancements in fault diagnosis methodologies and improve the accuracy, efficiency, and applicability of fault diagnosis systems.

1.2. Background

Fault detection has been approached from various perspectives in different fields. In the control engineering community, fault detection is regarded as a subset of change detection, which also encompasses surveillance, parameter tracking, adaptive estimation, adaptive control, and hybrid systems [1], [5], [6], in addition to fault detection. In this context, the primary focus lies in identifying deviations in system behavior, often compared to a predefined model, that could indicate the presence of faults. The aim is to detect and address faults by providing relevant residuals. On the other hand, the Artificial Intelligence (AI) community treats fault detection as part of anomaly detection methodologies [7], [8]. Anomaly detection is applied in diverse domains, such as intrusion detection, fraud detection, and medical informatics [8]. Within this framework, fault detection involves identifying abnormal behavior that may suggest the existence of faults via utilizing AI algorithms and machine

learning techniques to detect deviations from expected patterns. These patterns are extracted through feature extraction from observed or measured data. As a result, terminologies may differ across the various fields. This study aligns more closely with the first approach, namely fault detection from a control engineering perspective, and borrows IFAC technical committees' terminologies.

Fault Detection and Diagnosis methods can be broadly categorized into two main approaches: model-based and data-driven. Model-based methods leverage physics of the failure of the system to detect and diagnose faults. This approach can be further classified into quantitative and qualitative techniques. The quantitative model employs static and dynamic interactions between system variables and parameters to mathematically describe the behavior of the system [1]. Conversely, the qualitative model utilizes static and dynamic relationships among system variables and parameters to describe the system's behavior using qualitative measures such as cause-effect relationships or conditional rules, such as if-then statements [1]. On the other hand, data-driven methods do not require prior knowledge of the system's physics. Instead, they directly analyze input and output signals to detect and diagnose faults, without relying on explicit mathematical models. These methods rely on statistical analysis, pattern recognition, or data-driven algorithms to identify anomalies or deviations in the signals, which may indicate the presence of faults. Figure 1-2 presents a tree diagram that provides a detailed breakdown of the various categories within the diagnosis process. This tree diagram is constructed based on a comprehensive study of the most popular categorizations found in the literature [1], [6]–[11].

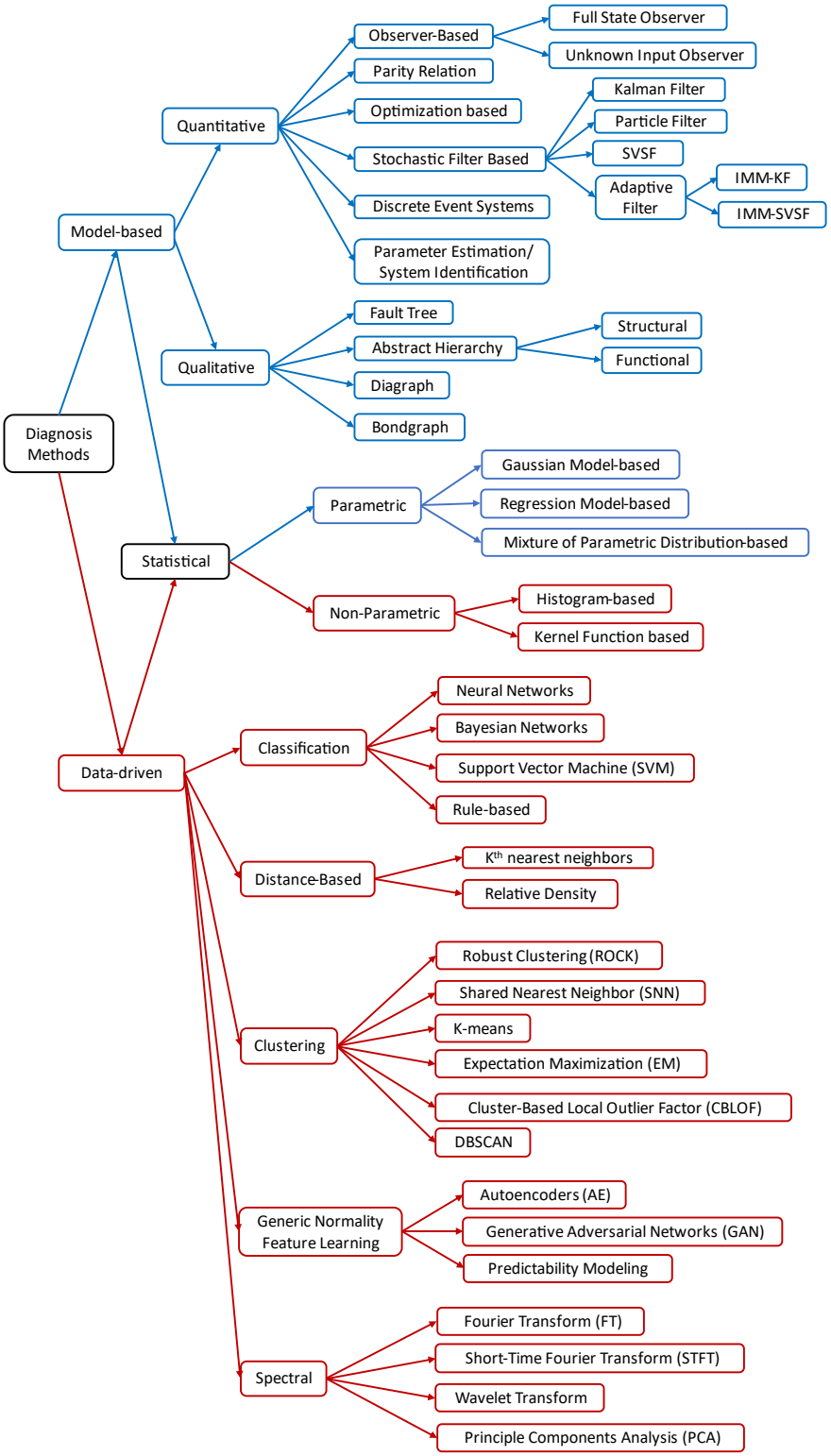

Figure 1-2. The tree diagram of different diagnosis approaches.

The distinction between these approaches may not always be well-defined, and in some cases, a combination of these methods is utilized. For example, chapter 3 utilizes spectral analysis on the chattering signal obtained from the quantitative model-based SVSF filter for fault diagnosis of a system. This approach can be considered as the combination of a model-based system with a data-driven method. This study lies in the specialization of quantitative model-based FDD approaches.

Faults in a dynamic system can manifest in various forms, including actuator, sensor, and component faults [6]. Actuator faults introduce additional disturbances or errors into the system, exhibiting an additive nature. Similarly, sensor faults commonly cause additive effects, resulting in inaccuracies or biases in the measured data. On the other hand, component faults, also referred to as parameter changes, have a multiplicative impact on the system. These faults alter the parameters or characteristics of the system components, leading to overall changes in system behavior. Modeling such component faults can be challenging for model-based FDD approaches.

FDD methods, in general, employ the redundancy concept, which can be achieved through hardware-based or analytical approaches [6]. Hardware redundancy involves comparing duplicate signals generated by different hardware components. For example, one can identify a faulty sensor by comparing the same signal from two or more sensors. In contrast, analytical redundancy utilizes multiple non-identical approaches, including mathematical process models in analytic form [2]. Analytical redundancy plays a critical role in the residual generation and diagnosis process for model-based FDD methods.

1.2.1. Residual Generation

The process of residual generation, serving as the initial step (depicted in Figure 1-1), plays a crucial role in quantitative model-based FDD approaches. As defined by the IFAC technical committees, a residual is a fault indicator that results from the deviation between measurements and computations derived from model equations [2], [3]. The objective of a residual generator is to produce a residual vector, denoted as $\boldsymbol{r}(t)$, which satisfies the following relationship [12]:

- $\boldsymbol{r}(t) = 0 \;\; if \;\; \boldsymbol{f}(t) = 0$, for invariance.
- $\boldsymbol{r}(t) \neq 0 \;\; if \;\; \boldsymbol{f}(t) \neq 0$, for fault detection.
- $r_i(t) \neq 0 \;\; if \;\; f_i(t) \neq 0$, for fault isolation.
- $\lim_{t\to\infty}[\boldsymbol{r}(t) - \boldsymbol{f}(t)] = 0$, for fault identification.

where $f_i(t)$ represents the ith fault and $r_i(t)$ is the corresponding subset of residuals. The prevailing techniques utilized for residual generation include observer-based methods, parity relations, optimization-based approaches, adaptive filter-based techniques, and system identification methods [6].

Observer-based methods involve generating residuals through an observer, where the observer tracks the actual plant's state and yields residuals with a zero mean, when no fault is present. Additionally, these observers are designed to facilitate fault isolation. On the other hand, the parity relations approach involves converting the input-output transfer function or state-space models of the plant to directly generate directional or structural residual vectors. Both the observer-based methods and the parity relations approach usually overlook multiplicative faults or model

uncertainties. Moreover, they are typically restricted to Linear Time-Invariant (LTI) systems [6].

In order to be able to isolate all possible faults, it is necessary to decouple the impact of each fault on the residual from the influences of other faults. Full decoupling is not feasible in most of the situations because of restrictive conditions, which are governed by the number of faults to be isolated, and the number of available sensor signals. To address this problem, approximate decoupling has been proposed using optimization based residual generation [12]–[14]. The basic concept is to enhance the effect of faults on the residuals, while minimizing the effect of unknown inputs and uncertainties on them.

The Kalman filter is a well-known algorithm, which is used in stochastic filter-based methods for fault detection and diagnosis. It can be seen as a specific instance of stochastic optimization employing linear quadratic techniques. In this approach, faults are identified through statistical assessments regarding the residuals' whiteness as well as their mean and covariance. The typical statistical approaches for evaluating Kalman filter residuals encompass the Maximum Likelihood approach or the Generalized Likelihood Ratio (GLR) test [8]. Filter-based approaches are usually implemented in an adaptive format using Multiple Model Adaptive Estimation (MMAE) structure [8], [15]. The implementation of adaptive filter-based methods is significantly more complex compared to observer-based or parity relations methods, especially in situations involving numerous fault conditions. However, the adaptive filter-based approach offers the advantage of achieving optimal filtering by combining Interacting Multiple Model with Kalman Filter (IMM-KF). To enhance estimator robustness, the IMM with Smooth Variable Structure Filter (IMM-SVSF) has been

introduced [16]. The parallel structure of these filters enables rapid adaptation, leading to accurate state estimation following a fault occurrence. To extend this multiple model approach to nonlinear or time-varying systems, nonlinear filters like the Extended Kalman Filters (EKF), Unscented Kalman Filters (UKF), and Particle Filter (PF) [17], also known as the sequential Monte Carlo method [18] have been employed. The adaptive filter-based approach is suitable for detecting both multiplicative (component) faults and additive faults.

Despite its advantages, MMAE approach exhibits two main drawbacks: it is computationally intensive; and it assumes that fault parameters take discrete values from a finite set [6], [19]. In order to enhance computational efficiency, this thesis introduces a more computationally efficient version of adaptive filtering by combining the Updated Interacting Multiple Model (UIMM) with a robust SVSF filter. This improved approach is employed to detect leakage and friction faults in an Electro-Hydraulic Actuator (EHA), a well-known FDD problem in aircrafts [6]. Regarding the second issue, for certain faults with continuous fault parameters, several fault models may be needed to describe a single fault with a varying level of intensity. This introduces additional complexity and may result in potentially higher false alarm rates. To address this challenge, a novel variation of IMM, known as Moving Window IMM (MWIMM), is proposed in this thesis specifically for FDD problems involving continuous faults.

System identification methods have broad applicability, extending to both linear and nonlinear systems. These approaches prove particularly valuable for detecting small or incipient faults. Nonetheless, the effectiveness of the system identification

method is highly dependent on the statistical decision-making techniques utilized to identify changes in parameters.

1.2.2. Decision-Making Tools

Once residuals are generated, the subsequent important step in the quantitative FDD process involves decision making as depicted in the flowchart shown in Figure 1-1. Various methods can be employed to make decisions based on the generated residuals. One commonly approach is the fixed threshold method, where a fault is identified if the residual exceeds a pre-established threshold. Alternatively, the adaptive threshold approach dynamically adjusts the threshold based on the system's operating conditions or statistical properties of the residuals.

Introduced by Wald in 1947, the Sequential Probability Ratio Test (SPRT) continuously monitors the likelihood of a fault based on the generated residual and updates the decision accordingly [6]. The Cumulative Sum (CUSUM) algorithm, also known as the Page–Hinkley Stopping Rule, was proposed by Page [20] to detect a change in the mean of the residuals by analyzing a weighted sum of recent observations. Page noted that this rule is equivalent to conducting an SPRT [6]. In [21], Lorden established the asymptotic minimax optimality, or the worst-case optimality, of the CUSUM algorithm. Lorden derived a lower bound for the worst mean delay for detection and demonstrated that the CUSUM algorithm achieves this lower bound. Extending the capabilities of the CUSUM algorithm, Nikiforov addressed both the change detection and isolation problem in [22]. This extension involved multiple hypotheses testing, and the statistical properties of the algorithm were thoroughly examined.

The Generalized Likelihood Ratio Test (GLRT) utilizes statistical likelihood ratios to make decisions based on the observed residuals [8]. It involves comparing the likelihood of the observed data under two competing hypotheses: one assumes a fault-free system, while the other considers a faulty system. The GLRT calculates a likelihood ratio to assess the relative likelihood of these hypotheses based on the observed data. Willsky and Jones [23] developed an iterative algorithm for the GLR test on the residual (or innovation) produced by a Kalman filter by leveraging the linear system property, the Gaussian noise characteristics, and the additive effect of faults on the system. Basseville and Benveniste [24] proposed a modified algorithm that utilizes the Maximum Likelihood Estimate (MLE) of the innovation instead of the likelihood ratio. Li and Kadirkamanathan [25] applied the GLR test in conjunction with a particle filter method to address the FDI problem in general nonlinear and non-Gaussian systems.

The local approach, first introduced by Nikiforov [26], adopts a Taylor's series expansion of the log likelihood function instead of conducting a direct test based on measurements. The test relies on the first-order derivative term in the Taylor's series expansion, which is known as the efficient score. Using the Central Limit Theorem, it can be demonstrated that the efficient score is asymptotically distributed as Gaussian Probability Density Function (PDF). This property allows a wide range of change detection problems to be transformed into the fundamental task of testing for a change in the mean value of a Gaussian vector [6].

The widely recognized statistical decision techniques, such as SPRT and CUSUM algorithms, are easily implementable. It is also relatively straightforward to

implement the GLR test, which is effective in detecting additive and component faults. Although more intricate, the local approach has shown a promising performance in detecting small or incipient faults [6].

1.2.3. Fault Supervision

The ultimate objective of fault detection is to effectively manage system faults that may occur during its operation. To achieve this, supervision involves actively monitoring the physical system and taking appropriate actions to ensure its continued functioning even in the presence of faults. For certain critical applications like flight control systems, it becomes crucial to identify the most suitable control actions following a fault in order to maintain the system's safe operation without interruption. This can be accomplished through reconfiguration control, which involves adjusting the controllers in real-time in response to faults, leading to the development of fault-tolerant control systems.

A well-known approach for fault supervision involves the utilization of multiple-model methods. These methods employ a collection of parallel models that describe the system's behavior under normal conditions and various fault scenarios. Corresponding controllers are designed for each model, and a switching mechanism is chosen to determine the system's mode at each time step. This enables the selection of the appropriate controller designed for that particular mode, resulting in improved performance and robustness across different operating conditions. The multiple-model control approaches are derived from multiple-model fault detection schemes such as IMM-KF and IMM-SVSF. In this thesis, a fault-tolerant control system based on the UIMM-SVSF strategy was devised to control the position of an Electro-

Hydraulic Actuator (EHA) – widely used in flight surface control – in the presence of leakage and friction faults [27].

Another commonly used approach for fault supervision is the utilization of an adaptive controller. This approach aims to ensure robust or acceptable performance levels in the face of sudden changes in system parameters. Adaptive control is generally classified into two methods: indirect adaptive control, which involves a parameter isolation process, and direct adaptive control, which does not require explicit parameter isolation. Adaptive control has been widely applied to design a fault tolerant control solution for flight surface control problems. For instance, in one study [28], adaptive flight control laws were devised to compensate for actuator faults or surface damage. Additionally, a joint effort between Honeywell Labs and NASA Langley Research Center led to the development of a Control Upset Prevention and Recovery System. This system provided reconfiguration of control laws, fault supervision, fault detection, fault isolation, and pilot cueing. Its performance was evaluated through piloted simulations on a civil transport aircraft [29], [30]. Moreover, Kim et al. [31] developed an indirect adaptive control algorithm for aircraft flight control systems to address unknown system parameters and actuator faults. The system parameters were estimated in an online manner using Fourier transformation and then used in the design of the control gain.

Recently, there has been a surge in the popularity of the online learning approach for fault supervision. This method involves the utilization of machine learning algorithms to continuously learn from the system's real-time behavior and adapt to changes induced by faults [32]. One prominent example of an online learning approach

for fault supervision is reinforcement learning [32]–[34]. Reinforcement learning is a form of machine learning in which an agent learns to make decisions by interacting with an environment and receiving feedback in the form of rewards or penalties. In the context of fault supervision, reinforcement learning can be employed to acquire a control policy that remains robust in the presence of faults by optimizing a reward function considering both the system's performance and the occurrence of faults [32]–[34]. Another notable example of an online learning approach for fault supervision is resilient learning [34]. Resilient learning entails using machine learning algorithms to learn from the system's behavior during fault occurrences and adapt to changes induced by these faults. It can be employed to acquire a control policy that exhibits resilience to faults by optimizing a cost function that considers both the system's performance and the occurrence of faults [34]. Nevertheless, it is important to acknowledge that implementing online learning for fault-tolerant control poses challenges, such as ensuring stability during the learning process, avoiding overfitting to specific fault scenarios, and managing computational complexity in real-time applications.

1.3.Thesis Outlines

The structure of this thesis is as follows: In Chapter 2, there is a comprehensive review of existing quantitative model-based fault detection and diagnosis methods, including a comparative analysis aimed at identifying areas where further research is needed and contributions of this thesis.

Chapter 3 delves into the exploration of information extraction from chattering, with the aim of identifying model mismatch based on the spectral characteristics of

the chattering signal. To assess the effectiveness of the developed framework for chattering analysis, two case studies are undertaken. First, the power spectrum of the chattering signal has been employed to identify mismatch and the potential of recovering the temporal information of the model mismatch from the spectrogram is studied, using Short Time Fourier Transform (STFT) for an underdamped second-order system. Then, the proposed strategy is applied to detect and measure the severity of leakage and friction faults as well as the bulk modulus mismatch in an electro-hydraulic actuator.

Chapter 4 introduces the UIMM-SVSF algorithm as an innovative approach for detecting and isolating leakage and friction faults within a standard EHA system. In this chapter, a Fault Tolerant Control System (FTCS) has been developed to show the application of the proposed Fault Detection and Diagnosis (FDD) strategy for managing faults within a closed-loop system.

Chapter 5 presents an innovative adaptive estimation technique known as the Moving Window Interacting Multiple Model (MWIMM). This chapter begins by offering an overview of adaptive estimation methods and proceeds to explain the MWIMM formulation for estimating fault intensity and Remaining Useful Life (RUL). Furthermore, it delves into the examination of the parameter estimation challenge. Comparative analysis with the augmented state Extended Kalman Filter (EKF) estimation is conducted, demonstrating that the MWIMM approach introduced in this study presents a viable and promising alternative for effectively managing significant parameter uncertainties and adapting to gradual changes in system parameters.

Chapter 6 is dedicated to summarizing concluding remarks and providing suggestions for future research.

2. Preliminary Analysis of Quantitative Model-based Fault Detection and Diagnosis Approach

Model-based approaches involve creating a system model using either a fundamental understanding of the system's physics or system identification. By utilizing the analytical redundancy concept, this model serves as a reference to establish mathematical relationships between inputs and measurements. In an FDD context the models can be used in conjunction with measurements from the system for, generating residuals that carry fault signatures. These residuals are then processed through a decision-making tool for diagnostic purposes. The physical meaning associated with each state and parameter of the model greatly aids the diagnostic procedure in this approach.

The fault diagnosis analytical redundancy schemes basically rely on signal processing techniques, such as state estimation, parameter estimation, adaptive filtering, and other related methods. consider a general system model as follows:

$$\boldsymbol{y}(t) = \boldsymbol{f}\big(\boldsymbol{u}(t), \boldsymbol{d}(t), \boldsymbol{x}(t), \boldsymbol{\theta}(t)\big) \tag{2.1}$$

where the measurable output and input vectors are denoted as $\boldsymbol{y}(t)$ and $\boldsymbol{u}(t)$ respectively, $\boldsymbol{x}(t)$ is the state vector, $\boldsymbol{d}(t)$ represents unknown inputs (or disturbances) and uncertainties, and $\boldsymbol{\theta}(t)$ is the system parameter vector. To estimate the unmeasured elements of $\boldsymbol{x}(t)$ and/or $\boldsymbol{\theta}(t)$ based on the observed $\boldsymbol{y}(t)$ and $\boldsymbol{u}(t)$, state estimation and parameter estimation methods are employed, with widely used techniques such as Kalman filters or observers [13] and least squares methods for online monitoring of parameter variation [9]. The residuals generated from these

estimation strategies are then utilized to diagnose and manage faults within the system. Figure 2-1 illustrates the fault diagnosis and supervision flowchart of a typical quantitative model-based approach. This section delves into the most frequently utilized model-based methods, providing discussions on their applications, and explaining the research gap and contributions of this study.

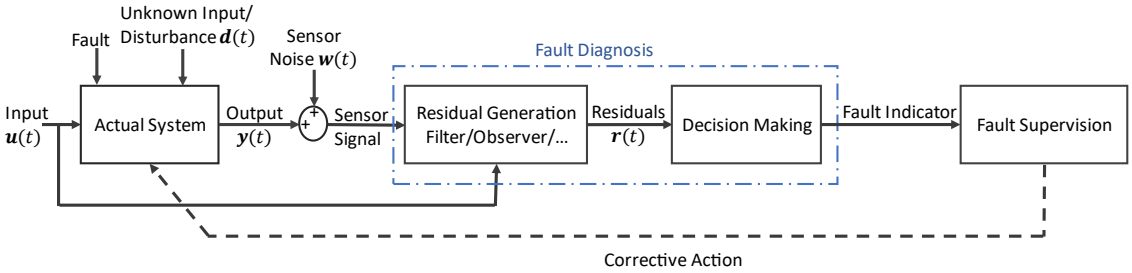

Figure 2-1. Quantitative model-based fault diagnosis and supervision flowchart.

2.1. Observer-Based Methods

In the field of diagnostics, observer-based approaches play an important role in comparing model-predicted values to actual measurement signals to obtain residuals. It is important to note that diagnosis observers, distinct from classical state observers utilized for control purposes, primarily serve as output observers and often operate in an open-loop configuration [12]. This configuration makes them more susceptible to modeling errors and uncertainties. Therefore, ensuring robustness is essential for reliable fault detection and accurate diagnosis, as cited in the literature [12], [13], [35]–[37]. Two widely recognized types of diagnostic observers are the full-state observer-based and the unknown input observer-based, which are briefly discussed in the forthcoming sections.

2.1.1. Full-State Observer-based FDD

In this part, the examination centers around exploring a simplified linear interpretation of the fault model. The aim is to clarify the foundational structure of the diagnosis method rooted in the full-state observer approach. Let us consider a linear additive fault model that does not account for measurement noise and disregards sensor anomalies, as depicted below:

$$\boldsymbol{x}(k+1) = \boldsymbol{A}\boldsymbol{x}(k) + \boldsymbol{B}\boldsymbol{u}(k) + \boldsymbol{E}\boldsymbol{d}(k) + \boldsymbol{F}\boldsymbol{f}_a(k), \tag{2.2}$$

$$\boldsymbol{z}(k) = \boldsymbol{C}\boldsymbol{x}(k). \tag{2.3}$$

where, $\boldsymbol{x}(k)$ is the state vector, $\boldsymbol{u}(k)$ denotes the input vector, $\boldsymbol{d}(k)$ represents the unknown inputs (or disturbance) and uncertainties, $\boldsymbol{f}_a(k)$ is the actuator fault vector, and $\boldsymbol{z}(k)$ stands for the measurement vector. These entities are all evaluated at time k. The full-state observer is derived as follows:

$$\hat{\boldsymbol{x}}(k+1) = \boldsymbol{A}\hat{\boldsymbol{x}}(k) + \boldsymbol{B}\boldsymbol{u}(k) + \boldsymbol{L}\big(\boldsymbol{z}(k) - \hat{\boldsymbol{z}}(k)\big), \tag{2.4}$$

$$\hat{\boldsymbol{z}}(k) = \boldsymbol{C}\hat{\boldsymbol{x}}(k). \tag{2.5}$$

Here, $\hat{\boldsymbol{x}}$ represents the estimated state and $\boldsymbol{L}$ is the matrix of observer gains. The subsequent step involves establishing the residuals by comparing the estimated state against the measured state, based on the redundancy concept. This is defined as follows:

$$\boldsymbol{r}(k) \triangleq \boldsymbol{W_o}\big(\boldsymbol{z}(k) - \hat{\boldsymbol{z}}(k)\big) = \boldsymbol{W_o}\boldsymbol{C}\boldsymbol{e}(k), \tag{2.6}$$

where, $\boldsymbol{W_o}$ is the weighting matrix of the residuals and $\boldsymbol{e}(k) \triangleq \boldsymbol{z}(k) - \hat{\boldsymbol{z}}(k)$ represents the error in estimation. The dynamics of the error are expressed as follows:

$$\boldsymbol{e}(k+1) = (\boldsymbol{A} - \boldsymbol{LC})\boldsymbol{e}(k) + \boldsymbol{Ed}(k) + \boldsymbol{Ff}_a(k). \tag{2.7}$$

The selection of gains $\boldsymbol{L}$ and $\boldsymbol{W_o}$ is conducted in a manner that ensures the asymptotic stability of $\boldsymbol{A} - \boldsymbol{LC}$ and imparts certain desired attributes to the residual. Two common strategies to obtain these weights are the methods related to eigen-structure assignment [38], [39] and the utilization of a fault detection filter [40].

In the context of eigen-structure assignment technique, the objective is to diminish the residual's susceptibility to disturbances by nullifying the transfer function matrix connecting $\boldsymbol{d}(k)$ to $\boldsymbol{r}(k)$. The transfer function is deduced from equations (2.6) and (2.7), resulting in the following expression:

$$\boldsymbol{W_o C}[z\boldsymbol{I} - (\boldsymbol{A} - \boldsymbol{LC})^{-1}]\boldsymbol{E} = 0. \tag{2.8}$$

where z represents the z-transform, and $\boldsymbol{I}$ denotes the identity matrix. The aim is to select appropriate values for $\boldsymbol{W_o}$ and $\boldsymbol{L}$ to satisfy equation (2.8). The procedures for designing the eigen-structure assignments are explained in [39]. This approach can also be harnessed to generate structural residuals. As an illustration, assume $f_i(k)$ represents a distinct fault component (namely, where $f_i(k)$ constitutes an element of $\boldsymbol{f}_a(k)$). By regarding it as a disturbance $\boldsymbol{d}(k)$, the residual $\boldsymbol{r}(k)$ can be engineered to be impervious to the $f_i(k)$ fault.

The concept of the fault detection filter was initially introduced by Beard [40] and later enhanced through a geometric interpretation by Jones and Massoumnia [41], [42]. Examining the error dynamics presented in equation (2.7), let us consider $\boldsymbol{f}_i$ as a specific fault component. The influence of the $f_i(k)$ fault on the estimation error can be expressed as follows:

$$\boldsymbol{e}(k+1) = (\boldsymbol{A} - \boldsymbol{LC})\boldsymbol{e}(k) + F_i f_i(k). \tag{2.9}$$

Within a fault detection filter, the selection of gain $\boldsymbol{L}$ is directed towards ensuring the stability of $\boldsymbol{A} - \boldsymbol{LC}$, and concurrently, the error $\boldsymbol{e}(k)$ linked to the fault f_i is confined to a consistent subspace, denoted as $\mathcal{U}_i$. Consequently, the correlated orientation of the residual aligns with $\boldsymbol{W_o L}\mathcal{U}_i$. Moreover, when each subspace of the residuals corresponding to different faults remains distinct, the potential to achieve fault isolation emerges. Notably, it is important to recognize that fault detection filters typically do not consider the impact of disturbances or noise.

2.1.2. Unknown Input Observer

The Unknown Input Observer (UIO) develops a set of observers each one of them is sensitive to a subset of faults while insensitive to the remaining faults and the unknown inputs. The set of these residuals is used to detect and isolate different faults. These residuals should be robust so that the decisions are not corrupted by unknown inputs like unstructured uncertainties. In a case with no fault, the observers track the process output closely and the residuals from the unknown inputs are designed to be small. If a fault occurs, all observers, which are made insensitive to the fault by design, continue to develop small residuals, while observers, which are designed to be sensitive to the fault, will have significant residuals. This approach was introduced by Watanabe and Himmelblau [43], and has subsequently been refined by Frank and Wünnenberg [44]. To illustrate the basic idea of the unknown input observer, consider a linear system similar to (2.2) and (2.3) as below:

$$\boldsymbol{x}(k+1) = \boldsymbol{A}\boldsymbol{x}(k) + \boldsymbol{B}\boldsymbol{u}(k) + \boldsymbol{E}\boldsymbol{d}(k) + \boldsymbol{F}\boldsymbol{f}(k), \tag{2.10}$$

$$\boldsymbol{z}(k) = \boldsymbol{C}\boldsymbol{x}(k) + \boldsymbol{w}(k). \tag{2.11}$$

Here, $\boldsymbol{f}(k)$ is the general additive fault vector including component and actuator fault, and $\boldsymbol{w}(k)$ is measurement noise. Assuming $\boldsymbol{x}(k) \in \mathbb{R}^n$ and $\boldsymbol{z}(k) \in \mathbb{R}^m$, a pth order unknown input observer can be obtained using the following transformation:

$$\boldsymbol{x}_o(k) \triangleq \boldsymbol{T}\boldsymbol{x}(k), \tag{2.12}$$

$$\hat{\boldsymbol{x}}_o(k+1) = \boldsymbol{L}_1\hat{\boldsymbol{x}}_o(k) + \boldsymbol{L}_2\boldsymbol{u}(k) + \boldsymbol{L}_3\boldsymbol{z}(k), \tag{2.13}$$

where, $\boldsymbol{x}_o(k) \in \mathbb{R}^p, n-m \leq p \leq n$, and the matrices $\boldsymbol{T}, \boldsymbol{L}_1, \boldsymbol{L}_2$ and $\boldsymbol{L}_3$ are chosen such that the system residual is independent from both system input $\boldsymbol{u}(k)$ and unknown input $\boldsymbol{d}(k)$. Based on this observer, the system error and residual are defined as follows:

$$\boldsymbol{e}_o(k) = \hat{\boldsymbol{x}}_o(k) - \boldsymbol{T}\boldsymbol{x}(k) \tag{2.14}$$

$$\boldsymbol{r}(k) = \boldsymbol{W}_{o_1}\boldsymbol{e}_o(k) + \boldsymbol{W}_{o_2}\boldsymbol{w}(k) \tag{2.15}$$

Here, $\boldsymbol{e}_o(k)$ is the estimation error of the unknown input observer, $\boldsymbol{r}(k)$ is the vector of the residuals, and $\boldsymbol{W}_{o_1}$ and $\boldsymbol{W}_{o_2}$ are the matrix weights of the residuals. In the observer design, some of the degrees of freedom are taken up by the condition $\boldsymbol{TE} = \boldsymbol{0}$ for rejecting modelling uncertainties. The lost degrees of freedom depend on the size and structure of the matrix $\boldsymbol{E}$. The other degrees of freedom can be utilized in decoupling fault effects for isolation and multiple fault identifiability. More detail about diagnostic observer design can be found in [23].

In their work, Chen et al. [45] put forth a structured approach for the selection of matrices $\boldsymbol{T}$, $\boldsymbol{L}_1$, $\boldsymbol{L}_2$, and $\boldsymbol{L}_3$ intended for a full-ordered unknown input observer. The paper also outlines the necessary and sufficient conditions for existence of this observer. The strength of the full-order observer lies in its capacity to grant designers the liberty to craft directed residuals to aid in isolating faults. Moreover, opting for

a full-order observer provides enhanced flexibility in attaining diverse design aims, encompassing aspects such as adjusting the convergence rate and the containment of estimation errors' variance.

As indicated in [45], an unknown input observer's existence relies on specific rank requirements. In instances where these conditions are not met, full decoupling between the residual and the unknown input is not attainable. Amato and Mattei [46] introduced an unknown input observer that decouples faults when it is achievable, while diminishing residual disturbances through H_∞ optimization.

2.2. Parity Relation Approach

At the core of the fault detection method based on parity relations is the generation of residuals through subtracting system outputs from model outputs. These residuals undergo a linear transformation, forming a residual generator for desired fault diagnosis properties. Various strategies exist for designing such residual generation filters (expressed as parity equations) to meet response criteria. These filters are intended to improve fault isolation, demonstrating directional properties for specific faults, while remaining robust to noise, disturbances, and model errors. The parity relations can be designed with transfer function or state-space models [6]. The state-space scheme, also known as Chow-Willsky scheme is introduced in [47]. For a simple example, consider a state-space model as follows:

$$\begin{aligned} \boldsymbol{x}(k+1) &= \boldsymbol{A}\boldsymbol{x}(k) + \boldsymbol{B}\boldsymbol{f}_a(k), \\ \boldsymbol{z}(k) &= \boldsymbol{C}\boldsymbol{x}(k) + \boldsymbol{f}_s(k), \end{aligned} \tag{2.16}$$

where, $\boldsymbol{f}_a$ is the actuator faults vector and $\boldsymbol{f}_s$ is sensor faults vector. Using this equation, the parity vector $\boldsymbol{p}(k)$ is obtained as:

$$\boldsymbol{p}(k) \coloneqq \boldsymbol{T}\boldsymbol{z}(k) = \boldsymbol{T}\boldsymbol{C}\boldsymbol{x}(k) + \boldsymbol{T}\boldsymbol{f}_s(k). \tag{2.17}$$

By selecting the matrix $\boldsymbol{T}$ in a way that $\boldsymbol{T}\boldsymbol{C} = \boldsymbol{0}$, we obtain,

$$\boldsymbol{p}(k) = \boldsymbol{T}\boldsymbol{f}_s(k). \tag{2.18}$$

The direction of the parity vector $\boldsymbol{p}(k)$ caused by the i$^{\text{th}}$ sensor fault corresponds to the i$^{\text{th}}$ column of $\boldsymbol{T}$. This approach is expanded upon by Chow and Willsky when they consider the output equations in the following manner:

$$\begin{aligned}
\boldsymbol{z}(k-n) &= \boldsymbol{C}\boldsymbol{x}(k-l) + \boldsymbol{f}_s(k-l),\\
\boldsymbol{z}(k-n+1) &= \boldsymbol{C}\boldsymbol{A}\boldsymbol{x}(k-l) + \boldsymbol{C}\boldsymbol{B}\boldsymbol{f}_a(k-l) + \boldsymbol{f}_s(k-l+1),\\
&\vdots\\
\boldsymbol{z}(k) &= \boldsymbol{C}\boldsymbol{A}^l\boldsymbol{x}(k-l) + \boldsymbol{C}\boldsymbol{A}^{l-1}\boldsymbol{B}\boldsymbol{f}_a(k-l) + \cdots + \boldsymbol{C}\boldsymbol{B}\boldsymbol{f}_a(k-1) + \boldsymbol{f}_s(k).
\end{aligned} \tag{2.19}$$

Assuming the parity vector to be $\boldsymbol{p}(k) = \boldsymbol{T}[z^{\mathsf{T}}(k-l) \quad \cdots \quad z^{\mathsf{T}}]^{\mathsf{T}}$, the i$^{\text{th}}$ column of the parity vector will become independent from the state vector, if for the i$^{\text{th}}$ row of $\boldsymbol{T}$ ($\boldsymbol{t}_i$) in the following equation is true:

$$\boldsymbol{t}_i[\boldsymbol{C} \quad \cdots \quad \boldsymbol{C}\boldsymbol{A}^l]^{\mathsf{T}} = 0. \tag{2.20}$$

Knowing that the dimension of $\boldsymbol{t}_i$ is $(l+1) \times m$ and the number of equations in (2.20) is equal to dimension of the state vector (n), the remaining degrees of freedom of $\boldsymbol{t}_i$ can be leveraged to separate the response from specific faults or disturbances.

Designing parity relation-based residual generation involves a trade-off: lower-order parity spaces mean simpler online implementation but reduced performance, while higher-order spaces improve performance but increase computation. To address this, Ye et al. [48] introduced stationary wavelet transforms to traditional parity filters. They demonstrated that using the same-order parity vectors, this approach

delivers an optimal performance compared to traditional methods. This enhances fault detection performance without any extra computational cost.

Ding et al. [49] examined fault detection based on parity relations with temporal redundancy. They demonstrated that enhancing the parity relation's order raises the parity space dimension (the parity vector's size), offering greater flexibility for designing residual generation filters and thereby enhancing the performance of the fault detector based on parity relations.

2.3. Optimization-Based Approach

Complete isolation is often impractical due to constraints related to the number of faults that must be separated and the number of available sensor signals. To tackle this issue, an alternative to complete isolation, known as approximate decoupling, has been introduced through optimization-driven residual generation [12]–[14]. The underlying idea is to amplify the influence of faults ($\boldsymbol{f}$) on the residuals ($\boldsymbol{r}$), while minimizing the impact of unknown inputs and uncertainties ($\boldsymbol{d}$) on the residuals. To put it in the form of an optimization problem, the goal is to maximize the cost function ($\boldsymbol{J}$) defined as follows:

$$\boldsymbol{J} = \frac{\|\partial \boldsymbol{r}/\partial \boldsymbol{f}\|}{\|\partial \boldsymbol{r}/\partial \boldsymbol{d}\|}. \tag{2.21}$$

Stoustrup and Niemann's work [50] surveyed this approach from a control-theoretic standpoint, highlighting the trade-off between effective fault detection and optimal closed-loop system performance under uncertainties. Song and Collins [51] tackled fault detection in uncertain linear systems through an estimator based on parameter-dependent bounding and multiplier theory [52]. This method is less

conservative compared to those relying on the small gain theorem and fixed Lyapunov function theory. The robust estimation problem is formulated as a parameter optimization problem, minimizing an upper bound while adhering to a Riccati equation constraint. Furthermore, a Broyden-Fletcher-Goldfarb-Shanno (BFGS) continuation algorithm is developed for problem resolution. This fault diagnosis technique has been deployed in a longitudinal flight control system.

Stoorvogel et al. [53] addressed fault detection and isolation by framing it as an optimal estimation problem. Their aim was to devise an optimal estimator that remains unaffected by disturbances, while ensuring the fault signal estimate is as accurate as possible, assessed through either an H2 or an H1 norm. Wang and Lam [54] tackled a similar problem in a linear time-invariant system with additive output uncertainty and system matrix uncertainty. They transformed the problem into a multi-objective optimization task, minimizing a linear combination of sensitivity to uncertainties and faults, observer gain size, and numerical conditioning. The optimization was facilitated through explicit gradient equations. This fault detection technique was showcased with applications in a robotic manipulator and a vertical takeoff and landing aircraft.

In [55], a fault detection filter was adapted for linear time-varying systems via a least-squares method. This problem was redefined as a min-max strategy, leveraging the Kalman filter's least-square derivation. For linear time-invariant systems, the filter aligns with an unknown input observer, effectively extending it to the time-varying domain. In a similar vein, Chen et al. introduced a detection filter in [56]. This filter maximizes transmission from the target fault to the projected output error,

while minimizing transmission from nuisance faults. Additionally, it minimizes transmission from process and sensor noise to residuals for enhanced robustness.

2.4. Stochastic Filter-Based Methods

Within the existing literature, Kalman filter stands out as a prominent filtering technique employed for fault detection and diagnosis. It can be considered as a particular type of stochastic optimization utilizing linear quadratic methods. In this strategy, faults are detected by subjecting the residuals to statistical evaluations related to their whiteness, mean, and covariance. General Likelihood Ratio (GLR) and Maximum Likelihood (ML) are the common statistical methods used to evaluate the residuals. To circumvent the prerequisites of linearity, Gaussian noise distribution, and a mostly familiar model, alternative versions of the Kalman filter such as Extended Kalman Filter (EKF) and the Unscented Kalman Filter (UKF) have been introduced [57]. For general nonlinear systems characterized by non-Gaussian Probability Density Functions (PDFs), a recursive Bayesian filter was proposed, known as the Particle Filter (PF) [17] or the sequential Monte Carlo method [18]. However, the effectiveness of this approach is tied to the quantity of particles used, reflecting computational requirements.

When the model does not match the real system, i.e., when a fault occurs in the system [58], the KF loses its effectiveness and can become unstable. Similar concerns apply to other Bayesian filters such as UKF and PF, which require solid knowledge of the system model [59]. Remedies include Cholesky and UD factorizations [60], [61], and introducing higher process noise [62]. An alternative is the Variable Structure Filter (VSF), a sliding mode-based predictor-corrector method, offering robust

estimation [63]. Extending VSF, the Smooth Variable Structure Filter (SVSF) combats sliding mode chattering with a smoothing boundary layer, while ensuring convergence of the estimated state trajectory to a neighborhood around the true state trajectory [64]. Figure 2-2 illustrates the convergence and chattering dynamics associated with VSF and SVSF filters schematically.

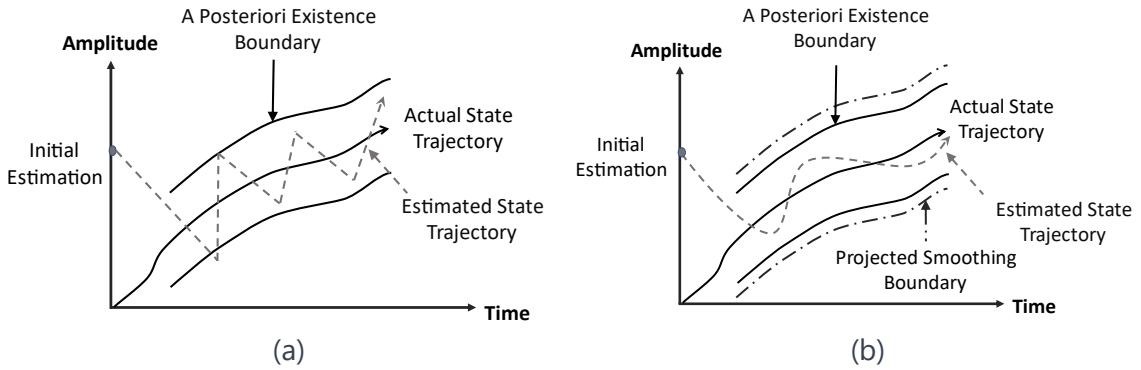

Figure 2-2. Variable structure filter estimation concept: (a) VSF; (b) SVSF.

A stochastic version of SVSF, optimized for linear systems to obtain a Variable Boundary Layer (VBL), reduces estimation error for systems with Gaussian noise using the newly formulated error covariance [16]. This approach is reported to outperform SVSF with a fixed boundary layer. Furthermore, due to its robustness, this method exhibits better performance compared to the Kalman filter. Further details on the method's development and its superiority over the Kalman filter are discussed in Chapter 4. There, the application of the SVSF-VBL filter and KF within an adaptive Multiple Model Adaptive Estimation (MMAE) framework is studied for real-time fault detection in an Electro-Hydraulic Actuator (EHA).

In the context of fault detection and diagnosis problems, the selection of the smoothing boundary layer has a significant impact. For a small boundary layer, faults will cause chattering, which can be used for detection purposes. Conversely, a large

boundary layer smoothens the estimation, but increases the risk of missing the faults in FDD algorithms. This implies that chattering carries footprints of mismatches that can be exploited to detect system faults and assess their magnitude. In Chapter 3, the exploration of extracting information from chattering is undertaken to identify the model mismatch through analysis of the chattering signal's spectral characteristics. This proposed approach is applied to detect and measure the severity of faults like leakage, friction faults, and bulk modulus mismatch within an electro-hydraulic actuator.

2.4.1. Adaptive Filter

Adaptive filtering approaches provide an alternative perspective that addresses large uncertainties and facilitates the estimation of abrupt changes in a system. This is particularly relevant in cases involving hybrid systems and fault detection scenarios. These approaches involve utilizing multiple models for hypothesis testing, referred to as Multiple Model Adaptive Estimation (MMAE), which is well-suited for managing large parameter uncertainties and hybrid systems characterized by different system models with distinct parameter configurations [15]. In fault diagnosis scenarios, each model corresponds to a specific fault condition, and the algorithm assigns mode probabilities to these models, which can serve as fault indicators [65]–[68].

Two distinct MMAE approaches are: static and dynamic methods. Static MMAE adheres to one model throughout the entire process, lacking transitions or jumps between the models. Therefore, it is not suitable for time-varying systems marked by parameter changes or model switches. Conversely, dynamic MMAE is designed for time-varying systems and finds application in online fault diagnosis scenarios [19],

[66]. Three prominent dynamic MMAE strategies are: General Pseudo-Bayesian estimator of first order (GPB1), General Pseudo-Bayesian estimator of second order (GPB2) and Interacting Multiple Model (IMM). While theoretically opting for higher orders should enhance estimation performance, it leads to an exponential increase in the number of filters that must be run in parallel. This becomes computationally impractical [66]. Of these, IMM has garnered attention due to its computational efficiency, while maintaining performance comparable to GPB2 [66]. Consequently, IMM presents a promising option for dynamic MMAE applications and serves as the basis for the proposed method in this thesis.

In the IMM approach, the occurrence or resolution of a failure within a dynamic system has been explicitly represented as a finite-state Markov chain with known transition probabilities. The IMM algorithm handles system structural changes using Gaussian approximations and a hypothesis merging technique known as "mixing." Integrating Kalman filters in an IMM structure, referred to as IMM-KF, is a widely recognized adaptive filter technique for fault detection and diagnosis, extensively explored in the literature [69]–[71]. To enhance robustness, IMM-SVSF has been recently introduced and demonstrated superior effectiveness compared to IMM-KF in the presence of system uncertainties [16], [67]. The growing computational power facilitates the practicality of these adaptive strategies for real-time fault diagnosis and supervision, leading to increased research in recent years. Chapters 4 and 5 of this thesis delve into adaptive filtering methods for fault diagnosis in greater detail and present novel contributions to enhance the performance of this approach.

2.5. Discrete Event and Hybrid Systems

Some researchers have explored fault detection and diagnosis problem for discrete-event or hybrid systems. One approach considers it as a hybrid state estimation problem, similar to the multiple model technique described for adaptive filtering. Here, the faulty modes of a plant or process are represented as the discrete states within a hybrid system framework. Solving the Fault Detection and Diagnosis (FDD) problem then involves estimating the hybrid state, which includes both continuous and discrete components. If the continuous state dynamics in each discrete state (or mode) are linear, the solution can be approached using MMAE or IMM algorithms. For situations where the continuous state dynamics in each mode are nonlinear, particle filters become a viable option [72], [73].

A technique for tracking and diagnosis of hybrid systems in real-time was introduced by Narasimhan and Biswas in [74]. Their approach involved creating parameterized plant models, where faults manifest as sudden changes in system parameters. They applied model-based diagnosis techniques, leveraging the analytical redundancy between the model and system measurements to address hybrid systems. In [75], Wang and Gao tackled FDD problem for uncertain continuous-time state delayed systems with Markovian jump parameters. They designed a fault detection filter as a Markovian jump system, which exhibited robustness to modeling inaccuracies, unknown inputs, and control inputs. The existence of these filters was established using linear matrix inequalities. Additionally, in another study [76], researchers addressed critical modeling and computational challenges that combine

model-based diagnosis methods with signature analysis, facilitating the effective detection and isolation of emerging and abrupt faults in hybrid systems.

In their work [77], Zhong and colleagues addressed the challenge of robust fault detection in a class of discrete-time linear Markovian jump systems with an unknown input. They developed an observer-based residual generation filter for fault detection, with matrices tailored to the specific system mode. In [78], Zhang and team delved into fault detection in periodic systems, resolving it through the solution of a difference periodic Riccati system. This approach strikes a balance between resilience against unknown disturbances and sensitivity to faults, ultimately leading to the design of an optimal fault detection system for linear discrete-time periodic systems.

Baroni et al. [79], explored model-based diagnosis within the realm of distributed discrete-event systems, specifically focusing on a category referred to as 'active systems.' These active systems are conceptualized as networks comprising communicating automata, where each automaton characterizes the behavior of an individual system component by responding to potential external threats. This diagnostic approach pertains to asynchronous events that do not necessitate the incorporation of a global diagnosis. Instead, it employs a method of online, step-by-step reconstruction of the active system's behavior guided by available observations. This technique demonstrates its efficacy when applied to large-scale active systems. It encompasses various phases, including planning for reconstruction, the actual reconstruction of behavior, and the generation of diagnostics.

2.6. System Identification Methods

Faults cause a change in the physical parameters of a system. Consequently, employing parameter estimation is an effective approach for identifying, isolating, and even measuring the magnitude of faults within a system. In this methodology, one seeks to construct a model of the normal operational state of the physical system, either offline or online. The underlying assumption is that any fault within the system would manifest itself as a change in the parameters within this model. Therefore, the task of identifying such changes in the system's parameters falls under the scope of the problem of fault detection and diagnosis. Isermann established that diagnosing process problems could potentially be performed by estimating unobservable process parameters and/or state variables in a review paper [80]. Comprehensive insights into fault diagnosis utilizing system identification are provided in a book authored by Simani et al. [81] and Isermann's survey paper [82].

Joint state and parameter estimation, which views the changing parameters as an augmented state and estimates that using state estimation techniques such as EKF, is a well-known method to estimate the faulty parameter [68], [83]–[88]. However, this method has certain drawbacks because it relies on nonlinear filtering, which calls for solving challenging nonlinear Partial Differential Equations (PDEs) in order to obtain the best answer. The use of the augmented state EKF offers a suboptimal solution, which is vulnerable to bias estimation and divergence for the following reasons [89]:

- Augmented states lack meaningful dynamics, hence, determining the artificially introduced noise through engineering judgment is challenging [15].

- Reliability of the covariance linearization employed in the EKF would be compromised when significant parameter uncertainty is present.
- Inclusion of augmented states has the potential to make the system unobservable [89].
- Discriminative training methods used to obtain the process noise covariance matrix rely on measured states, and the incorporation of augmented states will have a negative impact on the training process [90], [91].

Another approach involves utilization of subspace-based techniques for both system identification and detection of faults [92], [93]. These subspace-based methods [94] are linear algorithms for identifying systems, relying on measurements in the time domain or covariance matrices of system outputs, where different subspaces of Gaussian random vectors play a pivotal role. A system identification-driven FDD method is introduced, tailored for monitoring structures that experience rapid unmeasured environmental fluctuations alongside gradual changes in their modal (vibrational) characteristics. The paper explores various applications, including development of an online monitoring system for aeroelastic flutter in aircraft.

2.7. Comparative Analysis: Identifying Research Opportunities

In this section, a comparison is made between various model-based FDD methods discussed in this chapter, with a focus on their performance, residual characteristics, complexity, and robustness. The identification of research gaps addressed in this thesis relies on the foundation provided by this comparative analysis. Performance of a fault detection algorithm is typically assessed in terms of the trade-offs between the false alarm rate and the mean detection delay [6].

Observer-based techniques, such as eigen-structure assignments and unknown input observers, yield the same residuals as an equivalent parity relation method, as outlined in [6]. However, the key distinction lies in how these methods generate residuals for direct use in the fault detection and diagnosis process. Observer-based methods create residuals using observers, while the parity relation method transforms the input-output transfer function or state-space models of the system to derive the directional or structural residual vector directly, allowing for fault isolation capability before the design phase. Despite their ease of implementation and computational efficiency, both observer-based and parity relation approaches have well-documented limitations:

- They operate deterministically without considering noise distributions and their impact on the system.
- They are designed primarily for additive faults and do not account for multiplicative faults or model uncertainties [6].
- They are typically suitable for linear time-invariant systems.
- In scenarios involving unmodeled disturbances or model uncertainties, the fault detection algorithm may fail to produce zero-mean residuals in the absence of faults. This discrepancy can be addressed by raising the detection threshold in the statistical decision test for the residual, albeit at the cost of longer detection delays.
- Due to limited measurement availability, achieving complete fault isolation is often impossible.

Optimization-based approaches tackle the challenge of fault isolability by utilizing a cost function that accentuates the influence of faults, while minimizing the impact of noise, disturbances, and model uncertainties on the residuals. The optimization-based technique has been applied to extend the fault detection filter or unknown input observer to nonlinear or time-varying systems. However, the effectiveness of these methods can vary significantly depending on the specific case, when implementing them in practical applications. Generally, they offer solutions to FDD issues by optimizing specific mathematical objective functions, but there is no assurance of the effectiveness and performance of these solutions in practical applications. In certain cases, formulating the optimization approach, including the choice of design parameters within the objective functions, can become challenging.

System identification techniques can be applied to both linear and nonlinear systems. They are capable of detecting minor or incipient faults using joint state and parameter estimation. However, solving the partial differential equations required for parameter estimation can be exceedingly difficult. Additionally, introduction of augmented states has the potential to make the system unobservable [89]. To address the observability challenge, one approach is to employ Multiple Model Adaptive Estimation (MMAE) methods, which are discussed in Chapter 4 and Chapter 5.

2.8. Research Contributions

The rise in computational power has opened up new possibilities for devising advanced algorithms in fault detection. Consequently, there is increased interest in recent years in use of stochastic filters. This thesis focuses on these techniques for fault detection and diagnosis. An advantage of stochastic filters is their consideration

of the system noise distribution. However, these filters rely on the availability of a system model that is largely known. When the system dynamics deviates from this model, due to a fault, modeling uncertainties can cause instability.

When the behaviour of a system is subject to change over time, particularly in contexts like fault detection, it is important to either have a robust estimation strategy or present various scenarios to adaptively characterize the system. The first contribution of this thesis, discussed in Chapter 3, is grounded in the former approach, using the smooth variable structure filter as a robust estimation strategy for addressing fault diagnosis problems. The latter approach forms the underlying concept of Multiple Model Adaptive Estimation (MMAE) which is a widely recognized framework for fault detection and diagnosis problems. This serves as the basis for the second and third contributions of this research that have been presented in chapters 4 and 5. In the following subsections, a brief overview of each of these contributions is provided before delving into more detailed explanations in the subsequent chapters.

2.8.1. Chapter 3: Information Extraction Using Spectral Analysis of the Chattering Signal of the Smooth Variable Structure Filter

The smooth variable structure filter enhances robustness and ensures stability, particularly in cases of bounded system uncertainties, making it an ideal choice for fault detection problems. Additionally, beyond the innovation vector used in filtering algorithms to adjust the predicted state vector, SVSF provides an additional set of indicators that can be used for information extraction, namely the chattering signals associated with various state variables. In the event of model mismatch due to factors

such as a fault condition, SVSF ensures stability through corrective actions, albeit leading to chattering as shown in Figure 2-3 [95]. This unique characteristic makes SVSF a suitable option for FDD problems.

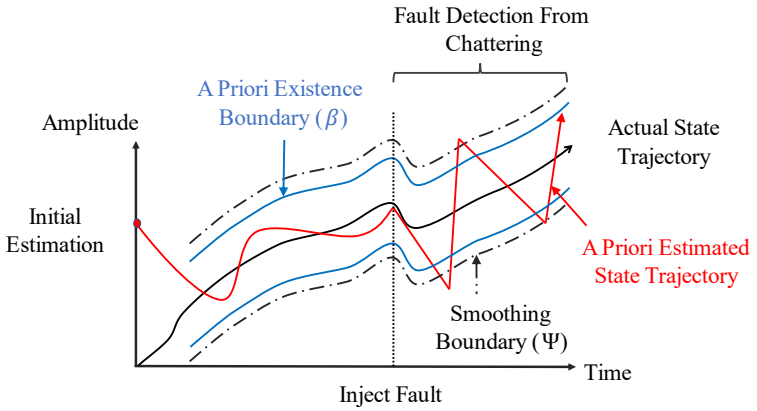

Figure 2-3. Fault detection from chattering signal of smooth variable structure filter[95].

As outlined in section 2.4, the SVSF employs a robust estimation technique through the utilization of a sliding mode-based predictor-corrector method. However, this robustness comes with the expense of chattering. The chattering occurs when a priori estimation error is larger than the boundary layer [95].

$$Chattering_i(k) = \begin{cases} 0 & |e_i(k|k-1)| < \psi_i \\ (|e_i(k|k-1)| - \psi_i)\, sgn\big(e_i(k|k-1)\big) & |e_i(k|k-1)| \geq \psi_i \end{cases} \quad (2.22)$$

where $Chattering_i(k)$ denotes the chattering, $e_i(k|k-1)$ is the a priori estimation error, and ψ_i is the smoothing boundary layer for state i.

The chattering phenomenon within SVSF contains distinctive change footprints that can be effectively utilized for identifying system faults and assessing their severity through spectral analysis. This forms the foundation for the first contribution of the thesis, built upon the following hypothesis:

- **Hypothesis 1:** information contained within the chattering of the robust Smooth Variable Structure Filter can be utilized to identify changes in system behavior, applicable in FDD problems.

Spectral analysis provides a powerful tool for extracting information from the noisy chattering signal through techniques like Fast Fourier Transform (FFT), Short-Time Fourier Transform (STFT) and wavelet transforms. Examining the spectrogram of the chattering signal proves to be highly insightful in this context. The spectrogram illustrates the frequency distribution of the chattering signal as it changes over time, offering insights into events like faults that impact the system and result in model mismatch. Three distinct approaches can be employed for fault diagnosis through spectral analysis.

1. **Expected value of spectral density of the chattering signal.**

The spectral density of the chattering signal reveals information about the frequency content of the system fault. In a healthy system, the power spectral density contains no information and should align with the expected value, as indicated by the dashed red line in Figure 2-4. Nevertheless, there will be some inherent random fluctuations attributed to system noise. When a fault occurs in the system, the distinctive signature of that fault manifests as alterations in the frequency content of the power spectral density of the chattering signal. However, in many cases this information is buried under the system noise and cannot be achieved from a single realization, specially when the system noise is large compared to the effect of the fault. For example, Figure 2-4 shows the power spectrum of the chattering signal for

a faulty system, featuring a spike at a specific low frequency. Yet, this characteristic is not easily discernible from a single realization due to the presence of noise.

Considering the characteristics of process and measurement noise, the expected power spectrum of the chattering signal can be calculated under normal conditions. Building on the concept of Monte Carlo simulation, one can compare the average of power spectrum of chattering signal for fault diagnosis, using the law of large numbers. This method requires multiple realizations to derive the expected value, as depicted in Figure 2-4. Consequently, it is not suitable for real-time applications. Also, temporal information cannot be extracted using this approach.

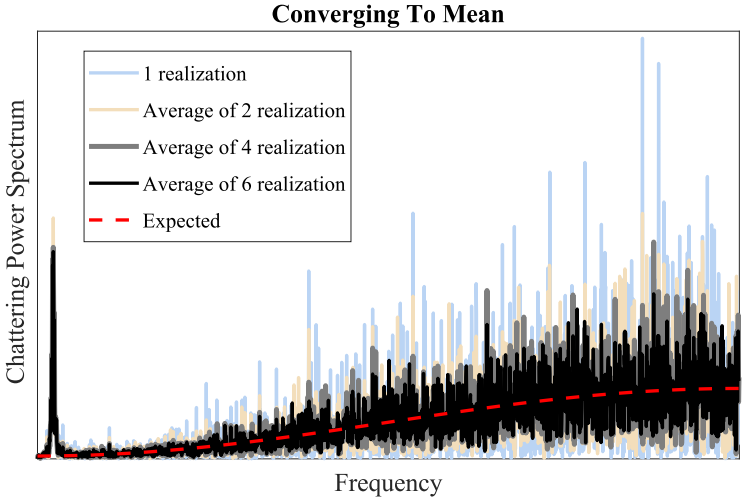

Figure 2-4. Fault detection based on expected chattering power spectrum.

2. **Find a threshold for spectral density of the chattering signal.**

In this approach, it is necessary to derive the Probability Distribution Function (PDF) of the power spectrum of the chattering signal for normal condition, considering both measurement and process noise. Under the faulty condition the PDF

of the chattering power spectral density will change accordingly. Following that, a threshold can be determined within a specific confidence interval.

Figure 2-5 provides a conceptual representation of the threshold selection process, depicting a balance aimed at minimizing the risk of missed detection while avoiding false alarms. Under normal conditions, a higher noise levels contributes to a heavier tail in the PDF, thereby increases the probability of missed detection or false alarm. On the other hand, a higher level of fault result in a more substantial shift in the PDF, which makes detection easier. The benefit of this method lies in its reliance on a single realization, making it well-suited for near real-time applications. However, it is more susceptible to false alarms or missed detections, especially when the impact of the fault is small compared to noise.

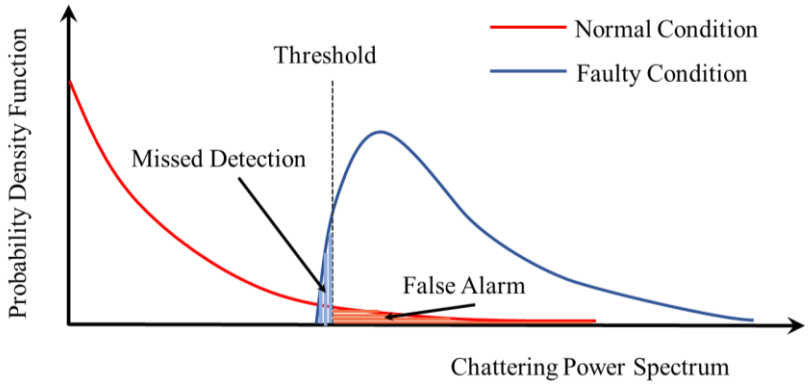

Figure 2-5. Fault detection using a threshold based on the confidence interval obtained from PDF of the chattering's power spectrum.

3. Spectrogram Analysis

Changes in the frequency content of the chattering signal indicate the occurrence of a system mismatch or fault. Consequently, it is advantageous for fault detection to capture temporal information regarding the frequency content of nonstationary

signals. The time-varying spectrum, commonly known as the spectrogram, is a tool for extracting both temporal and spectral information from the signal. Two established techniques, namely the Short-Time Fourier Transform (STFT) and the wavelet transform, can be employed to generate the spectrogram. This approach offers the benefit of not only recovering temporal details related to the fault but also reducing the likelihood of false alarms and missed detections due to the inherent averaging process in spectrogram calculation. However, there exists a trade-off between the periodic and temporal information attainable from the spectrogram, governed by the Heisenberg-Gabor limit.

In chapter 3, mathematical expressions are formulated to describe the chattering signal of the SVSF in scenarios involving both full-state and partial-state measurements. An investigation is conducted into the spectrogram of the chattering signal to extract both temporal and spectral information. Leveraging the concept of Monte Carlo simulation and considering the characteristics of process and measurement noise, the expected power spectrum of the chattering signal is derived under normal conditions. A proposal is made to select a threshold for Fault identification, balancing the avoidance of false alarms with the minimization of the risk of overlooking the faults. This threshold selection strategy takes into account the probability distribution of the chattering signal's power spectrum, establishing a confidence interval that facilitates real-time fault detection using a single realization of the event sequence. Additionally, for retrieval of temporal information related to a mismatch, the short-time Fourier transform of the chattering signal is studied. The efficacy of the proposed method for fault detection and mismatch identification is

demonstrated across various scenarios involving a typical second-order system and an electro-hydraulic actuator.

2.8.2. Chapter 4: A Robust Model-based Strategy for Real-time Fault Detection and Diagnosis in an EHA Using Updated Interacting Multiple Model Smooth Variable Structure Filter.

As mentioned at section 2.4.1 the dynamic MMAE approaches are for time-varying systems such as online fault diagnosis scenarios. The parallel structure inherent in MMAE algorithm enables rapid adaptation of the system, ensuring precise state estimation following a fault occurrence. Additionally, it tackles the observability challenge encountered in alternative strategies like observer-based, parity relation-based, and joint state and parameter estimation (i.e., system identification) approaches. Consider a general multiple model process governed by a hybrid system as below:

$$\begin{aligned} \boldsymbol{x}(k) &= \boldsymbol{f}_{M(k)}\big(\boldsymbol{x}(k-1), \boldsymbol{u}(k-1), \boldsymbol{v}(k-1)\big), \\ \boldsymbol{z}(k) &= \boldsymbol{h}_{M(k)}\big(\boldsymbol{x}(k), \boldsymbol{u}(k), \boldsymbol{w}(k)\big). \end{aligned} \tag{2.23}$$

Where the subscript $M(k)$ describes which system model and which measurement model is active in the time interval $(k-1, k]$. The active model in this interval is assumed to be among the r total possible model.

$$M(k) \in \{M_i\}_{i=1}^{r}, \tag{2.24}$$

Where $\boldsymbol{M_i}$ stands for i$^{\text{th}}$ model which corresponds to a pair of specific models, namely the system model $\boldsymbol{f}_{M_i}$ and the measurement model $\boldsymbol{h}_{M_i}$. Assuming the possibility of a Markov jump between different models at any time step, number of regime histories grows exponentially over time, as shown in Figure 2-6. Therefore, the conceptual solution to the MMAE algorithm becomes infeasible in practice.

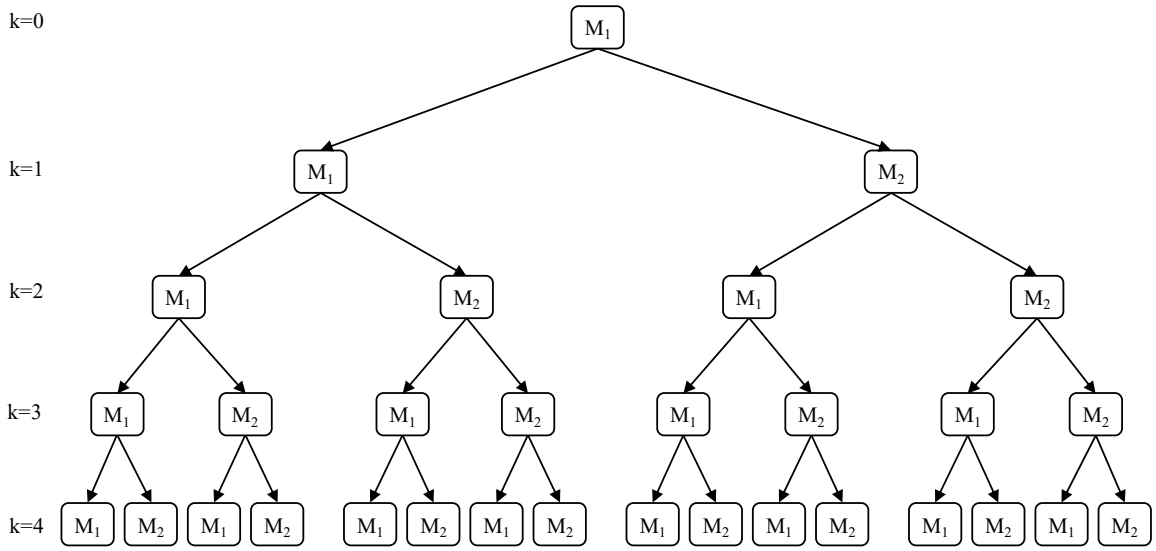

Figure 2-6. Model hypothesis tree for two-model jump-Markov MMAE algorithm. In the figure, it is assumed that M_1 is valid at time k=0. For a general system with r model the number of regime histories (number of tree branches), is r^k which grows exponentially with time.

One strategy to reduce the number of regime sequences is hypothesis merging. The Interacting Multiple Model (IMM) serves as a popular sub-optimal solution for MMAE, utilizing merging to reduce the branches in the model hypothesis tree. It utilizes and merges the regime histories from only the two preceding time steps. Therefore, when the total number of the possible models is r, the number of regime histories remains proportional to r^2, preventing exponential growth over time [66]. However, it's crucial to note that even IMM filter-based methods can be notably complex to implement, particularly when dealing with a high number of fault modes (e.g. large r).

The second contribution of this thesis aims to address this complexity within the context of the fault detection and diagnosis problem, guided by the following hypothesis:

- **Hypothesis 2:** Assuming that faults are irreversible in an FDD problem and modifying the IMM algorithm to account for this information can improve the computational efficiency and reduce the rate of false alarm.

Filter-based IMM is a well-known adaptive estimation method widely utilized in model-based FDD problems. Specifically, in IMM-SVSF approach, employing a robust bank of SVSF filters has proven to be efficient in detecting faults even in the presence of modeling uncertainties and has been used to detect leakage and friction faults in an EHA system [16]. However, as the number of models running in parallel (representing the number of faults studied) increases, the IMM method faces two main challenges: computational intensity and combinatorial explosion.

Chapter 4 introduces an efficient variant of IMM called Updated IMM (UIMM), which is integrated with the SVSF filter to establish a robust model-based approach for real-time fault detection and diagnosis. The UIMM method progresses through a subset of the fault condition-related models, rather than considering all models concurrently as in IMM. This is achieved by updating the filter bank when a fault is detected in the system, assuming the faults are irreversible. This update accommodates the alterations in the bank of potential model scenarios, describing the system's behavior specifically influenced by the detected fault, as illustrated in Figure 2-7. Consequently, the UIMM algorithm operates with significantly fewer models running in parallel compared to the IMM algorithm, as indicated in Table

2-1. This approach offers two key advantages: improved computational efficiency and avoidance of combinatorial complexity [67].

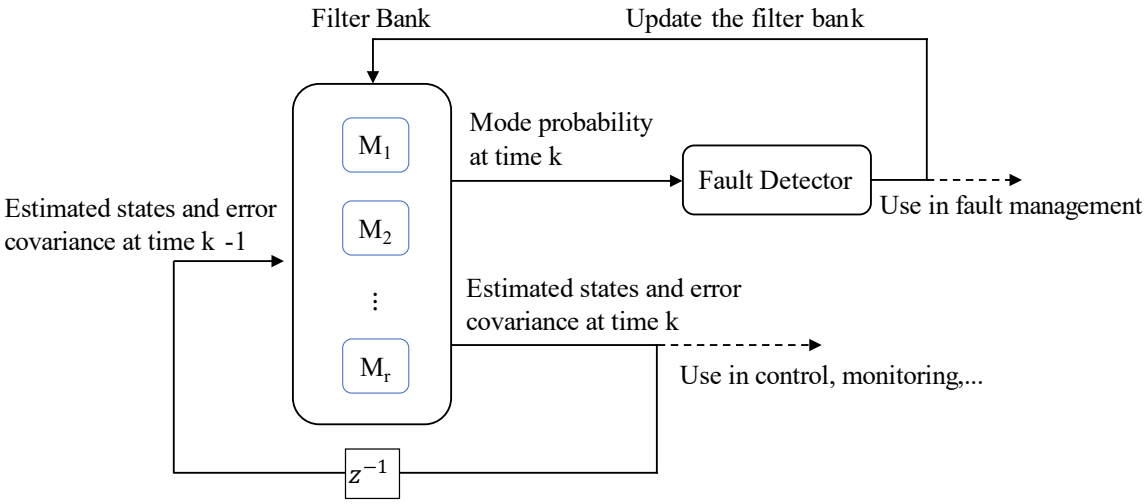

Figure 2-7. UIMM algorithm flow diagram.

Table 2-1: Comparing the number of filters in IMM and UIMM algorithms [67].

Number of Faults	**1**	**2**	**3**	**4**	**r**
Number of Filters in IMM	2	4	8	16	2^r
Number of Filters in UIMM	2	3	4	5	r+1

In chapter 4, the performance of the UIMM-SVSF method is validated through fault condition simulations for a typical Electro-Hydraulic Actuator (EHA). Leveraging the computational efficiency of the proposed algorithm for fault diagnosis, a Fault Tolerable Control System (FTCS) is developed in chapter 4, according to the flow diagram shown in Figure 2-8, to illustrate the application of this strategy in managing faults within a closed-loop system.

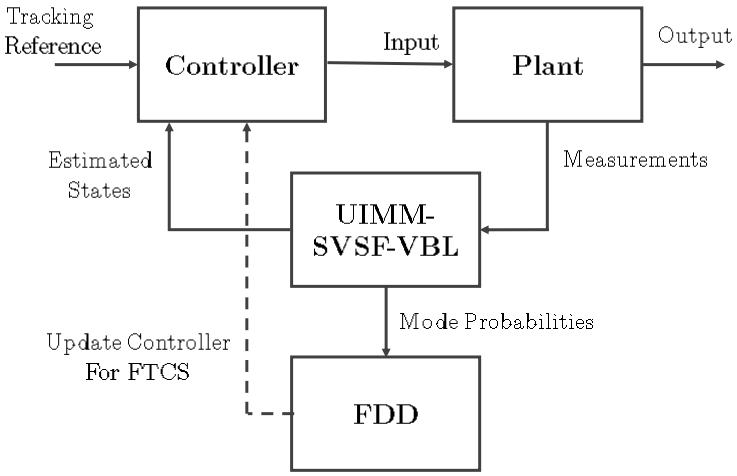

Figure 2-8. Block diagram of the UIMM-SVSF-VBL in a closed-loop application for fault-tolerant control system [67].

2.8.3. Chapter 5: Adaptive Estimation Using Interacting Multiple Model with Moving Window

Apart from its inherent complexity, another constraint of the IMM-based approach is its dependence on the assumption that fault parameters adhere to discrete values from a finite set. In cases where certain faults involve fault parameters with continuously drifting values, it may be necessary to employ multiple fault models to describe a single fault. Accounting for all the possible fault levels for a single fault simultaneously, introduces greater complexity and the potential for higher false alarm rates. A similar approach is needed for addressing problems characterized by a gradual progression of faults, where the set of models used in the multiple model approach have an inherent chronological order. In these circumstances, equation (2.24) can be regarded as having leveled member [95]:

$$M(k) \in \{M_{L[i]}\}_{i=0}^{N-1}. \tag{2.25}$$

In this context, $\boldsymbol{M(k)}$ shows the active model in the time interval $(k-1, k]$ and $\boldsymbol{M_{L[i]}}$ represents the model corresponding to progression level "i".

The third contribution of this thesis is an effort to resolve this problem which forms the basis of the following hypothesis:

- **Hypothesis 3:** Directing attention to a neighboring subset of the IMM in each cycle will enhance the algorithm's performance and computational efficiency.

In Chapter 5, a novel adaptive estimation strategy called the Moving Window Interacting Multiple Model (MWIMM) is introduced based on this hypothesis. Unlike the IMM strategy, the MWIMM approach employs a filter bank containing only the adjacent models to the active model, integrating information in chronological order. Therefore, the number of filters running concurrently is determined by the selected size of the moving window that defines the neighborhood. As depicted in Figure 2-9, when there is a model transition indicating a change in the active model, the moving window adjusts accordingly.

MWIMM can be considered as an extension of UIMM algorithm which relaxes the irreversibility assumption and allows for the estimation of gradual or continuous changes within the system. This extends the application domain of the multiple model strategies for systems that are experiencing gradual changes, which is more common in physical systems, including fault intensity assessment and Remaining Useful Life (RUL) estimation. By utilizing a moving window, MWIMM enhances the identifiability and computational efficiency of multiple model algorithms by

concentrating on a subset of potential models at each stage, rather than considering all models simultaneously.

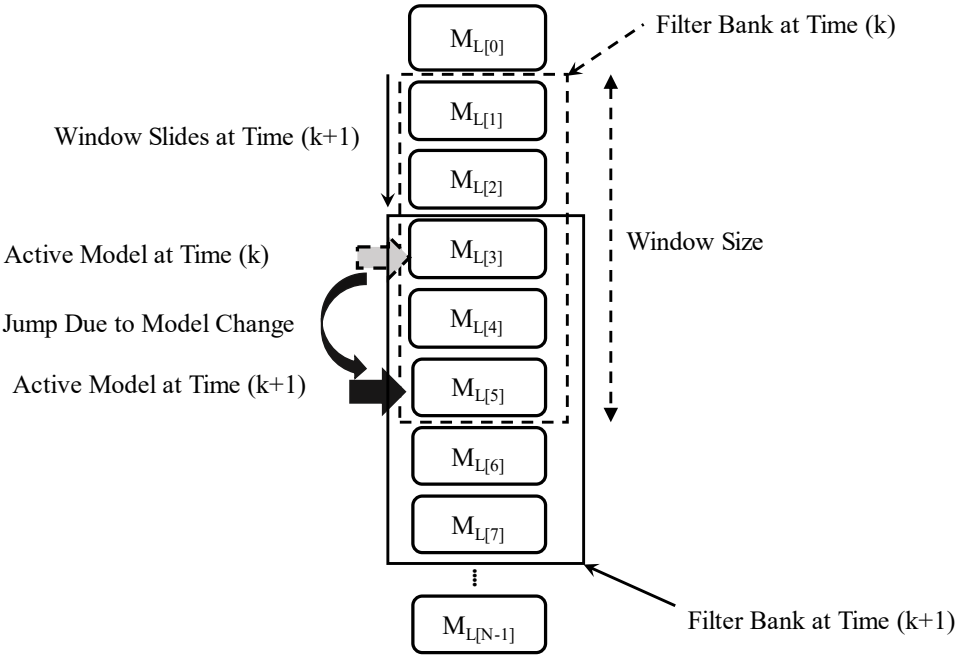

Figure 2-9. Flow diagram illustrating the MWIMM algorithm.

2.8.4. List of Primary and Secondary Contributions

The primary contributions of this thesis are outlined as follows:

1. Enhancing the computational efficiency and decreasing the false alarm rate through the modification of the IMM algorithm using UIMM-SVSF.
2. Information extraction from the chattering signal of the SVSF using spectral analysis.
3. Introduction of the Moving Window IMM (MWIMM) to improve identifiability and computational efficiency of IMM algorithm by narrowing down the search space for the true model.

The subsequent secondary contributions become possible due to the primary contributions:

1. Developing a fault-tolerant control system for an electro-hydraulic actuator utilizing the UIMM-SVSF-VBL diagnosis approach.
2. Employing spectral analysis of the chattering signal from the SVSF to diagnose leakage, friction fault, and bulk modulus changes in an electro-hydraulic actuator.
3. Quantifying fault intensity and predicting the remaining useful life (RUL) using the MWIMM algorithm.

These contributions have been presented in three papers as contained in Chapters three to five.

3. Information Extraction Using Spectral Analysis of the Chattering of the Variable Structure Filter

Ahsan Saeedzadeh*[1], Peyman Setoodeh[1], Saeid Habibi[1], Marjan Alavi[2]

[1] Department of Mechanical Engineering, McMaster University, Hamilton, ON, Canada

[2] W Booth School of Engineering Practice and Technology, McMaster University, Hamilton, ON, Canada

This paper is published in IEEE Access, vol. 11, pp. 104992-105008, 2023, DOI: 10.1109/ACCESS.2023.3318476. This paper is republished here with permission[1].

Abstract

SVSF is a model-based robust nonlinear filtering technique, based on the variable structure concept formulated in a predictor-corrector form. It is used for estimating the states of a system and is robust against noise and modeling uncertainties. It ensures stability in the face of model mismatch resulting from a poor model or fault, at the expense of corrective actions, which cause chattering. The chattering contains mismatch footprints that can be exploited to identify system faults and determine their severity. In this paper, information extraction from chattering is investigated to identify model mismatch based on the spectral contents of the chattering signal. To verify the effectiveness of the developed framework for chattering analysis, two case

[1] In reference to IEEE copyrighted material, which is used with permission in this thesis, the IEEE does not endorse any of McMaster's products or services. Internal or personal use of this material is permitted. If interested in reprinting/republishing IEEE copyrighted material for advertising or promotional purposes or for creating new collective works for resale or redistribution, please go to http://www.ieee.org/publications_standards/publications/rights/rights_link.html to learn how to obtain a License from RightsLink.

studies are considered. First, the power spectrum of the chattering signal has been employed to identify mismatch and the potential of recovering the temporal information of the model mismatch from the spectrogram is studied, using Short Time Fourier Transform (STFT) for an underdamped second-order system. Then, the proposed strategy is applied to detect and measure the severity of leakage and friction faults as well as the bulk modulus mismatch in an electro-hydraulic actuator.

Keywords: Fault Detection, Information Extraction, Smooth Variable Structure Filter, Spectral Analysis, STFT.

3.1. Introduction

Estimation is a process to obtain the states or parameters of interest using partial, noisy, and inaccurate measurements. It can be applied in areas such as tracking, control, system identification, statistical inference, signal processing, system monitoring, and fault management [1]. Kalman Filter (KF) is the best-known optimal state estimation strategy that minimizes the mean square error of the estimation for a stochastic linear system with zero-mean Gaussian noise. To overcome the requirement of linearity, gaussian noise distribution, and a fairly known model, different versions of KF such as the Extended Kalman Filter (EKF) and the Unscented Kalman Filter (UKF) have been proposed [2]. Later, a more computationally demanding recursive Bayesian estimator was proposed referred to as Particle Filter (PF) [3], also known as the sequential Monte Carlo method [liu1998sequential]. Particle Filters are applicable to general nonlinear systems with non-Gaussian Probability Density Functions (PDFs), but their performance is determined by the number of particles, which reflects the computational demand.

Conceptually, when the number of particles approaches infinity, the estimation error for a particle filter will converge to zero [4].

State estimation is the cornerstone of model-based Fault Detection and Diagnosis (FDD) strategies, be it online or offline. Model-based FDD methods involve the development of a system model through either a fundamental comprehension of the system's underlying physics or system identification. This model serves as a benchmark to create mathematical links between inputs and measurements and generate residuals that contain fault signatures using the concept of analytical redundancy. These residuals are then processed through a decision-making tool for diagnostic purposes. The benefit of this approach compared to data-driven methods lies in the meaningful interpretation of each physical state and parameter of the model, which significantly enhances the diagnostic process. The major model-based FDD approaches proposed in literature [5] can be classified into observer-based methods like full-state observers [6], [7] and unknown input observers [8], [9], parity relation [6], [10]–[12], optimization-based [13]–[15], stochastic filter-based methods like Kalman filters [16]–[18] and SVSF [19], [20], adaptive multiple model estimation [21]–[25], and parameter estimation [26]–[29]. Isolability and robustness (especially for online FDD) play an important role in the FDD process. Adaptive multiple model estimation can resolve the isolability problem, where perfect decoupling of estimation error residual is not possible, or the parameter estimation problem is not observable [30]. Fault or any other source of uncertainty will cause a model mismatch. Therefore, the robustness of the estimation is an important property of FDD problems.

The KF becomes sub-optimal and potentially unstable when the model used is not matching the real system [31]. The same problem exists in other Bayesian filters

such as UKF and PF, designed under the assumption that the system model is largely known [32]. The numerical instability of the KF, due to round-off error, can be resolved with square root forms such as the Cholesky and UD factorizations [33], [34], or using a larger process noise [4]. Variable Structure Filter (VSF) is a robust estimation method based on the sliding mode concept, in a predictor-corrector form [35]. The Smooth Variable Structure Filter (SVSF) is an extension of VSF, applicable to non-linear systems. Using SVSF, it is desired that the estimated state trajectory converges to an existence subspace around the ground truth and remains within this subspace. A large a priori error due to model mismatch or fault condition leads to chattering. SVSF uses a smoothing boundary layer to eliminate the chattering typical to sliding mode concept. If the smoothing boundary is larger than the width of the existence subspace, the estimated state trajectory will be smoothened, and chattering will not occur [35]. An optimal version of the SVSF has been proposed for linear systems and uses a Variable Boundary Layer (VBL) to minimize the estimation error for zero-mean Gaussian additive noise [36]. However, when it comes to FDD, choosing the smoothing boundary layer is a delicate matter. On one hand, model mismatch or fault condition may lead to chattering by reducing the effectiveness of the smoothing boundary layer [37]. Therefore, the chattering signal can be used as an indication of model mismatch or fault. On the other hand, increasing the width of the smoothing boundary layer smoothens the estimated state trajectory, which in turn, increases the chance of missing a fault by the deployed FDD algorithm.

This paper proposes a framework for model mismatch identification and fault detection based on the information content of the chattering signal obtained from the SVSF algorithm. The proposed framework relies on spectral analysis of the

chattering in the estimated state trajectory. To verify the effectiveness of the proposed strategy, it is applied to a linear stochastic dynamic system as well as an Electro-Hydraulic Actuator (EHA). It is shown that typical fault conditions seen in hydraulic systems involving bulk modulus mismatch, leakage, and friction faults can be identified using the chattering signal of the SVSF. Contributions of the paper can be summarized as follows:

- Exploration of the novel concept of utilizing chattering signals of the SVSF for fault diagnosis.
- Information extraction from spectral analysis of the chattering using the probability distribution of the chattering power spectrum.
- Examination of the ability to capture fault-related temporal details from chattering spectrogram using short time Fourier transform.
- Implementation of the developed approach to detect and measure the severity of leakage and friction faults as well as the bulk modulus mismatch within an electro-hydraulic actuator.

The organization of this paper is as follows. In section 3.2, the chattering signal of the smooth variable structure filter is defined while briefly outlining the filtering strategy. Development of the chattering equation based on model mismatch, process noise, and measurement noise is covered in Section 3.3. The section considers the information content in chattering for systems with both full and partial state measurements. In a case study for a second-order system, the potential of applying the chattering equation to derive information about model mismatch is then demonstrated. Section 3.4 focuses on spectral analysis of the chattering signal using the Fast Fourier Transform (FFT) and spectrogram. The proposed approach is

applied to an EHA system to detect bulk modulus, leakage, and friction faults in section 3.5. Concluding remarks are provided in section 3.6.

3.2. The Chattering Signal of The Smooth Variable Structure Filter

Consider a general linear stochastic dynamic system with zero-mean Gaussian process and measurement noise denoted by $\mathbf{v}(k)$ and $\mathbf{w}(k)$, which are characterized by the covariance matrices $\mathbf{Q}(k)$ and $\mathbf{R}(k)$, respectively.

$$\boldsymbol{x}(k+1) = \boldsymbol{A}\boldsymbol{x}(k) + \boldsymbol{B}\boldsymbol{u}(k) + \boldsymbol{v}(k). \tag{3.1}$$

$$\boldsymbol{z}(k) = \boldsymbol{C}\boldsymbol{x}(k) + \boldsymbol{w}(k). \tag{3.2}$$

Let us assume the modeling uncertainties $\boldsymbol{\Delta}\mathbf{A}(k)$, $\boldsymbol{\Delta}\mathbf{B}(k)$, and $\boldsymbol{\Delta}\mathbf{C}(k)$ to be as follows:

$$\begin{aligned} \Delta\boldsymbol{A} &= \boldsymbol{A} - \widehat{\boldsymbol{A}}, \\ \Delta\boldsymbol{B} &= \boldsymbol{B} - \widehat{\boldsymbol{B}}, \\ \Delta\boldsymbol{C} &= \boldsymbol{C} - \widehat{\boldsymbol{C}}, \end{aligned} \tag{3.3}$$

where $\widehat{\boldsymbol{A}}$, $\widehat{\boldsymbol{B}}$, and $\widehat{\boldsymbol{C}}$ contain the nominal parameters of the model. The SVSF then iteratively repeats the following four steps to estimate the states of the system [35].

1) The states are predicted according to the system model and a priori estimates are obtained.

$$\hat{\boldsymbol{x}}(k+1|k) = \widehat{\boldsymbol{A}}\hat{\boldsymbol{x}}(k|k) + \widehat{\boldsymbol{B}}\boldsymbol{u}(k|k). \tag{3.4}$$

$$\hat{\boldsymbol{z}}(k+1|k) = \widehat{\boldsymbol{C}}\hat{\boldsymbol{x}}(k+1|k). \tag{3.5}$$

2) A priori and a posteriori output error estimates are obtained.

$$\boldsymbol{e}_{\boldsymbol{z}}(k+1|k) = \boldsymbol{z}(k+1) - \hat{\boldsymbol{z}}(k+1|k), \tag{3.6}$$

$$\boldsymbol{e}_{\boldsymbol{z}}(k|k) = \boldsymbol{z}(k) - \hat{\boldsymbol{z}}(k|k). \tag{3.7}$$

3) The corrective term is calculated.

- If measurements are available for all states:

$$\boldsymbol{K}(k+1) = \widehat{\boldsymbol{C}}^{-1}(|\boldsymbol{e_z}(k+1|k)| + \gamma|\boldsymbol{e_z}(k|k)|) \odot sat(\boldsymbol{e_z}(k+1|k), \boldsymbol{\psi}), \quad (3.8)$$

where γ is the convergence rate, $\boldsymbol{\psi}$ is the smoothing boundary layer, and $\odot$ is the Schur product.

- If measurements are not available for some states but the system is observable, then the corrective term will be calculated based on Luenberger's reduced-order observer. For states with associated measurements, the corrective term is the same as above.

$$\boldsymbol{K}_u(k+1) = \widehat{\boldsymbol{C}}_1^{-1}(|\boldsymbol{e_z}(k+1|k)| + \gamma|\boldsymbol{e_z}(k|k)|) \odot sat(\boldsymbol{e_z}(k+1|k), \boldsymbol{\psi}), \quad (3.9)$$

$$\begin{aligned}\boldsymbol{K}_l(k+1) = \big(&\big|\widehat{\boldsymbol{\phi}}_{22}\widehat{\boldsymbol{\phi}}_{12}\boldsymbol{e_z}(k+1|k)\big| \\ &+ \gamma\big|\widehat{\boldsymbol{\phi}}_{12}^{-1}\boldsymbol{e_z}(k|k)\big|\big) \odot sat\big(\widehat{\boldsymbol{\phi}}_{22}\widehat{\boldsymbol{\phi}}_{12}^{-1}\boldsymbol{e_z}(k+1|k), \boldsymbol{\psi}\big),\end{aligned} \quad (3.10)$$

$$\boldsymbol{K}(k+1) = \begin{bmatrix}\boldsymbol{K}_u(k+1) \\ \boldsymbol{K}_l(k+1)\end{bmatrix}. \quad (3.11)$$

Assuming the system has n states and m outputs, the measurement matrix will have two blocks: $\boldsymbol{C} = [\boldsymbol{C}_1 \quad \boldsymbol{C}_2]$, where $\boldsymbol{C}_1$ is a full rank $m \times m$ matrix associated with measured states and $\boldsymbol{C}_2$ is an $m \times (m\text{-}n)$ matrix corresponding to the unmeasured states. Subscript u is used for state vectors directly linked to measurements, while subscript l refers to the states without corresponding measurements. Matrix $\widehat{\boldsymbol{\Phi}} = \boldsymbol{T}^{-1}\widehat{\boldsymbol{A}}\boldsymbol{T} = \begin{bmatrix}\widehat{\boldsymbol{\Phi}}_{11} & \widehat{\boldsymbol{\Phi}}_{12} \\ \widehat{\boldsymbol{\Phi}}_{21} & \widehat{\boldsymbol{\Phi}}_{22}\end{bmatrix}$ is calculated using transformation $\boldsymbol{T}$, which rearranges the state vector based on the mentioned two subsets of states [35].

4) The a posteriori state estimate is then updated by refining the a priori estimate using the corrective term.

$$\hat{\boldsymbol{x}}(k+1|k+1) = \hat{\boldsymbol{x}}(k+1|k) + \boldsymbol{K}(k+1). \tag{3.12}$$

The chattering occurs when a priori estimation error is larger than the boundary layer as shown below:

$$Chattering_i(k) = \begin{cases} 0 & |e_i(k|k-1)| < \psi_i \\ (|e_i(k|k-1)| - \psi_i)\, sgn\big(e_i(k|k-1)\big) & |e_i(k|k-1)| \geq \psi_i \end{cases} \tag{3.13}$$

where $\boldsymbol{Chattering_i(k)}$ denotes the chattering, $\boldsymbol{e_i(k|k-1)}$ is the a priori estimation error, and ψ_i is the smoothing boundary layer for state i. To avoid chattering under the normal condition, the smoothing boundary layer should be larger than the upper bound of the uncertain dynamics associated with the a priori state estimate ($\boldsymbol{\beta}$). This upper bound is obtained based on system uncertainties and noise as [38]:

$$\boldsymbol{\beta} = \sup\Big(\boldsymbol{C}\Big(\Delta\boldsymbol{A}\Big(\boldsymbol{C}^{-1}\big(\boldsymbol{z}(k) - \boldsymbol{w}(k)\big)\Big) + \Delta\boldsymbol{B}\boldsymbol{u}(k) + \boldsymbol{v}(k)\Big) + \boldsymbol{w}(k+1)\Big). \tag{3.14}$$

For an observable system with fewer measurements, states should be transformed, then $\boldsymbol{\beta}$ can be calculated as explained in [38].

$$\begin{bmatrix} \boldsymbol{d}_1(k) \\ \boldsymbol{d}_2(k) \end{bmatrix} = \Delta\boldsymbol{\Phi}\begin{bmatrix} \boldsymbol{z}(k) \\ \boldsymbol{y}(k) \end{bmatrix} + \Delta\mathbf{G}\boldsymbol{u}(k) + \begin{bmatrix} \overline{\boldsymbol{v}}_1(k) \\ \overline{\boldsymbol{v}}_2(k) \end{bmatrix}, \tag{3.15}$$

$$\begin{aligned} \boldsymbol{\beta} = max\big((\boldsymbol{I}-\gamma)^{-1}\big|\widehat{\boldsymbol{\phi}}_{22}\big|, \gamma^{-1}\big|\widehat{\boldsymbol{\phi}}_{22}\big|, (\boldsymbol{I}-\gamma)^{-1}, \gamma^{-1}, \boldsymbol{I}\big) \\ \times \sup\big(\big|\boldsymbol{d}_2(k) - \widehat{\boldsymbol{\phi}}_{22}\widehat{\boldsymbol{\phi}}_{12}^{-1}\boldsymbol{d}_1(k)\big| + \big|\widehat{\boldsymbol{\phi}}_{12}^{-1}\boldsymbol{d}_1(k-1)\big|\big). \end{aligned} \tag{3.16}$$

The existence boundary can be determined based on an upper bound on $\boldsymbol{d}(k)$ due to uncertain dynamics, $\boldsymbol{\Phi} = \boldsymbol{T}^{-1}\boldsymbol{A}\boldsymbol{T} = \begin{bmatrix} \boldsymbol{\Phi}_{11} & \boldsymbol{\Phi}_{12} \\ \boldsymbol{\Phi}_{21} & \boldsymbol{\Phi}_{22} \end{bmatrix}$, $\boldsymbol{G} = \boldsymbol{T}^{-1}\boldsymbol{B}$, and $\begin{bmatrix} \overline{\boldsymbol{v}}_1(k) \\ \overline{\boldsymbol{v}}_2(k) \end{bmatrix} = \boldsymbol{T}^{-1}\boldsymbol{v}(k) - \begin{bmatrix} \boldsymbol{\phi}_{11} \\ \boldsymbol{\phi}_{21} \end{bmatrix}\boldsymbol{w}(k+1)$.

To avoid chattering, $\boldsymbol{\psi}$ should be larger than $\boldsymbol{\beta}$. However, choosing a very large smoothing boundary layer ($\Psi_i \gg \beta_i \; for \; all \; i$) reduces the robustness of the filter.

The SVSF estimation inside the smoothing boundary layer can be improved by finding an optimal variable boundary layer [36].

To detect fault conditions from the chattering effect in the SVSF (or SVSF-VBL), the upper bound on the smoothing boundary layer should be chosen based on system uncertainties (Figure 2-9(a)). As shown in Figure 2-9(c), when the smoothing boundary layer is smaller than $\boldsymbol{\beta}$, chattering occurs even during normal system conditions. On the other hand, as shown in Figure 2-9(b), if the smoothing boundary layer is larger than $\boldsymbol{\beta}$, fault cannot be detected. Assuming that matrix $\boldsymbol{C}$ is exactly known, the existence boundary layer obtained from equation (3.14) can be considered as an approximate value for the smoothing boundary layer [38].

3.3. Information Extraction from Chattering Signal

When a model mismatch or fault is detected from the chattering signal of the SVSF-VBL, an auxiliary filter is run in parallel to extract information from the chattering signal. This auxiliary filter is a variant of the mentioned SVSF that has the same recursive steps with one exception. In equations (3.8), (3.9), and (3.10), the saturation function, $sat(\cdot, \boldsymbol{\Psi})$, is replaced with the sign function, $sgn(\cdot)$. In other words, the auxiliary filter does not use any smoothing boundary layer.

3.3.1. Chattering Signal for Full Measurement of the State Variables

According to equation (2.22), the chattering for the auxiliary filter that uses sign function is equal to the a priori error:

$$\begin{aligned} \boldsymbol{chattering}(k+1) &= \boldsymbol{e_z}(k+1|k) = \boldsymbol{z}(k+1) - \hat{\boldsymbol{z}}(k+1|k) \\ &= \boldsymbol{z}(k+1) - \widehat{\boldsymbol{C}}\hat{\boldsymbol{x}}(k+1|k). \end{aligned} \tag{3.17}$$

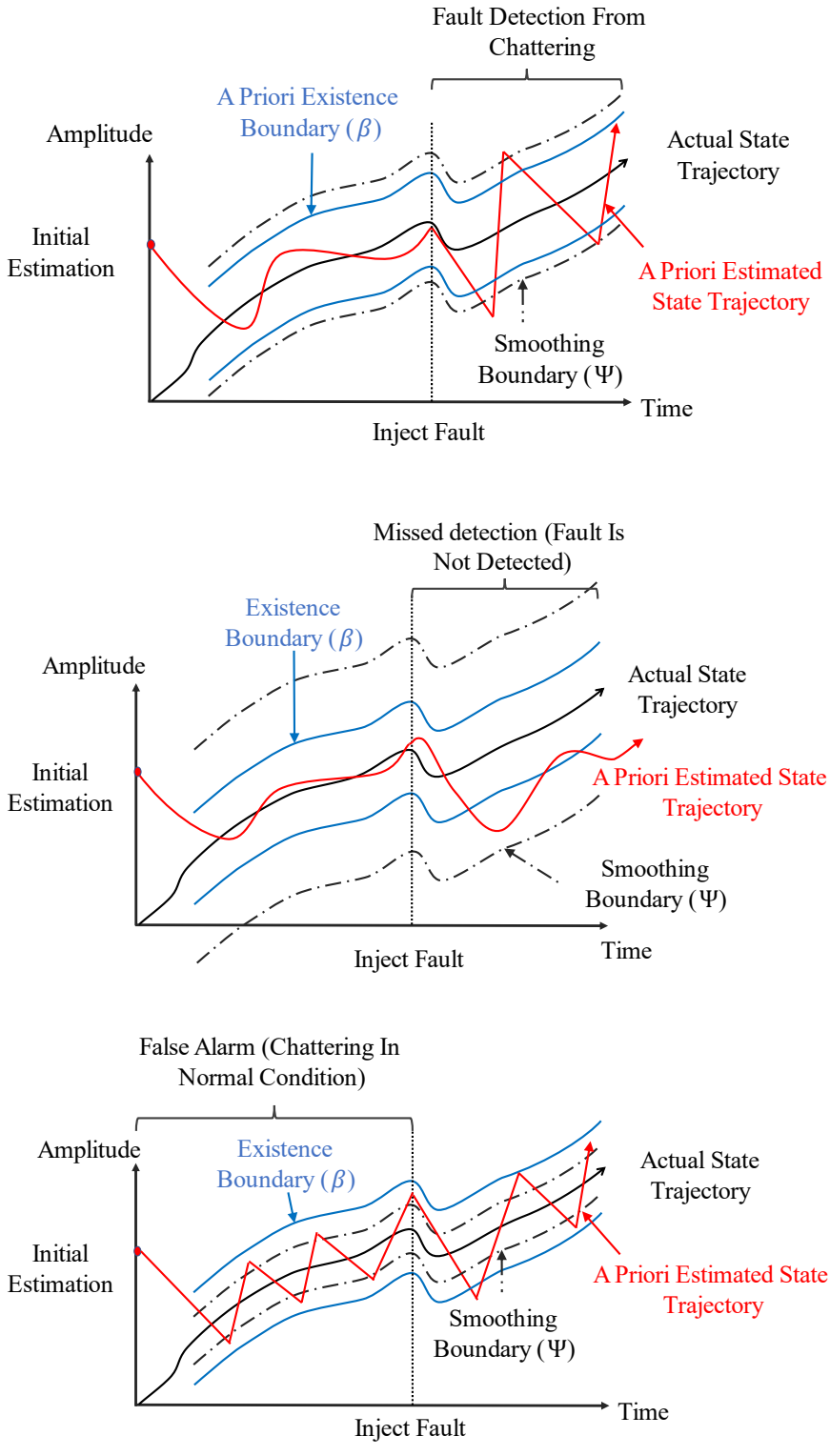

Figure 3-1. Fault detection from chattering signal of SVSF for different relative values of existence and smoothing boundary layers.

Substituting (3.4) and (3.2) into (3.17) yields:

$$\boldsymbol{chattering}(k+1) = \boldsymbol{C}x(k+1) + \boldsymbol{w}(k+1) - \widehat{\boldsymbol{C}}\left(\widehat{\boldsymbol{A}}\widehat{\boldsymbol{x}}(k|k) + \widehat{\boldsymbol{B}}\boldsymbol{u}(k)\right). \tag{3.18}$$

Substituting the states from (3.1) gives:

$$\begin{aligned}\boldsymbol{chattering}(k+1)& \\ &= \boldsymbol{CA}\boldsymbol{x}(k) + \boldsymbol{CB}\boldsymbol{u}(k) + \boldsymbol{C}\boldsymbol{v}(k) + \boldsymbol{w}(k+1) \\ &- \widehat{\boldsymbol{C}}\left(\widehat{\boldsymbol{A}}\widehat{\boldsymbol{x}}(k|k) + \widehat{\boldsymbol{B}}\boldsymbol{u}(k)\right).\end{aligned} \tag{3.19}$$

The a posteriori state estimate obtained by the auxiliary filter is calculated as follows:

$$\begin{aligned}\widehat{\boldsymbol{x}}(k|k) = \widehat{\boldsymbol{x}}(k|k-1) + \boldsymbol{K}(k)& \\ &= \widehat{\boldsymbol{x}}(k|k-1) \\ &+ \widehat{\boldsymbol{C}}^{-1}(|\boldsymbol{e_z}(k|k-1)| \\ &+ \gamma|\boldsymbol{e_z}(k-1|k-1)|)\odot sgn\big(\boldsymbol{e_z}(k|k-1)\big) \\ &= \widehat{\boldsymbol{x}}(k|k-1) \\ &+ \widehat{\boldsymbol{C}}^{-1}\Big(\boldsymbol{e_z}(k|k-1) \\ &+ \gamma|\boldsymbol{e_z}(k-1|k-1)|\odot sgn\big(\boldsymbol{e_z}(k|k-1)\big)\Big),\end{aligned} \tag{3.20}$$

where the estimation error decays with rate γ [38].

$$|\boldsymbol{e_z}(k-1|k-1)| = \gamma|\boldsymbol{e_z}(k-2|k-2)| = \gamma^{k-1}|\boldsymbol{e_z}(0|0)|. \tag{3.21}$$

Substituting (3.19) into (3.20) and further simplifying it using (3.6), (3.5), and (3.2) yields:

$$\begin{aligned}\widehat{\boldsymbol{x}}(k|k) = \widehat{\boldsymbol{x}}(k|k-1) + \widehat{\boldsymbol{C}}^{-1}\big(\boldsymbol{z}(k) - \widehat{\boldsymbol{z}}(k|k-1)\big)& \\ + \widehat{\boldsymbol{C}}^{-1}\gamma^{k-1}|\boldsymbol{e_z}(0|0)|\odot sgn\big(\boldsymbol{e_z}(k|k-1)\big)& \\ = \widehat{\boldsymbol{C}}^{-1}\boldsymbol{z}(k) + \widehat{\boldsymbol{C}}^{-1}\gamma^{n-1}|\boldsymbol{e_z}(0|0)| \circ\ sgn\big(\boldsymbol{e_z}(k|k-1)\big)& \\ = \widehat{\boldsymbol{C}}^{-1}\boldsymbol{C}\boldsymbol{x}(k) + \widehat{\boldsymbol{C}}^{-1}\boldsymbol{w}(k)& \\ + \widehat{\boldsymbol{C}}^{-1}\gamma^{k-1}|\boldsymbol{e_z}(0|0)|\odot sgn\big(\boldsymbol{e_z}(k|k-1)\big).&\end{aligned} \tag{3.22}$$

By substituting (3.22) into (3.19) and rearranging it, the chattering can be formulated as a function of model mismatch and system noise:

$$\begin{aligned}\boldsymbol{chattering}(k+1)\\ &= \big(\boldsymbol{CA} - \widehat{\boldsymbol{C}}\widehat{\boldsymbol{A}}\widehat{\boldsymbol{C}}^{-1}\boldsymbol{C}\big)\boldsymbol{x}(k) + \big(\boldsymbol{CB} - \widehat{\boldsymbol{C}}\widehat{\boldsymbol{B}}\big)\boldsymbol{u}(k) + \boldsymbol{C}v(k)\\ &- \widehat{\boldsymbol{C}}\widehat{\boldsymbol{A}}\widehat{\boldsymbol{C}}^{-1}\boldsymbol{w}(k) + \boldsymbol{w}(k+1)\\ &+ \widehat{\boldsymbol{C}}\widehat{\boldsymbol{A}}\widehat{\boldsymbol{C}}^{-1}\gamma^{k-1}|\boldsymbol{e_z}(0|0)|\odot sgn\big(\boldsymbol{e_z}(k|k-1)\big).\end{aligned} \tag{3.23}$$

3.3.2. Chattering Signal for Fewer Measurements Than State Variables

For an observable system, the chattering of the state estimates of the auxiliary filter can be obtained based on Luenberger's reduced order observer [38]. Applying Luenberger's transformation, equation (3.19) can be written as follows:

$$\begin{aligned}\boldsymbol{chattering}_u(k+1)\\ &= \boldsymbol{C}_1\boldsymbol{\Phi T}\boldsymbol{x}(k) - \widehat{\boldsymbol{C}}_1\widehat{\boldsymbol{\Phi}}\boldsymbol{T}\widehat{\boldsymbol{x}}(k|k) + \big(\boldsymbol{C}_1\boldsymbol{G} - \widehat{\boldsymbol{C}}_1\widehat{\boldsymbol{G}}\big)\boldsymbol{u}(k)\\ &+ \overline{\boldsymbol{v}}_1(k),\end{aligned} \tag{3.24}$$

where subscript u refers to the states that are measured. The a posteriori state estimate can be obtained from (3.9), (3.10), and (3.11):

$$\begin{aligned}\widehat{\boldsymbol{x}}(k|k) &= \widehat{\boldsymbol{x}}(k|k-1) + \begin{bmatrix}K_u(k)\\ K_l(k)\end{bmatrix}\\ &= \begin{bmatrix}\widehat{\boldsymbol{x}}_u(k|k-1) + \widehat{\boldsymbol{C}}_1^{-1}\big(\boldsymbol{z}(k) - \widehat{\boldsymbol{z}}(k|k-1)\big) + \widehat{\boldsymbol{C}}_1^{-1}\gamma^{k-1}|\boldsymbol{e_z}(0|0)|\odot sgn\big(\boldsymbol{e_z}(k|k-1)\big)\\ \widehat{\boldsymbol{x}}_l(k|k-1) + \widehat{\boldsymbol{\phi}}_{22}\widehat{\boldsymbol{\phi}}_{12}^{-1}\big(\boldsymbol{z}(k) - \widehat{\boldsymbol{z}}(k|k-1)\big) + \gamma^{k-1}\left|\widehat{\boldsymbol{\phi}}_{12}^{-1}\boldsymbol{e_z}(0|0)\right|\odot sgn\left(\widehat{\boldsymbol{\phi}}_{12}^{-1}\boldsymbol{e_z}(k|k-1)\right)\end{bmatrix}\\ &= \begin{bmatrix}\widehat{\boldsymbol{C}}_1^{-1}\boldsymbol{C}_1\boldsymbol{x}_u(\boldsymbol{k}) + \widehat{\boldsymbol{C}}_1^{-1}\gamma^{n-1}|\boldsymbol{e_z}(0|0)|\odot sgn\big(\boldsymbol{e_z}(k|k-1)\big)\\ \boldsymbol{x}_l(k) + \widehat{\boldsymbol{\phi}}_{22}\widehat{\boldsymbol{\phi}}_{12}^{-1}\boldsymbol{d}_1(k-1) + \boldsymbol{d}_2(k-1) + \gamma^{k-1}\left|\widehat{\boldsymbol{\phi}}_{12}^{-1}\boldsymbol{e_z}(0|0)\right|\odot sgn\left(\widehat{\boldsymbol{\phi}}_{12}^{-1}\boldsymbol{e_z}(k|k-1)\right)\end{bmatrix}.\end{aligned} \tag{3.25}$$

Then, chattering can be obtained by substituting (3.25) into (3.24):

$$\begin{aligned}&\boldsymbol{chattering}_u(k+1)\\ &= \boldsymbol{C}_1\boldsymbol{\Phi T}\boldsymbol{x}(k) + \big(\boldsymbol{C}_1\boldsymbol{G} - \widehat{\boldsymbol{C}}_1\widehat{\boldsymbol{G}}\big)\boldsymbol{u}(k) + \overline{\boldsymbol{v}}_1(k)\\ &- \widehat{\boldsymbol{C}}_1\widehat{\boldsymbol{\Phi}}\boldsymbol{T}\begin{bmatrix}\widehat{\boldsymbol{C}}_1^{-1}\boldsymbol{C}_1\boldsymbol{x_u}(\boldsymbol{k}) + \widehat{\boldsymbol{C}}_1^{-1}\gamma^{n-1}|\boldsymbol{e_z}(0|0)|\odot\ sgn\big(\boldsymbol{e_z}(k|k-1)\big)\\ \boldsymbol{x}_l(k) + \widehat{\boldsymbol{\phi}}_{22}\widehat{\boldsymbol{\phi}}_{12}^{-1}\boldsymbol{d}_1(k-1) + \boldsymbol{d}_2(k-1) + \gamma^{k-1}\left|\widehat{\boldsymbol{\phi}}_{12}^{-1}\boldsymbol{e_z}(0|0)\right|\odot sgn\left(\widehat{\boldsymbol{\phi}}_{12}^{-1}\boldsymbol{e_z}(k|k-1)\right)\end{bmatrix}\end{aligned} \tag{3.26}$$

Ignoring the impact of the initial error, assuming $\widehat{\boldsymbol{C}}_1 = \boldsymbol{C}_1$, and $\boldsymbol{T}$ being identity, which can be achieved by rearranging the states, equation (3.26) can be simplified as follows:

$$\begin{aligned} &\boldsymbol{chattering}_u(k+1) \\ &\quad = \boldsymbol{C}_1\boldsymbol{\Delta\Phi x}(k) + \boldsymbol{C}_1\boldsymbol{\Delta G u}(k) + \bar{\boldsymbol{v}}_1(k) \\ &\quad - \boldsymbol{C}_1 \begin{bmatrix} \widehat{\boldsymbol{\phi}}_{12}\widehat{\boldsymbol{\phi}}_{22}\widehat{\boldsymbol{\phi}}_{12}{}^{-1}\boldsymbol{d}_1(k-1) + \widehat{\boldsymbol{\phi}}_{12}\boldsymbol{d}_2(k-1) \\ \widehat{\boldsymbol{\phi}}_{22}^2\widehat{\boldsymbol{\phi}}_{12}{}^{-1}\boldsymbol{d}_1(k-1) + \widehat{\boldsymbol{\phi}}_{22}\boldsymbol{d}_2(k-1) \end{bmatrix}. \end{aligned} \tag{3.27}$$

The chattering of the states without an associated measurement can be obtained based on the chattering of the measured states, using Luenberger's transformation [38]:

$$\begin{aligned} \boldsymbol{chattering}_l(k+1) &= \boldsymbol{e}_{\boldsymbol{y}}(k+1|k) \\ &= \widehat{\boldsymbol{\phi}}_{22}\widehat{\boldsymbol{\phi}}_{12}^{-1}\boldsymbol{chattering}_l(k+1) - \widehat{\boldsymbol{\phi}}_{22}\widehat{\boldsymbol{\phi}}_{12}^{-1}\boldsymbol{d}_1(k) + \boldsymbol{d}_2(k) \end{aligned} \tag{3.28}$$

where subscript l refers to the states without an associated measurement.

The modified upper bound of the uncertain dynamics associated with the a priori state estimate can be calculated from the following equation:

$$\boldsymbol{\beta}_{estimated} = sup\big(\boldsymbol{chattering}(k)\big). \tag{3.29}$$

To avoid chattering, the smoothing boundary layer ($\boldsymbol{\Psi}$) should be larger than $\boldsymbol{\beta}_{estimated}$.

3.3.3. Model Mismatch Detection from Chattering Signal of the SVSF

In this section, the model mismatch detection for a second-order system from the chattering signal of the SVSF is investigated. The discretized state-space model of a general second-order system with damping ratio ζ, natural frequency ω_0,

measurement noise $\boldsymbol{w}(k)$, and process noise $\boldsymbol{v}(k)$ is given in (3.30), assuming only the first state has been measured.

$$\begin{cases} x_1(k+1) = x_1(k) + T_s x_2(k) + v_1(k) \\ x_2(k+1) = -T_s\omega_0^2 x_1(k) + (1 - 2T_s\zeta\omega_n)x_2(k) + T_s b u(k) + v_2(k) \\ z(k) = x_1(k) + w(k), \end{cases} \tag{3.30}$$

where T_s denotes the time-step and u is the system input. Under normal condition, let us assume an undamped (zeta=0) system with $\omega_0 = 2Hz$, $b = 100$, uncorrelated process noise $v_1(k) \sim \mathcal{N}(0, 10^{-10})$ and $v_2(k) \sim \mathcal{N}(0, 10^{-8})$, measurement noise $w(k) \sim \mathcal{N}(0, 10^{-8})$, and $T_s = 0.001s$. For the estimated parameters being equal to the normal condition, model matrices are obtained as follows:

$$\widehat{\boldsymbol{A}} = \boldsymbol{A} = \begin{bmatrix} 1 & 0.001 \\ -0.0125 & 1 \end{bmatrix}, \qquad \widehat{\boldsymbol{B}} = \boldsymbol{B} = \begin{bmatrix} 0 \\ 0.1 \end{bmatrix}, \qquad \widehat{\boldsymbol{C}} = \boldsymbol{C} = [1 \quad 0]. \tag{3.31}$$

If the smoothing boundary layer is chosen to be larger than the SVSF chattering under normal conditions, then chattering in the SVSF indicates a model mismatch. For state x_1, which is directly measured, width of the smoothing boundary layer can be calculated by substituting (3.31) and (3.27) into (3.29). Ignoring the effect of initial error, we obtain:

$$\psi_1 \geq \beta_{1,estimated} = \sup\Big(\bar{\boldsymbol{v}}_1(k) - \widehat{\boldsymbol{\phi}}_{12}\widehat{\boldsymbol{\phi}}_{22}\widehat{\boldsymbol{\phi}}_{12}{}^{-1}\boldsymbol{d}_1(k-1) + \widehat{\boldsymbol{\phi}}_{12}\boldsymbol{d}_2(k-1)\Big). \tag{3.32}$$

Let us denote the argument of the supremum function in the above equation by δ_1. Substituting the numerical values of the parameters, we have:

$$\begin{aligned} \delta_1(\mathrm{k}) = v_1(k) - v_1(k-1) - 0.001v_2(k-1) - w(k) \\ + (1 - 1.25e-5)w(k-1). \end{aligned} \tag{3.33}$$

Considering that the measurement noise and process noise are independent and white, distribution of δ_1 is obtained as:

$$\begin{aligned}\delta_1(k)\sim N\big(&\mu_{v_1(k)} - \mu_{v_1(k-1)} - 0.001\mu_{v_2(k-1)} - \mu_{w(k)} + \mu_{w(k-1)}, \sigma^2_{v_1(k)} \\ &+ \sigma^2_{v_1(k-1)} + 10^{-6}\sigma^2_{v_2(k)} + \sigma^2_{w(k)} + \sigma^2_{w(k-1)}\big) \\ &\approx \mathcal{N}(0, 2.02 \times 10^{-8}).\end{aligned} \tag{3.34}$$

Since δ_1 has a zero-mean normal distribution, if the assigned value to the smoothing boundary layer is between $3\sigma_{\delta_1(k)}$ and $4\sigma_{\delta_1(k)}$, then chattering will occur with a probability of 0.2% to 0.01%. Therefore, it would not be necessary to consider a larger smoothing boundary layer. As mentioned previously, choosing a large smoothing boundary layer suppresses the chattering, and in effect, therefore, decreases the sensitivity for model mismatch detection. This increases the chance of missing faults. On the other hand, choosing a small boundary layer increases the probability of chattering occurrence even under normal conditions. This will lead to false alarms. Hence, the smoothing boundary layer must be chosen based on a trade-off between reducing the probability of missing faults and reducing the probability of false alarms. Choosing $\psi_1 = 5 \times 10^{-4} \approx 3.5\sigma_{\delta_1(k)}$, the probability of the chattering is calculated as follows according to the normal distribution table:

$$\Pr\big(\psi_1 < \beta_{1,estimated}\big) = \Pr(5 \times 10^{-4} < |\delta_1(k)|) \approx 0.067\ \%. \tag{3.35}$$

This means that chattering is almost impossible during normal operation and any chattering reflects a fault or model mismatch in the system. For the unmeasured state x_2, the smoothing boundary is obtained by substituting (3.32), (3.28), and (3.21) into (3.29):

$$\begin{aligned}\psi_2 \geq \beta_{2,estimated} = \sup\Bigg(&1000\Big(\bar{v}_1(k) - \widehat{\boldsymbol{\phi}}_{12}\widehat{\boldsymbol{\phi}}_{22}{\widehat{\boldsymbol{\phi}}_{12}}^{-1}\boldsymbol{d}_1(k-1) + \\ &\widehat{\boldsymbol{\phi}}_{12}\boldsymbol{d}_2(k-1)\Big) - 1000v_1(k) + 1000w(k) + v_2(k) - 12.5w(k)\Bigg).\end{aligned} \tag{3.36}$$

Similarly, denoting the argument of the supremum function in the above equation by δ_2, distribution of δ_2 is calculated as:

$$\delta_2(\mathrm{k}) \sim \mathcal{N}(0, 3.0135 \times 10^{-2}). \tag{3.37}$$

Sensitivity of the chattering signal to fault or model mismatch depends on the smoothing boundary layer, which is determined by process and measurement noise. A higher noise level needs a larger smoothing boundary layer, which will overshadow the fault or model mismatch. Comparing (3.34) with (3.37), δ_1 has a sharper distribution than δ_2 due to its lower variance, which reflects a lower level of uncertainty. This is rational, because x_2 is not measured directly. Therefore, the chattering signal of the measured state x_1 is used to detect the model mismatch here.

The state-space model of the second-order system described in (3.30) includes two parameters: damping ratio and natural frequency. Hence, in this case, model mismatch refers to any difference between the values of these two parameters in the system whose states are estimated and the model of this system, which is used by the filter that estimates the states. To evaluate the capability of the proposed model mismatch detection method based on the chattering signal of the SVSF, the following scenario is considered for creating model mismatch. While the model used by SVSF remains unchanged, for the system whose states are estimated, during the time interval [1s, 2s], natural frequency is changed from 2Hz to 3Hz, and during the time interval [3s, 4s], damping ratio is changed from zero to 0.1. Three different smoothing boundary layers are selected for the measured state based on δ_1, while keeping the smoothing boundary layer of the unmeasured state the same for comparison. As shown in Figure 3-2, when the smoothing boundary layer is too large ($\psi_1 = 0.002 \gg \sigma_{\delta_1(k)}$), chattering does not occur. Since chattering signal is used as a secondary

indicator along with the innovation vector as the primary indicator of model mismatch, in the absence of chattering in this case, there is not any extra information that can be used for detecting model mismatch. Conversely, when the smoothing boundary layer is too small ($\psi_1 = 0.0001 < \sigma_{\delta_1(k)}$), chattering occurs even under normal conditions, and again analysis of the chattering signal is not helpful for model-mismatch detection. Hence, the value of ψ_1 must be selected carefully. This figure also shows that the estimation error increases when there is a model mismatch in the system. It is more severe for x_2, which is not measured directly and relies more on a correct model. This error is larger for a smaller boundary layer, because it means that SVSF has more confidence in the model, which is not correct anymore.

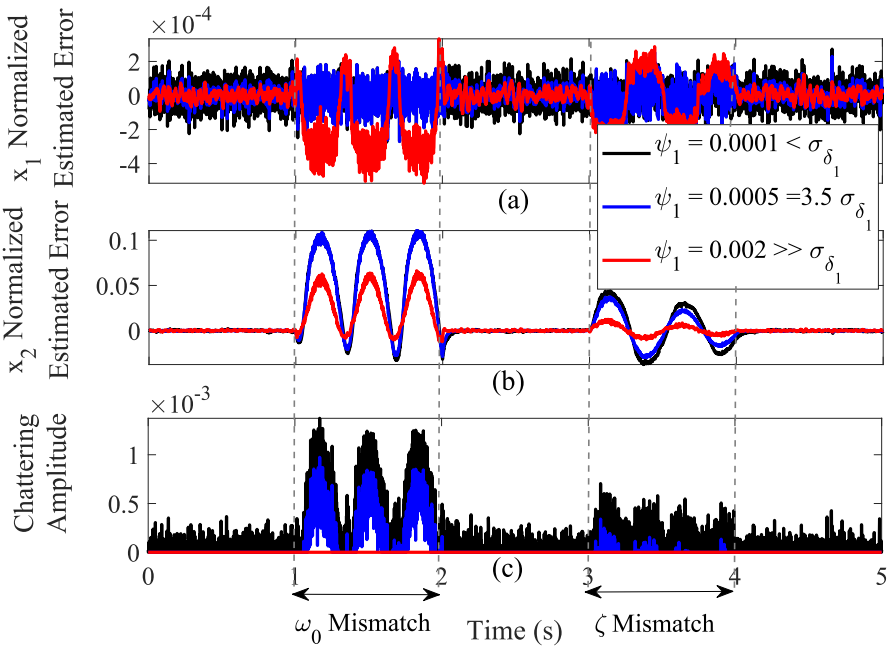

Figure 3-2. Model mismatch detection from chattering signal of SVSF for a second order system. Normalized estimation error for (a) measured and (b) unmeasured states. (c) Chattering signal of the measured state for three different smoothing boundary values. For a small smoothing boundary layer (black), chattering occurs even during normal conditions. For a large smoothing boundary layer (red), chattering does not occur when there is model mismatch. Only for a medium smoothing boundary layer (blue), chattering signal is helpful for model-mismatch-detection.

3.4. Spectral Analysis of the Chattering Signal

In state estimation, it is not straightforward to distinguish between noise and model mismatch based on their effects on the innovation vector. Deploying SVSF for state estimation, the corresponding chattering signals provide a secondary set of indicators that can be used for model-mismatch detection. To extract information from the chattering signal, an auxiliary SVSF without a smoothing boundary layer is used. As indicated in (3.23), (3.27), and (3.28), the chattering signal contains information about severity of mismatch between the state-space model used by the SVSF and dynamics of the actual system whose states are estimated by the filter. Spectral analysis provides a powerful tool for extracting this information from the noisy chattering signal using strategies such as Fast Fourier Transform (FFT) and Short-Time Fourier Transform (STFT). In this regard, looking at the spectrogram of the chattering signal will be very revealing. Spectrogram represents the frequency content of the chattering signal as it varies over time. Hence, it provides clues on occurrence of events such as faults that change the system, and lead to model mismatch. Power spectrum is defined as squared modulus of the Fourier transform. For a random signal, the power spectrum will similarly exhibit randomness. In certain contexts, when studying random signals, the expected power spectrum (or the expected value of squared modulus of the Fourier transform) is simply referred to as the power spectrum. In this study, the power spectrum shown by $\mathcal{S}$, is a random variable and when needed, we explicitly denote the expected power spectrum using the notation $\mathbb{E}[\mathcal{S}]$. Sources of randomness in the system dynamics are process noise and measurement noise, which are zero-mean white Gaussian processes. To lay the groundwork for deriving mathematical expressions for power spectrum of the

chattering signal, first, Lemma 1 presents the probability distribution of the real and imaginary parts of the discrete Fourier transform coefficients for zero-mean white Gaussian processes, emphasizing on the orthogonality of these real and imaginary parts. Building on the results of Lemma 1, Lemma 2 expresses that power spectrum of a stationary zero-mean white Gaussian noise at each frequency follows a chi-squared distribution. Result of Lemma 2 is then used to find the distribution of the power spectrum of the chattering signal. This distribution is needed to calculate the confidence interval for model mismatch detection.

- **Lemma 1.** *The discrete Fourier transform coefficients of a stationary zero-mean white Gaussian noise,* $v(k) \sim \mathcal{N}(0, \sigma^2)$*, with N samples are independent and zero-mean white Gaussian with the variance of* $\frac{N\sigma^2}{2}$ *.*

$$\Re\{V^{(N)}(\omega_n)\} \sim \mathcal{N}\left(0, \frac{N\sigma^2}{2}\right) \;\&\; \Im\{V^{(N)}(\omega_n)\} \sim \mathcal{N}\left(0, \frac{N\sigma^2}{2}\right) \;\&\; \Re\{V^{(N)}(\omega_n)\} \perp \Im\{V^{(N)}(\omega_n)\}, \quad for\ \omega_n = \frac{2\pi}{N}n, \quad where: \; -\left\lfloor \frac{(N-1)}{2} \right\rfloor \leq n \leq \left\lfloor \frac{N}{2} \right\rfloor, \tag{3.38}$$

where, $V^{(N)}(\omega_n)$ *is discrete Fourier transform of noise signal* v *at* n^{th} *frequency,* $\Re$ *and* $\Im$ *denote real and imaginary parts respectively, and* $\lfloor x \rfloor$ *denotes the floor function (the largest integer, which is less than or equal to* x*).*

Proof. Let us define the normalized $V^{(N)}(\omega_n)$ as follows:

$$\tilde{V}^{(N)}(\omega_n) = \frac{1}{\sqrt{2\pi N}} V^{(N)}(\omega_n) = \frac{1}{\sqrt{2\pi N}} \sum_{k=1}^{N} v(k) e^{-i\omega_n k}. \tag{3.39}$$

According to [39], $\tilde{V}^{(N)}(\omega_n)$ is a zero-mean complex Gaussian random variable with the following distribution:

$$\tilde{V}^{(N)}(\omega_n) \sim \mathcal{N}_C\big(0, f(\omega_n)\big), \tag{3.40}$$

where f is the spectral density function. For white noise, it is flat and equal to $\frac{\sigma^2}{2\pi}$. Since the family of normal distributions is closed under linear transformation, distribution of $V^{(N)}(\omega_n)$ can be obtained from (3.40) as:

$$V^{(N)}(\omega_n) \sim \mathcal{N}_C\big(0, 2\pi N f(\omega_n)\big) \Longrightarrow V^{(N)}(\omega_n) \sim \mathcal{N}_C(0, N\sigma^2). \tag{3.41}$$

Real and imaginary parts are obtained as a direct consequence of (3.41):

$$V^{(N)}(\omega_n) \sim \mathcal{N}_C(0, N\sigma^2) \Leftrightarrow \begin{cases} \Re\{V^{(N)}(\omega_n)\} \perp \Im\{V^{(N)}(\omega_n)\} \\ \Re\{V^{(N)}(\omega_n)\} \sim \mathcal{N}\left(0, \frac{N\sigma^2}{2}\right) \\ \Im\{V^{(N)}(\omega_n)\} \sim \mathcal{N}\left(0, \frac{N\sigma^2}{2}\right) \end{cases}. \tag{3.42}$$

■

- **Lemma 2.** *The power spectrum of a stationary zero-mean white Gaussian noise, $v(k) \sim \mathcal{N}(0, \sigma^2)$, with N evenly spaced samples follows a central chi-squared distribution of order 2 with the expected value of σ^2:*

$$\frac{2\mathcal{S}_v^{(N)}(\omega_n)}{\sigma^2} \sim \chi_2^2 \;\; \& \;\; \mathbb{E}\Big[\mathcal{S}_v^{(N)}(\omega_n)\Big] = \sigma^2 \;\; for\ \omega_n = \frac{2\pi}{N} n, \quad where: \;\; 0 \le n \le \left\lfloor \frac{N}{2} \right\rfloor - 1, \tag{3.43}$$

where $\mathcal{S}_v^{(N)}(\omega_n)$ is the power spectrum of noise signal v at n^{th} frequency.

Proof. Based on the power spectrum definition, the following equation holds:

$$\mathcal{S}_v^{(N)}(\omega_n) = \frac{1}{N}\left|V^{(N)}(\omega_n)\right|^2 = \frac{1}{N}\left(\Re\{V^{(N)}(\omega_n)\}^2 + \Im\{V^{(N)}(\omega_n)\}^2\right). \quad (3.44)$$

The following is valid because the family of normal distributions is closed under the linear transformation:

$$\begin{aligned}\Re\{V^{(N)}(\omega_n)\} &\sim \mathcal{N}\left(0, \frac{N\sigma^2}{2}\right) \Rightarrow \frac{\sqrt{2}\Re\{V^{(N)}(\omega_n)\}}{\sigma\sqrt{N}} \sim \mathcal{N}(0,1),\\ \Im\{V^{(N)}(\omega_n)\} &\sim \mathcal{N}\left(0, \frac{N\sigma^2}{2}\right) \Rightarrow \frac{\sqrt{2}\Im\{V^{(N)}(\omega_n)\}}{\sigma\sqrt{N}} \sim \mathcal{N}(0,1).\end{aligned} \quad (3.45)$$

Knowing that $\Re\{V^{(N)}(\omega_n)\} \perp \Im\{V^{(N)}(\omega_n)\}$ from lemma 1, definition of chi-squared distribution yields:

$$\begin{aligned}&\frac{2\Re\{V^{(N)}(\omega_n)\}^2}{N\sigma^2} + \frac{\Im\{V^{(N)}(\omega_n)\}^2}{N\sigma^2} \sim \chi_2^2\\ &\Rightarrow \frac{2}{\sigma^2}\left(\frac{1}{N}\left(\Re\{V^{(N)}(\omega_n)\}^2 + \Im\{V^{(N)}(\omega_n)\}^2\right)\right) \sim \chi_2^2\\ &\Rightarrow \frac{2\mathcal{S}_v^{(N)}(\omega_n)}{\sigma^2} \sim \chi_2^2.\end{aligned} \quad (3.46)$$

Knowing that the expected value of central chi-squared distribution is equal to the degrees of freedom, the expected value of the power spectrum is obtained as:

$$\mathbb{E}\left[\frac{2\mathcal{S}_v^{(N)}(\omega_n)}{\sigma^2}\right] = 2 \Rightarrow \mathbb{E}\left[\mathcal{S}_v^{(N)}(\omega_n)\right] = \sigma^2. \quad (3.47)$$

■

The power spectrum of the chattering signal for each frequency is defined as follows:

$$\boldsymbol{S}^{(\boldsymbol{N})}_{\boldsymbol{chattering}}(\omega_n) = \frac{1}{\mathrm{N}}|\mathcal{F}(\boldsymbol{chattering}_k)_n|^{\odot 2}$$
$$= \frac{1}{\mathrm{N}}\left|\sum_{k=1}^{N} \boldsymbol{chattering}(k)e^{-i\omega_n k}\right|^{\odot 2}, \qquad (3.48)$$
$$for\ \omega_n = \frac{2\pi}{N}n, \qquad where:\ N = \frac{t}{T_s}\ and\ \ 0 \le n \le \left\lfloor\frac{N}{2}\right\rfloor - 1.$$

$\mathcal{S}_{chattering_i}$ is the power spectrum (only for half of the frequencies because it is symmetric) of the chattering signal of the state i at n^{th} frequency, $\mathcal{F}$ denotes the discrete Fourier transform, N is the number of samples, $\boldsymbol{chattering}_k \coloneqq \boldsymbol{chattering}(1), \boldsymbol{chattering}(2), \dots, \boldsymbol{chattering}(N)$ is a sequence of chattering vectors, $\odot$ is element-wise also known as Schur operation ($\boldsymbol{B} = \boldsymbol{A}^{\odot 2} \Rightarrow b_{ij} = a_{ij}^2$), t is signal duration, and T_s is sampling time. To obtain frequency in Hz, the following transformation is applied on ω_n:

$$\omega = F_s\omega_n \quad where:\ F_s = \frac{1}{T_s}. \qquad (3.49)$$

ω is the frequency in Hz and F_s is the sampling rate. As shown in (3.48) and (3.49) the resolution and upper bound of ω depends on the signal duration and sampling frequency, respectively. Hence, the sampling size, N, is a crucial parameter that affects the spectrogram. Hereafter, the superscript N is removed since it is considered that the number of samples is fixed. Substituting (3.23) into (3.49) and ignoring the impact of the initial error, the power spectrum of chattering signal is obtained as follows using the linearity property of the discrete Fourier transform:

$$\begin{aligned}\boldsymbol{S_{chattering}}(\omega_n) &= \frac{1}{N}\left|\left(\boldsymbol{CA}-\widehat{\boldsymbol{C}}\widehat{\boldsymbol{A}}\widehat{\boldsymbol{C}}^{-1}\boldsymbol{C}\right)\mathcal{F}(\boldsymbol{x}_k)_n+\left(\boldsymbol{CB}-\widehat{\boldsymbol{C}}\widehat{\boldsymbol{B}}\right)\mathcal{F}(\boldsymbol{u}_k)_n\right. \\ &\left.+\boldsymbol{C}\mathcal{F}(\boldsymbol{v}_k)_n-\widehat{\boldsymbol{C}}\widehat{\boldsymbol{A}}\widehat{\boldsymbol{C}}^{-1}\mathcal{F}(\boldsymbol{w}_k)_n+\mathcal{F}(\boldsymbol{w}_{k+1})_n\right|^{\odot 2}.\end{aligned} \tag{3.50}$$

Under the normal condition with no model mismatch, equation (3.50) can be rewritten as:

$$\begin{aligned}\boldsymbol{S_{chattering}}(\omega_n) &= \frac{1}{N}\left|\boldsymbol{C}\mathcal{F}(\boldsymbol{v}_k)_n-\widehat{\boldsymbol{C}}\widehat{\boldsymbol{A}}\widehat{\boldsymbol{C}}^{-1}\mathcal{F}(\boldsymbol{w}_k)_n+\mathcal{F}(\boldsymbol{w}_{k+1})_n\right|^{\odot 2} \\ &= \frac{1}{N}\left|\boldsymbol{C}\mathcal{F}(\boldsymbol{v}_k)_n-\widehat{\boldsymbol{C}}\widehat{\boldsymbol{A}}\widehat{\boldsymbol{C}}^{-1}\mathcal{F}(\boldsymbol{w}_k)_n+e^{i\omega_n}\mathcal{F}(\boldsymbol{w}_k)_n\right|^{\odot 2} \\ &= \frac{1}{N}\left|\boldsymbol{C}\mathcal{F}(\boldsymbol{v}_k)_n+\left(e^{i\omega_n}\boldsymbol{I}-\widehat{\boldsymbol{C}}\widehat{\boldsymbol{A}}\widehat{\boldsymbol{C}}^{-1}\right)\mathcal{F}(\boldsymbol{w}_k)_n\right|^{\odot 2}.\end{aligned} \tag{3.51}$$

Using the shift theorem for discrete Fourier transform, (3.51) is further simplified as:

$$\begin{aligned}\boldsymbol{S_{chattering}}(\omega_n) &= \frac{1}{N}\left|\boldsymbol{C}\mathcal{F}(\boldsymbol{v}_k)_n-\widehat{\boldsymbol{C}}\widehat{\boldsymbol{A}}\widehat{\boldsymbol{C}}^{-1}\mathcal{F}(\boldsymbol{w}_k)_n+e^{i\omega_n}\mathcal{F}(\boldsymbol{w}_k)_n\right|^{\odot 2} \\ &= \frac{1}{N}\left|\boldsymbol{C}\mathcal{F}(\boldsymbol{v}_k)_n+\left(e^{i\omega_n}\boldsymbol{I}-\widehat{\boldsymbol{C}}\widehat{\boldsymbol{A}}\widehat{\boldsymbol{C}}^{-1}\right)\mathcal{F}(\boldsymbol{w}_k)_n\right|^{\odot 2}.\end{aligned} \tag{3.52}$$

Let us consider independent stationary white process and measurement noise with zero mean Gaussian distributions as:

$$\boldsymbol{Q}(k)=\boldsymbol{v}(k)\boldsymbol{v}(k)^{\intercal}=diag(\boldsymbol{\sigma}_v^2), \tag{3.53}$$

$$\boldsymbol{R}(k)=\boldsymbol{w}(k)\boldsymbol{w}(k)^{\intercal}=diag(\boldsymbol{\sigma}_w^2), \tag{3.54}$$

where $\boldsymbol{Q}(k)$ and $\boldsymbol{R}(k)$ are the covariance matrices of the process and measurement noise respectively, $\sigma_{v_i}^2$is the variance of the process noise for state i, and $\sigma_{w_j}^2$ is the variance of measurement noise for measurement j.

Regarding the predictor-corrector form of the SVSF, at each time instant, chattering depends on measurement noise for both predictions, $\boldsymbol{w}(k-1)$, and correction, $\boldsymbol{w}(k)$. Therefore, as shown in (3.52), the chattering signal exhibits autocorrelation due to the implicit accumulation of the effect of delayed measurement noise terms over time. The expected value of the power spectrum of the chattering signal is obtained using lemmas 1 and 2 (all the cross-correlation terms become zero due to independence and zero mean condition of discrete Fourier transform from lemma 1):

$$\begin{aligned}
&\mathbb{E}\left[\boldsymbol{S}_{\boldsymbol{chattering}}(\omega_n)\right] \\
&\qquad = \boldsymbol{C}^{\odot 2}\mathbb{E}\left[\frac{1}{N}|\mathcal{F}(\boldsymbol{v}_k)_n|^{\odot 2}\right] \\
&\qquad + \left|e^{i\omega_n}\boldsymbol{I} - \widehat{\boldsymbol{C}}\widehat{\boldsymbol{A}}\widehat{\boldsymbol{C}}^{-1}\right|^{\odot 2}\mathbb{E}\left[\frac{1}{N}|\mathcal{F}(\boldsymbol{w}_k)_n|^{\odot 2}\right] \\
&\qquad = \boldsymbol{C}^{\odot 2}\mathbb{E}[\boldsymbol{S}_{\boldsymbol{v}}] + \left|e^{i\omega_n}\boldsymbol{I} - \widehat{\boldsymbol{C}}\widehat{\boldsymbol{A}}\widehat{\boldsymbol{C}}^{-1}\right|^{\odot 2}\mathbb{E}[\boldsymbol{S}_{\boldsymbol{w}}] \\
&\qquad = \boldsymbol{C}^{\odot 2}\boldsymbol{\sigma}_{\boldsymbol{v}}^2 + \left|e^{i\omega_n}\boldsymbol{I} - \widehat{\boldsymbol{C}}\widehat{\boldsymbol{A}}\widehat{\boldsymbol{C}}^{-1}\right|^{\odot 2}\boldsymbol{\sigma}_{\boldsymbol{w}}^2,
\end{aligned} \tag{3.55}$$

Due to the exponential term in equation (3.55), which depends on frequency, it can be concluded that in general, the expected value of the power spectrum of the chattering signal is not flat under normal conditions (Figure 3-4).

3.4.1. Find the Threshold for Spectral Density of the Chattering Signal Under Normal Condition

To identify model mismatch, a threshold must be determined for the spectral density of the chattering signal that reflects normal conditions. This threshold should be intelligently specified in a way to decrease the chance of missing any model mismatch while avoiding false alarms. According to (3.52), there is an element of randomness in the power spectrum of the chattering signal. Therefore, the threshold should be

obtained by taking account of the probability distribution of the power spectrum of the chattering signal, using a confidence interval. To be more precise, the following equation must hold to ensure that the probability of a false alarm is smaller or equal to $\alpha\%$:

$$\Pr\left(\mathcal{S}_{chattering_i}(\omega_n) > threshold_i \middle| Normal\ Condition\right) \leq \alpha\%, \tag{3.56}$$

where $\mathcal{S}_{chattering_i}$is the power spectrum of the chattering signal for measured state i, and $threshold_i$ is its corresponding threshold. Let us define the matrices $\boldsymbol{M}$ and $\boldsymbol{\Lambda}$ as follows:

$$\begin{gathered} \boldsymbol{M} \coloneqq -\widehat{\boldsymbol{C}}\widehat{\boldsymbol{A}}\widehat{\boldsymbol{C}}^{-1} \\ \lambda_{ij} \coloneqq \begin{cases} m_{ij} & for\ i \neq j \\ m_{ij} + 1 & for\ i = j\ and\ m_{ij} \geq 0 \\ m_{ij} - 1 & for\ i = j\ and\ m_{ij} < 0 \end{cases}. \end{gathered} \tag{3.57}$$

Given that $-1 \leq e^{i\omega_n} \leq 1$, the above definition leads to $\boldsymbol{\Lambda} > \left(e^{i\omega_n}\boldsymbol{I} - \widehat{\boldsymbol{C}}\widehat{\boldsymbol{A}}\widehat{\boldsymbol{C}}^{-1}\right)$. This inequality along with independence of process and measurement noise, will lead to the following inequality:

$$\begin{aligned} \boldsymbol{S_{chattering}}(\omega_n) &= \frac{1}{N}\left|\boldsymbol{C}\mathcal{F}(\boldsymbol{v}_k)_n + \left(e^{i\omega_n}\boldsymbol{I} - \widehat{\boldsymbol{C}}\widehat{\boldsymbol{A}}\widehat{\boldsymbol{C}}^{-1}\right)\mathcal{F}(\boldsymbol{w}_k)_n\right|^{\odot 2} \\ &\leq \frac{1}{N}\left|\boldsymbol{C}\mathcal{F}(\boldsymbol{v}_k)_n + \boldsymbol{\Lambda}\mathcal{F}(\boldsymbol{w}_k)_n\right|^{\odot 2}. \end{aligned} \tag{3.58}$$

Based on the linearity property of the DFT, equation (3.58) can be rewritten as:

$$\boldsymbol{S_{chattering}}(\omega_n) \leq \frac{1}{N}\left|\mathcal{F}(\boldsymbol{C}\boldsymbol{v}_k + \boldsymbol{\Lambda}\boldsymbol{w}_k)_n\right|^{\odot 2}. \tag{3.59}$$

Since $\boldsymbol{v_k}$ and $\boldsymbol{w_k}$ are mutually independent stationary white zero-mean Gaussian vectors, their linear combination is also a stationary white zero-mean Gaussian vector:

$$\begin{aligned} \boldsymbol{\Gamma}_k = \boldsymbol{C v}_k + \boldsymbol{\Lambda w}_k \quad where: \boldsymbol{\Gamma}_k \sim \mathcal{N}\big(0, \boldsymbol{\Sigma_\Gamma}(k)\big) \;\&\; \boldsymbol{\Sigma_\Gamma}(k) \\ = \boldsymbol{CQ}(k)\boldsymbol{C}^T + \boldsymbol{\Lambda R}(k)\boldsymbol{\Lambda}^T. \end{aligned} \tag{3.60}$$

Substituting (3.60) into (3.59), and using lemma 2, we have:

$$\boldsymbol{\mathcal{S}_{chattering}}(\omega_n) \leq \frac{1}{N}|\mathcal{F}(\boldsymbol{\Gamma}_k)_n|^{\odot 2} = \boldsymbol{\mathcal{S}_\Gamma} \qquad where: \; \frac{2\mathcal{S}_{\Gamma_i}}{\Sigma_{\Gamma_{ii}}} \sim \chi_2^2, \tag{3.61}$$

where $\mathcal{S}_{\Gamma_i}$ is the power spectrum of the random signal associated with state i, which has a chi-squared distribution. Therefore, a threshold for the chattering signal under normal conditions will be obtained based on equation (3.56), using the chi-squared distribution table. When there is a model mismatch, a spike in the chattering power spectrum is expected according to the frequency content of the states and input signals as shown in (3.50). Higher peaks will result from a larger model mismatch, which can be used to evaluate the severity of the fault. If the chattering signal's power spectrum exceeds the threshold, it indicates a model mismatch in the system. Additionally, it is possible to acquire the frequency content of system states (such as natural frequencies) to be used for mismatch identification.

Since the threshold plays a key role in correctly detecting mismatch, it must be selected by taking account of system's measurement and process noise levels as well as the required confidence interval based on the probability distribution of the power spectrum of chattering signal. Figure 3-3 conceptually illustrates how the threshold is chosen based on a trade-off between reducing the chance of missing model mismatches and avoiding false alarms regarding the PDF of the chattering's power

spectrum for both normal and mismatch conditions. Under normal conditions, a higher level of noise leads to a heavier tail in the PDF, which in turn, increases the likelihood of missed detection and false alarm. However, a higher level of mismatch corresponds to a larger shift in the PDF, which makes detection easier.

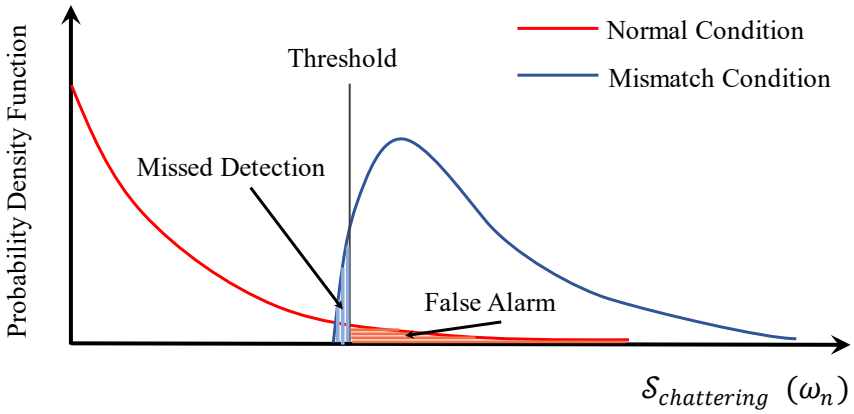

Figure 3-3. PDF of the chattering's power spectrum for normal and mismatched conditions.

3.4.2. Mismatch Identification in a Second-Order System using Spectral Analysis of the Chattering Signal

Let us consider a second-order system as (3.30), with the natural frequency of $\omega_0 = 10Hz$, damping ratio $\zeta = 0.1$, $b = 100$, and $T_s = 0.001s$. The process and measurement noise are assumed to be independent white zero-mean Gaussian with the following covariance matrices:

$$\boldsymbol{Q} = \begin{bmatrix} 10^{-8} & 0 \\ 0 & 10^{-6} \end{bmatrix}, \quad \boldsymbol{R}_{low} = \begin{bmatrix} 10^{-8} & 0 \\ 0 & 10^{-6} \end{bmatrix}, \quad \boldsymbol{R}_{high} = \begin{bmatrix} 10^{-6} & 0 \\ 0 & 10^{-4} \end{bmatrix}.$$

In order to study the impact of noise level on mismatch identification, two levels of measurement noise are considered with one being 10 times higher than the other. Under normal conditions, system matrices are obtained as below:

$$\widehat{\boldsymbol{A}} = \boldsymbol{A} = \begin{bmatrix} 1 & 0.001 \\ -3.1978 & 0.9887 \end{bmatrix}, \quad \widehat{\boldsymbol{B}} = \boldsymbol{B} = \begin{bmatrix} 0 \\ 0.1 \end{bmatrix}, \quad \widehat{\boldsymbol{C}} = \boldsymbol{C} = \begin{bmatrix} 1 & 0 \\ 0 & 1 \end{bmatrix} \tag{3.62}$$

A unit step is applied as the input, and system's behavior is observed for 4 seconds. Since $\boldsymbol{T_s = 0.001s}$, simulation generates 4000 data points over 4 seconds. Figure 3-4 displays the power spectrum of the chattering signal for both states under normal conditions. As shown, the higher noise level requires a higher threshold. Higher measurement noise skews the power spectrum more, increasing the power density in high frequencies. The shift property in equation (3.52) is the cause of skewness. The power spectrum of the chattering signal remains below the threshold for the $\boldsymbol{0.1\%}$ false alarm level (99.9% confidence interval from chi-squared distribution), but for the $\boldsymbol{1\%}$ level, there are several false alarms in high frequencies, which is acceptable for 500 samples. To avoid false alarms completely, the number of samples ($\boldsymbol{N}$) should be taken into account when selecting $\boldsymbol{\alpha}$. A conservative upper bound for the probability of false alarm in all frequencies is obtained as below:

$$\begin{aligned} &\Pr\left(\begin{array}{c} \left(\mathcal{S}_{chattering_i}(\omega_1) > threshold_i\right) \cup \left(\mathcal{S}_{chattering_i}(\omega_1) > threshold_i\right) \\ \cup \ldots \cup \left(\mathcal{S}_{chattering_i}\left(\omega_{\frac{N}{2}}\right) > threshold_i\right) \end{array} \middle| Normal\ Condition \right) \\ &\leq \sum_{n=1}^{N/2} \Pr\left(\mathcal{S}_{chattering_i}(\omega_n) > threshold_i \middle| Normal\ Condition\right) \leq \frac{N}{2}\alpha\% \end{aligned} \tag{3.63}$$

In Figure 3-5, the power spectrum of the chattering signal for the second state, $\boldsymbol{chattering_2}$, has been used to identify model mismatch. In this case, a very small change in natural frequency ($\boldsymbol{\omega_0 = 11\,Hz}$ compared to $\boldsymbol{\omega_0 = 10\,Hz}$ for normal condition) is considered, while all other parameters remain unchanged. Accordingly, the state matrix of the system will change to $\boldsymbol{A} = \begin{bmatrix} 1 & 0.001 \\ -4.7769 & 0.9862 \end{bmatrix}$, while input

and measurement matrices do not change ($\widehat{\boldsymbol{B}} = \boldsymbol{B}$, $\widehat{\boldsymbol{C}} = \boldsymbol{C}$). It can be seen from (3.23) or (3.50) that $\boldsymbol{chattering_1}$will not change when only ω_0 changes. Thus, the mismatch is not observable in $\boldsymbol{chattering_1}$.

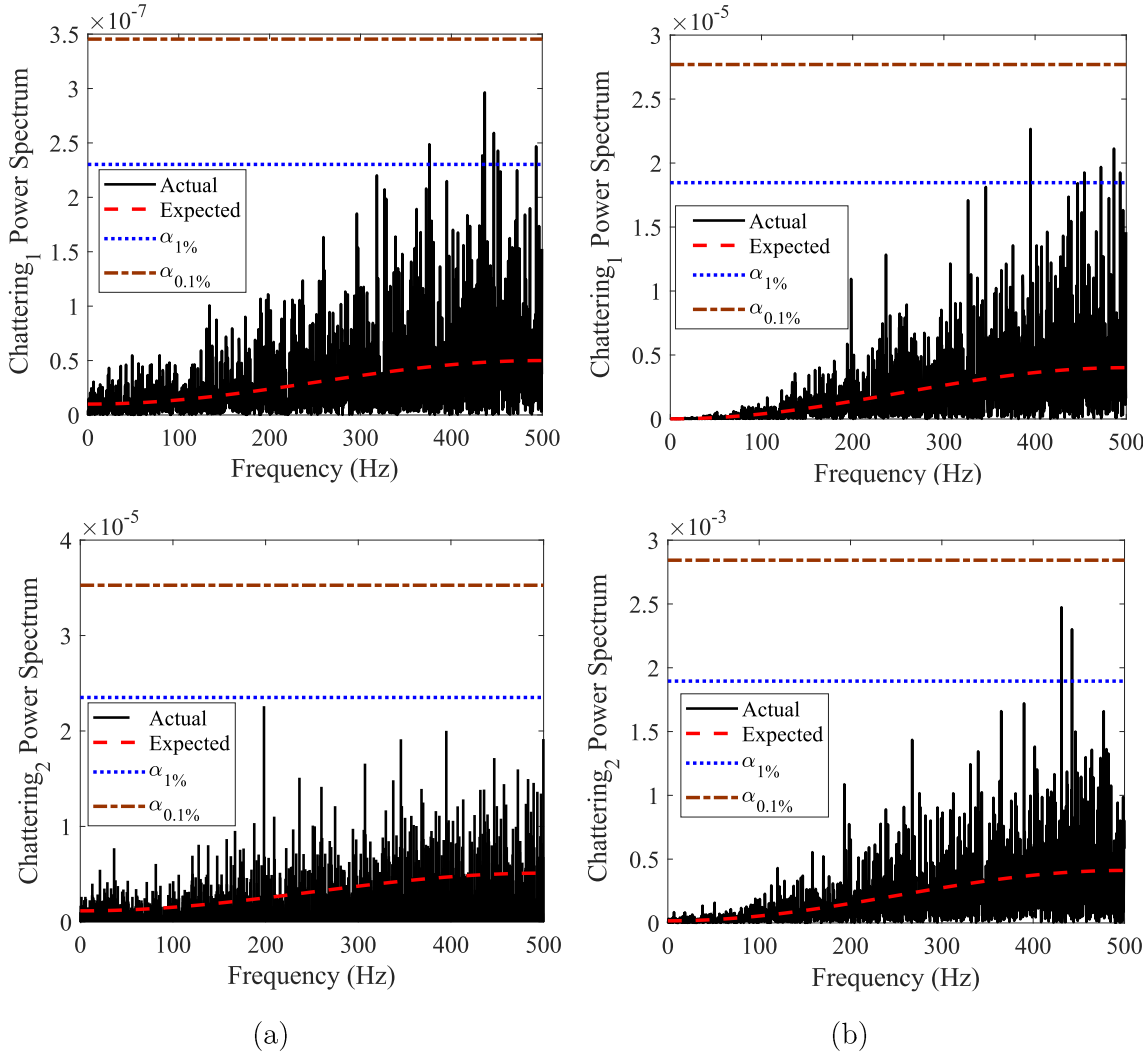

Figure 3-4. Power spectrum of the chattering signal under normal conditions for (a) low measurement noise level and (b) high measurement noise level, where $\boldsymbol{\alpha}$ denotes the error probability.

As shown, the mismatch causes a spike in the spectral density at 11 Hz, which coincides with the natural frequency of the actual system. For the high measurement

noise level shown in Figure 3-5(b), this peak is lower than the threshold, which means it cannot be separated from the noise effect. Using the expected power spectrum is one strategy to resolve this issue. For this purpose, using the idea of Monte Carlo simulation, average of the spectrogram is obtained for many realizations of the same event with the same input and identical conditions. Then, the averaged power spectrum of the noise will converge to the expected value, while the peak at 11 Hz remains the same as demonstrated in Figure 3-6. Nevertheless, this approach cannot be used for real-time mismatch identification.

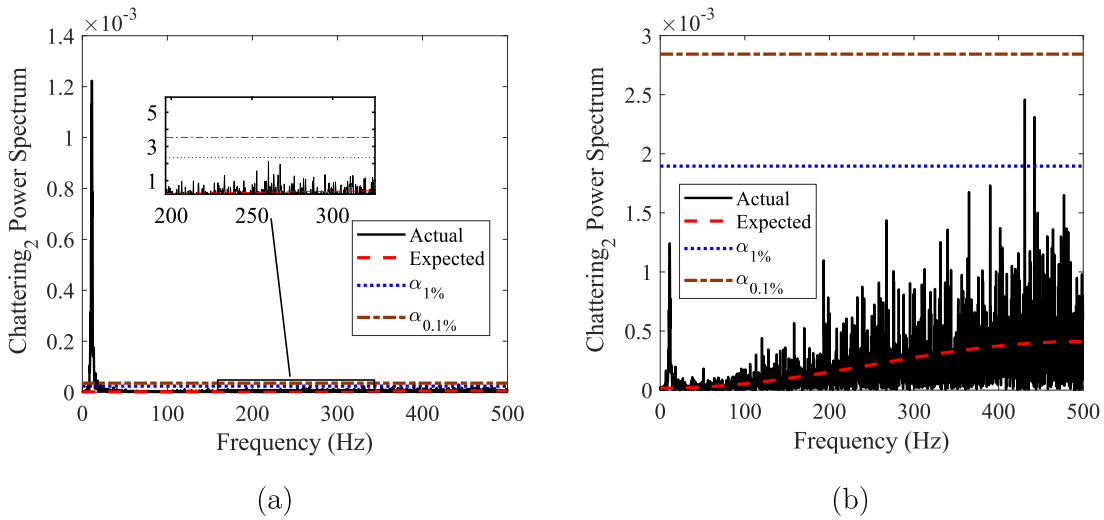

Figure 3-5. Power spectrum of the chattering signal with a mismatch ($\omega_0 = 11Hz$) for (a) low measurement noise level and (b) high measurement noise level, where α denotes the error probability.

Figure 3-7 depicts the power spectrum of the chattering for different levels of mismatch, where the natural frequency of the real system is changed to $\omega_0 = 9Hz, 12Hz,$ and $15\,Hz$ as opposed to the nominal model with $\omega_0 = 10Hz$. Results demonstrate that the proposed approach is capable of separating various levels of mismatch and indicating the intensity of the mismatch based on the amplitude of

the peak. As mentioned previously, frequency resolution of the spectrogram depends on the duration of data gathering and the sampling rate.

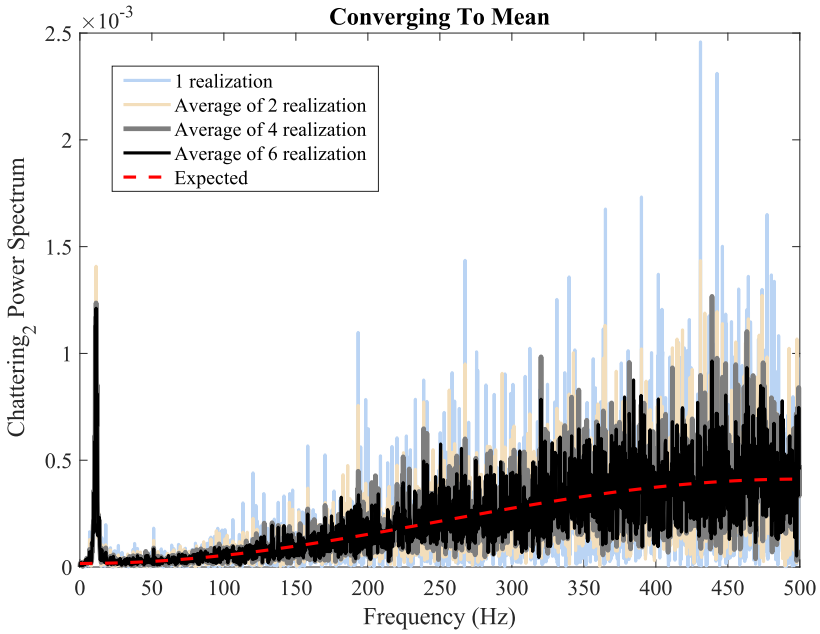

Figure 3-6. Detection of mismatch by averaging over different realizations.

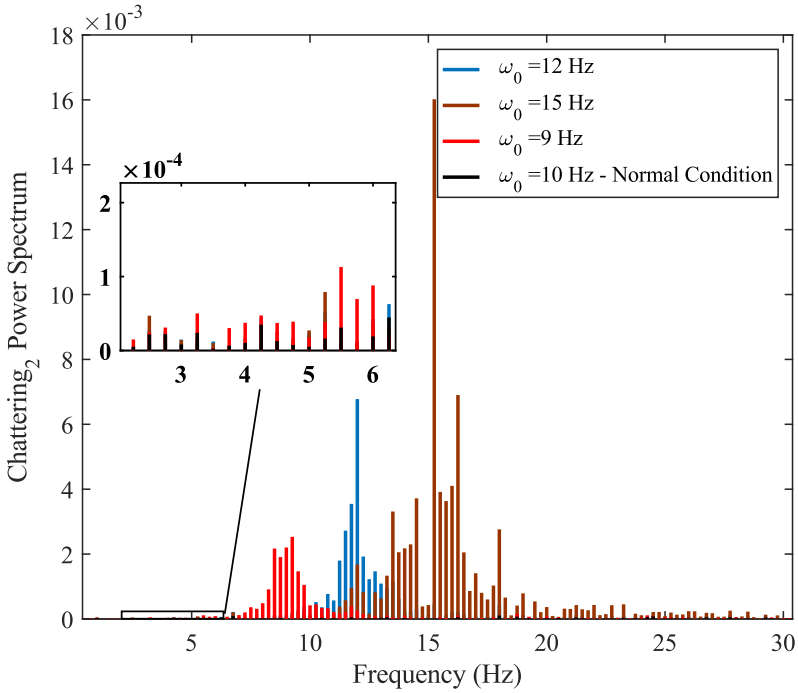

Figure 3-7. Power spectrum of the chattering signal for different levels of mismatch.

3.4.3. Extract Temporal Information of the Mismatch from the Spectrogram of The Chattering Signal

Frequency content of the chattering signal changes when a mismatch or fault occurs in a system. Therefore, it would be beneficial for mismatch detection to extract the temporal information about the frequency content of nonstationary signals. Time-varying spectrum, also known as the spectrogram, is a powerful tool to recover the temporal information along with the frequency content of the signal. Two well-known techniques can be deployed to generate the spectrogram: the Short-Time Fourier Transform (STFT) and the wavelet transform. The STFT method is used in this part to identify the mismatch from the chattering signal.

Let us assume the following scenario for the general second-order system presented in (3.30), where the process and measurement noise are independent white zero-mean Gaussian with $\boldsymbol{Q} = \begin{bmatrix} 10^{-8} & 0 \\ 0 & 10^{-6} \end{bmatrix}$ and $\boldsymbol{R} = \begin{bmatrix} 10^{-6} & 0 \\ 0 & 10^{-4} \end{bmatrix}$:

- Under normal conditions, the natural frequency of the system is 5 Hz with no damping ratio.
- For the first 2 seconds, a model mismatch is introduced to the system by changing the natural frequency to 8Hz.
- Then, for 2 seconds system goes back to the normal condition.
- Then again, for 2 seconds, a model mismatch is introduced, this time by changing the damping ratio to 0.1.
- Finally, the system becomes normal again until the end of the simulation.

According to the Heisenberg-Gabor limit, the periodical and temporal resolution of the spectrogram, which are both governed by the STFT window, have an inverse

relationship. A long window improves the frequency resolution but decreases the temporal resolution and vice versa. Therefore, the length of the window should be chosen carefully based on the application at hand. For this problem, the length of the window has been chosen to be one second, which gives a 1 Hz frequency resolution and 1 second time resolution. The shift time is set to be 0.2s (or 0.8s overlap) to have a sharper edge for detecting the start and end of each mismatch period, and the Hamming window function is used as the taper. The spectrogram of the chattering signal is shown in Figure 3-8 for two input signals: a unit constant function and a step function.

Results accurately pinpoint the frequency and damping mismatches as well as their temporal details. Note that for a constant input, the effect of damping ratio mismatch fades away after a while, because the system stops moving due to damping. However, when the system is excited at $t=5s$, with the step function input, the impact of the mismatch will become visible in the chattering signal. This shows the importance of the persistence excitation specially when system has a large damping.

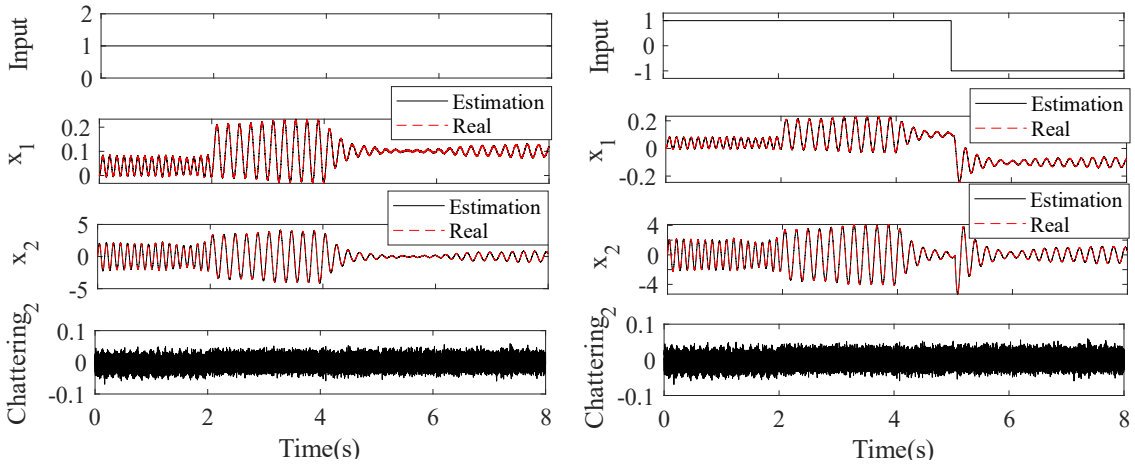

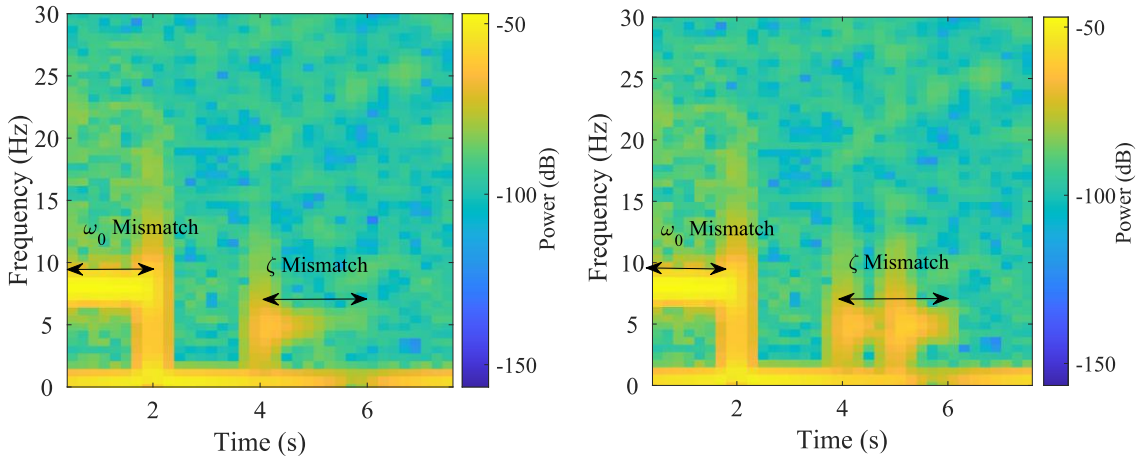

Figure 3-8. Mismatch identification using the spectrogram of the chattering signal for (a) a constant unit input and (b) a step function input.

3.5. Simulation Results for Fault Detection in an Electro-Hydraulic Actuator

The discrete model of the EHA system as described in [40] is used to illustrate the application of the suggested approach for identifying leakage, friction, and bulk modulus mismatch faults. The EHA is a third-order system with state variables that correspond to its position, velocity, and differential pressure, as given in the following state-space model:

$$\begin{cases} x_1(k+1) = x_1(k) + T_s x_2(k) + v_1(k) \\ x_2(k+1) = \left(1 - \frac{T_s a}{M}\right) x_2(k) + \frac{T_s A_c}{M} x_3(k) + v_2(k) \\ x_3(k+1) = \left(1 - \frac{T_s \beta_e L_t}{V_0}\right) x_3(k) + \frac{T_s \beta_e D_p}{V_0} u(k) - \frac{T_s \beta_e A_c}{V_0} x_2(k) + v_3(k) \end{cases}, \quad (3.64)$$

$$\begin{cases} z_1(k) = x_1(k) + w_1(k) \\ z_2(k) = x_2(k) + w_2(k), \\ z_3(k) = x_3(k) + w_3(k) \end{cases}$$

where T_s is the sampling time, which is assumed to be $0.001s$, $\boldsymbol{v}(k)$ and $\boldsymbol{w}(k)$ are zero-mean white Gaussian noise with the following covariance matrices:

$$\begin{aligned} \boldsymbol{v}\boldsymbol{v}^{\mathsf{T}} = \boldsymbol{Q} &= \begin{bmatrix} 10^{-12} & 0 & 0 \\ 0 & 10^{-6} & 0 \\ 0 & 0 & 1 \end{bmatrix}, \\ \boldsymbol{w}\boldsymbol{w}^{\mathsf{T}} = \boldsymbol{R} &= \begin{bmatrix} 10^{-10} & 0 & 0 \\ 0 & 10^{-6} & 0 \\ 0 & 0 & 10^{6} \end{bmatrix}. \end{aligned} \tag{3.65}$$

Table 3-1 provides the nominal values of the parameters in the state-space model (64) [41]. When a leakage fault, friction fault, or bulk modulus mismatch occurs in the system, it causes a change in the associated parameter values L_t, a, or β_e. Following [41], Table 6-1 summarizes the mismatch scenarios, which are considered to evaluate the ability of the proposed method for handling different levels of defects and faults. This table also shows the corresponding changes in system's dynamics for each fault regarding damping ratio and natural frequency with respect to their nominal values presented in Table 3-1.

Table 3-1: EHA Parameters.

Physical Significance	Parameter	Value
Piston Area	A_c	1.52×10^{-3} m^2
Pump Displacement	Dp	5.57×10^{-7} m^3
Mass	M	7.38 kg
Leakage Coefficient	L_t	$4.8 \times 10^{-12} \frac{m^3}{s.pa}$
Friction Coefficient	a	$2144\, N.s/m$
Bulk Modulus	β_e	5×10^8 Pa
System Volume	V_0	1.08×10^{-3} m^3

Table 3-2: Fault Levels.

Fault	**Level**	**Affected Parameter**	**Value**	**Natural Frequency**	**Damping Ratio**
Healthy	*N/A*	*N/A*	N/A	38.9Hz	0.5924
Leakage	*Minor*	L_t	$3\times10^{-11}\frac{m^3}{s.pa}$	38.43Hz	0.5895
	Medium	L_t	$6\times10^{-11}\frac{m^3}{s.pa}$	37.88Hz	0.5861
	Major	L_t	$9\times10^{-11}\frac{m^3}{s.pa}$	37.32Hz	0.5826
Friction	*Minor*	a	$4000\ N.s/m$	38.82Hz	1.1091
	Major	a	$7000\ N.s/m$	38.7Hz	1.9484
Bulk Modulus	*50% down*	β_e	$0.5\beta_e$	27.5Hz	0.8392
	25% down	β_e	$0.75\beta_e$	33.69Hz	0.6846
	25% up	β_e	$1.25\beta_e$	43.49Hz	0.5295
	50% up	β_e	$1.5\beta_e$	47.64Hz	0.4830

The system matrices are obtained from (3.64) as follows:

$$\widehat{\boldsymbol{A}}=\begin{bmatrix}0 & T_s & 0\\ 0 & 1-\frac{T_s a}{m} & \frac{T_s A_c}{m}\\ 0 & \frac{T_s A_c \beta_e}{V_0} & 1-\frac{T_s \beta_e L_t}{V_0}\end{bmatrix},\quad \widehat{\boldsymbol{B}}=\begin{bmatrix}0\\ 0\\ \frac{T_s \beta_e D_p}{V_0}\end{bmatrix},\quad \widehat{\boldsymbol{C}}=\begin{bmatrix}1 & 0 & 0\\ 0 & 1 & 0\\ 0 & 0 & 1\end{bmatrix}. \tag{3.66}$$

Substituting (3.65) and (3.66) into (3.55), (3.60), and (3.61), the expected value and the threshold can be calculated for the power spectrum of the chattering signal under normal conditions. An input chirp signal with a frequency ranging from 10 to 100Hz is used to excite the system below and above its natural frequency. Figure 3-9 shows the power spectrum of the chattering signal under the healthy condition. For the error probability $\alpha = 0.1\%$, power spectrum of the chattering signal follows the expected value trend and remains below the threshold for the corresponding

chattering signals of the three state variables. For $\alpha = 1\%$, there are several false alarms in high frequencies, which would be acceptable considering the number of data points (*N=4000*). However, these false alarms can be avoided by a lower level of α using equation (3.63).

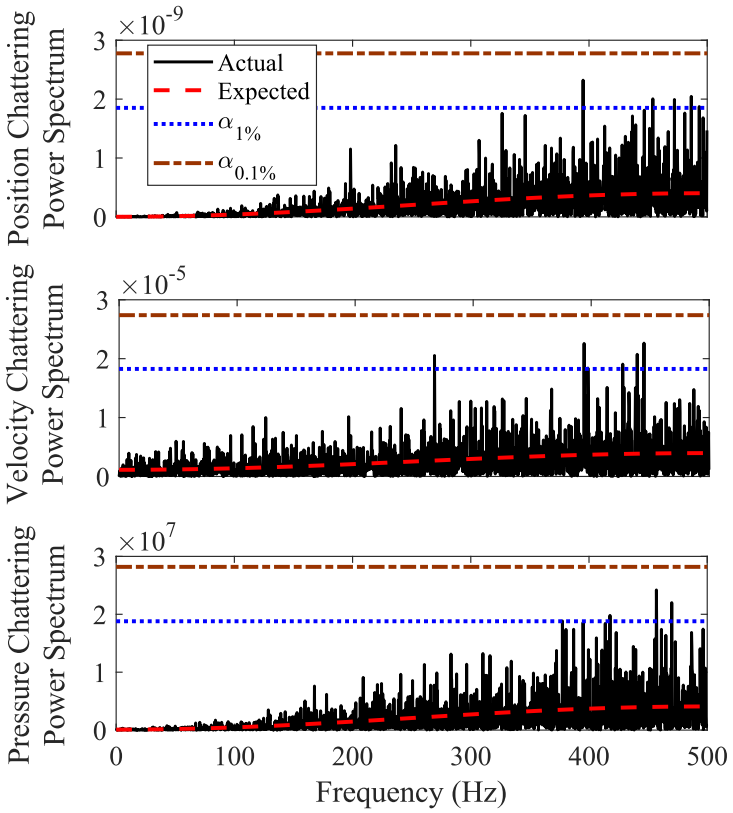

Figure 3-9. Power spectrum of the chattering signal for the EHA system under the healthy condition, where α denotes the error probability.

Ignoring the negligible impact of initial error $\boldsymbol{e_z}(0|0)$ in (3.23), the chattering signal of the EHA for leakage condition is obtained as:

$$\begin{bmatrix} chattering_1(k+1) \\ chattering_2(k+1) \\ chattering_3(k+1) \end{bmatrix}$$
$$= \begin{bmatrix} v_1(k) + T_s w_2(k) + w_1(k+1) \\ v_2(k) + \left(1 - \frac{T_s a}{m}\right) w_2(k) + \left(\frac{T_s A_c}{m}\right) w_3(k) + w_2(k+1) \\ \left(1 - \frac{T_s \beta_e \Delta L_t}{V_0}\right) x_3(k) + v_3(k) + \left(\frac{T_s A_c \beta_e}{V_0}\right) w_2(k) + \left(1 - \frac{T_s \beta_e L_t}{V_0}\right) w_3(k) + w_3(k+1) \end{bmatrix}, \quad (3.67)$$

where ΔL_t is the mismatch in the leakage coefficient due to leakage fault. As shown in (3.67), leakage fault is observable from the chattering signal of the third state variable that represents differential pressure. Thus, the power spectrum of the pressure chattering signal is used for leakage fault detection. Figure 3-10 shows that the power spectrum of the chattering signal deviates from the expected value when leakage occurs, with higher leakage levels leading to a larger divergence. However, only a major leakage can be detected based on the 0.1% threshold, derived from system noise. This issue can be improved to some extent by deploying a more accurate sensor with a lower level of noise. Additionally, following the idea of Monte Carlo simulation, as shown in Figure 3-6, the experiment can be repeated, and average of the power spectrum can be calculated. Then, detection can be performed based on the expected power spectrum. As indicated in Table 6-1, leakage has a small Impact on natural frequency. Hence, power spectrum has a peak at the natural frequency of the system.

Similar to (3.67), the following equation is used to obtain the chattering signal when there is a friction fault:

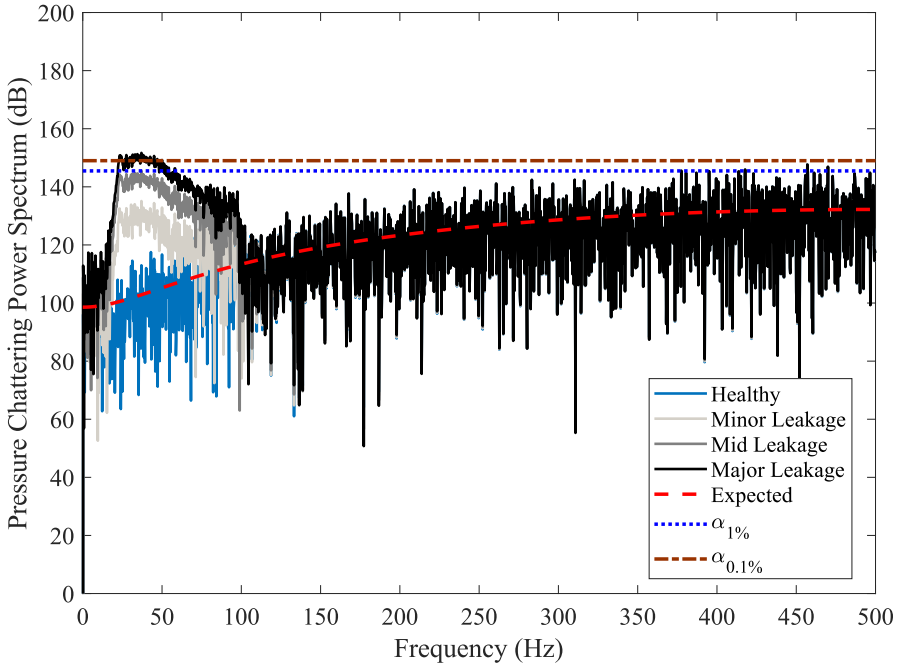

Figure 3-10. Leakage fault detection using spectral analysis of the pressure chattering signal.

$$\begin{bmatrix} chattering_1(k+1) \\ chattering_2(k+1) \\ chattering_3(k+1) \end{bmatrix} = \begin{bmatrix} v_1(k) + T_s w_2(k) + w_1(k+1) \\ -\frac{T_s \Delta a}{m} x_2(k) + v_2(k) + \left(1 - \frac{T_s a}{m}\right) w_2(k) + \left(\frac{T_s A_c}{m}\right) w_3(k) + w_2(k+1) \\ v_3(k) + \left(\frac{T_s A_c \beta_e}{V_0}\right) w_2(k) + \left(1 - \frac{T_s \beta_e L_t}{V_0}\right) w_3(k) + w_3(k+1) \end{bmatrix}, \quad (3.68)$$

where Δa is the mismatch in the friction coefficient due to the fault. Power spectrum of the velocity chattering signal is employed for friction fault identification. As demonstrated in (3.68), friction fault can be observed from the chattering signal of the second state variable that represents velocity. Figure 3-11 shows that both minor and major frictions can be detected from spectral analysis. The friction fault has a negligible impact on the natural frequency, but it increases the damping ratio of the

system and makes it overdamped (Table 6-1). Power spectrum does not peak at the natural frequency, because the system becomes overdamped for minor and major friction faults.

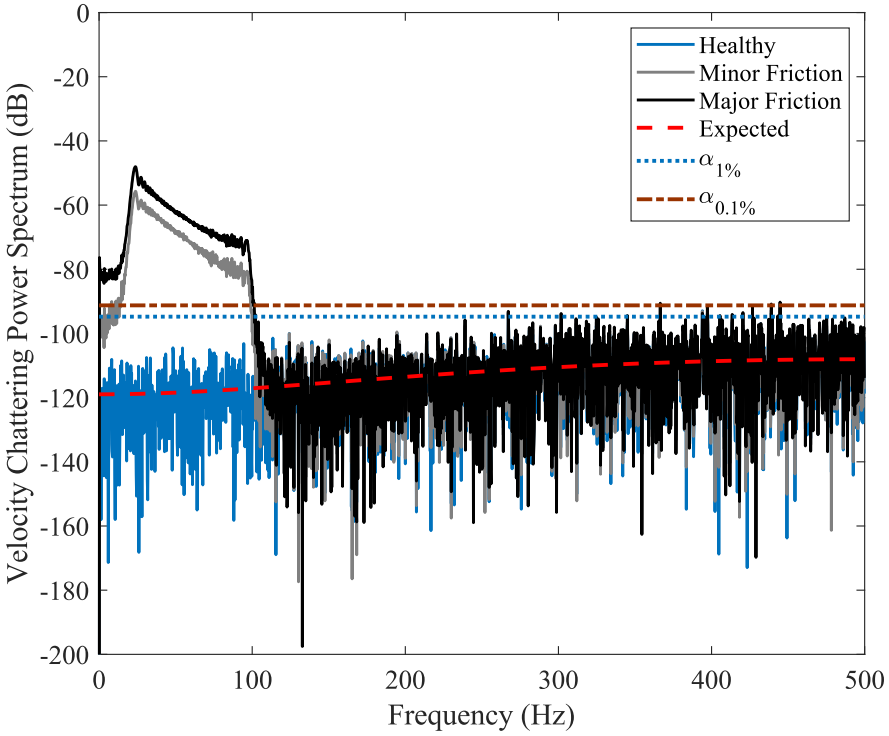

Figure 3-11. Friction fault detection using spectral analysis of the velocity chattering signal.

The chattering for the bulk modulus mismatch is obtained from the following equation:

$$\begin{bmatrix} chattering_1(k+1) \\ chattering_2(k+1) \\ chattering_3(k+1) \end{bmatrix} = \begin{bmatrix} v_1(k) + T_s w_2(k) + w_1(k+1) \\ v_2(k) + \left(1 - \frac{T_s a}{m}\right) w_2(k) + \left(\frac{T_s A_c}{m}\right) w_3(k) + w_2(k+1) \\ \frac{T_s A_c \Delta\beta_e}{V_0} x_2(k) - \frac{T_s \Delta\beta_e L_t}{V_0} x_3(k) + \frac{T_s \Delta\beta_e D_p}{V_0} u(k) + v_3(k) + \left(\frac{T_s A_c \beta_e}{V_0}\right) w_2(k) + \left(1 - \frac{T_s \beta_e L_t}{V_0}\right) w_3(k) + w_3(k+1) \end{bmatrix}, \quad (3.69)$$

where $\Delta\beta_e$ is the mismatch in the bulk modulus due to the fault. The bulk modulus mismatch is detectable from the pressure chattering signal, as indicated in (3.69). Figure 3-12 shows that the bulk modulus mismatch can be identified using the

deviation from the expected power spectrum. Furthermore, a larger mismatch leads to a higher degree of deviation. According to Table 6-1, a higher bulk modulus increases the natural frequency and decreases the damping ratio of the system. This phenomenon is illustrated in Figure 3-12.

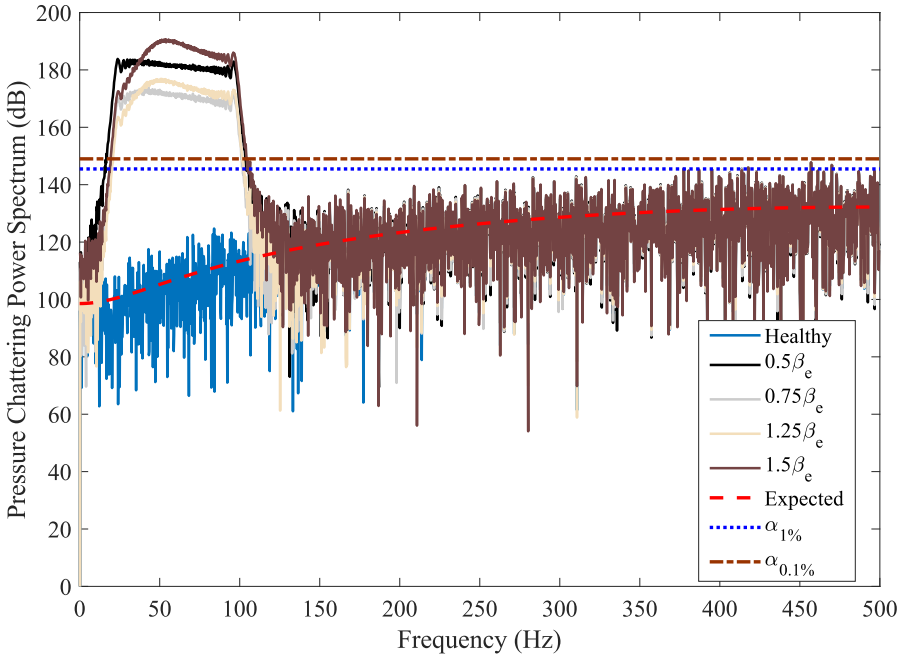

Figure 3-12. Bulk modulus mismatch detection using the spectral analysis of the pressure chattering signal.

3.6. Conclusion

In addition to the innovation vector, which is used in filtering algorithms to correct the predicted state vector in light of the most recent estimation, SVSF benefits from a secondary set of indicators that are the chattering signals associated with different state variables. This paper entertained the idea of using the chattering signal for fault detection and model mismatch identification. In this paper, mathematical expressions were derived for chattering signal of the SVSF for both full-state and partial-state measurement scenarios. Spectrogram of the chattering signal was investigated to

extract temporal and spectral information. Building on the idea of Monte Carlo simulation, and taking account of process and measurement noise characteristics, expected value of the chattering signal's power spectrum was obtained under normal conditions. It was proposed to select a threshold for mismatch identification based on a trade-off between avoiding false alarms and minimizing the chance of missing any event that leads to a change in the system under study and causes model mismatch such as fault occurrence. The proposed strategy for choosing this threshold takes the probability distribution of the chattering signal's power spectrum into consideration. A confidence interval is determined using such a distribution that paves the way for fault detection using one realization of the sequence of events, which is suitable for real-time applications. Furthermore, to recover the temporal information regarding a mismatch, the chattering signal can be analyzed using the short-time Fourier transform. Effectiveness of the proposed method for fault detection and mismatch identification was demonstrated through considering a number of scenarios for a typical second order system and an electro-hydraulic actuator. Furthermore, the proposed framework allows for determining the severity of the mismatch. Future research can study the implementation of this approach within a closed-loop system for fault diagnosis and development of a Fault Tolerant Control System (FTCS). Considering that the majority of closed-loop systems are designed to demonstrate overdamped dynamics and regarding the fact that the input excitation originates from the controller, addressing challenges in achieving the persistent excitation necessary for fault detection calls for an in-depth exploration.

3.7. References

[1] Y. Bar-Shalom, X. R. Li, and T. Kirubarajan, *Estimation with applications to*

tracking and navigation: theory algorithms and software. John Wiley & Sons, 2004.

[2] E. A. Wan and R. Van Der Merwe, "The unscented Kalman filter for nonlinear estimation," in *Proceedings of the IEEE 2000 Adaptive Systems for Signal Processing, Communications, and Control Symposium (Cat. No. 00EX373)*, 2000, pp. 153–158.

[3] B. Ristic, S. Arulampalam, and N. Gordon, *Beyond the Kalman filter: Particle filters for tracking applications*. Artech house, 2003.

[4] D. Simon, *Optimal state estimation: Kalman, H infinity, and nonlinear approaches*. John Wiley & Sons, 2006.

[5] I. Hwang, S. Kim, Y. Kim, and C. E. Seah, "A survey of fault detection, isolation, and reconfiguration methods," *IEEE Trans. Control Syst. Technol.*, vol. 18, no. 3, pp. 636–653, 2009.

[6] R. J. Patton and J. Chen, "Robust fault detection using eigenstructure assignment: A tutorial consideration and some new results," in *Proceedings of the 30th IEEE Conference on Decision and Control*, 1991, vol. 3, pp. 2242–2247.

[7] R. J. Patton and J. Chen, "On eigenstructure assignment for robust fault diagnosis," *Int. J. Robust Nonlinear Control IFAC-Affiliated J.*, vol. 10, no. 14, pp. 1193–1208, 2000.

[8] K. Watanabe and D. M. Himmelblau, "Instrument fault detection in systems with uncertainties," *Int. J. Syst. Sci.*, vol. 13, no. 2, pp. 137–158, 1982.

[9] J. Wünnenberg and P. M. Frank, "Sensor fault detection via robust observers," in *System Fault Diagnostics, Reliability and Related Knowledge-Based Approaches: Volume 1 Fault Diagnostics and Reliability Proceedings of the First European Workshop on Fault Diagnostics, Reliability and Related Knowledge-Based Approaches, Island of Rhodes,* 1987, pp. 147–160.

[10] J. Gertler and D. Singer, "A new structural framework for parity equation-based failure detection and isolation," *Automatica*, vol. 26, no. 2, pp. 381–388, 1990.

[11] H. Ye, G. Wang, and S. X. Ding, "A new parity space approach for fault

detection based on stationary wavelet transform," *IEEE Trans. Automat. Contr.*, vol. 49, no. 2, pp. 281–287, 2004.

[12] H. M. Odendaal and T. Jones, "Actuator fault detection and isolation: An optimised parity space approach," *Control Eng. Pract.*, vol. 26, pp. 222–232, 2014.

[13] P. M. Frank and X. Ding, "Frequency domain approach to optimally robust residual generation and evaluation for model-based fault diagnosis," *Automatica*, vol. 30, no. 5, pp. 789–804, 1994.

[14] J. Stoustrup and H. H. Niemann, "Fault estimation—a standard problem approach," *Int. J. Robust Nonlinear Control IFAC-Affiliated J.*, vol. 12, no. 8, pp. 649–673, 2002.

[15] R. H. Chen, D. L. Mingori, and J. L. Speyer, "Optimal stochastic fault detection filter," *Automatica*, vol. 39, no. 3, pp. 377–390, 2003.

[16] R. K. Mehra and J. Peschon, "An innovations approach to fault detection and diagnosis in dynamic systems," *Automatica*, vol. 7, no. 5, pp. 637–640, 1971.

[17] P. D. Hanlon and P. S. Maybeck, "Characterization of Kalman filter residuals in the presence of mismodeling," *IEEE Trans. Aerosp. Electron. Syst.*, vol. 36, no. 1, pp. 114–131, 2000.

[18] Y. Chinniah, R. Burton, and S. Habibi, "Failure monitoring in a high performance hydrostatic actuation system using the extended Kalman filter," *Mechatronics*, vol. 16, no. 10, pp. 643–653, 2006.

[19] S. A. Gadsden, Y. Song, and S. R. Habibi, "Novel model-based estimators for the purposes of fault detection and diagnosis," *IEEE/ASME Trans. Mechatronics*, vol. 18, no. 4, pp. 1237–1249, 2013.

[20] H. H. Afshari, S. A. Gadsden, and S. R. Habibi, "Robust fault diagnosis of an electro-hydrostatic actuator using the novel dynamic second-order SVSF and IMM strategy," *Int. J. Fluid Power*, vol. 15, no. 3, pp. 181–196, 2014.

[21] P. D. Hanlon and P. S. Maybeck, "Multiple-model adaptive estimation using a residual correlation Kalman filter bank," *IEEE Trans. Aerosp. Electron. Syst.*, vol. 36, no. 2, pp. 393–406, 2000.

[22] S. Kim, J. Choi, and Y. Kim, "Fault detection and diagnosis of aircraft

actuators using fuzzy-tuning IMM filter," *IEEE Trans. Aerosp. Electron. Syst.*, vol. 44, no. 3, pp. 940–952, 2008.

[23] S. A. Gadsden, S. R. Habibi, and T. Kirubarajan, "A novel interacting multiple model method for nonlinear target tracking," in *2010 13th International Conference on Information Fusion*, 2010, pp. 1–8.

[24] Q. Zhang, "Adaptive Kalman filter for actuator fault diagnosis," *Automatica*, vol. 93, pp. 333–342, 2018.

[25] X. Sun, X. Wang, and S. Lin, "Multi-Fault Diagnosis Approach Based on Updated Interacting Multiple Model for Aviation Hydraulic Actuator," *Information*, vol. 11, no. 9, p. 410, 2020.

[26] R. Isermann, "Process fault detection based on modeling and estimation methods—A survey," *automatica*, vol. 20, no. 4, pp. 387–404, 1984.

[27] R. Isermann, "Supervision, fault-detection and fault-diagnosis methods—an introduction," *Control Eng. Pract.*, vol. 5, no. 5, pp. 639–652, 1997.

[28] E. Che Mid and V. Dua, "Model-based parameter estimation for fault detection using multiparametric programming," *Ind. Eng. Chem. Res.*, vol. 56, no. 28, pp. 8000–8015, 2017.

[29] V. Stojanovic and D. Prsic, "Robust identification for fault detection in the presence of non-Gaussian noises: application to hydraulic servo drives," *Nonlinear Dyn.*, vol. 100, no. 3, pp. 2299–2313, 2020.

[30] A. Saeedzadeh, S. Habibi, and M. Alavi, "A Model-Based FDD Approach for an EHA Using Updated Interactive Multiple Model SVSF," in *Fluid Power Systems Technology*, 2021, vol. 85239, p. V001T01A006.

[31] M. Al-Shabi, S. A. Gadsden, and S. R. Habibi, "Kalman filtering strategies utilizing the chattering effects of the smooth variable structure filter," *Signal Processing*, vol. 93, no. 2, pp. 420–431, 2013.

[32] L. Ortega, J. Vilà-Valls, E. Chaumette, G. Pagès, and F. Vincent, "Robust Tracking under Measurement Model Mismatch via Linearly Constrained Extended Kalman Filtering," in *2020 59th IEEE Conference on Decision and Control (CDC)*, 2020, pp. 2924–2929.

[33] P. Kaminski, A. Bryson, and S. Schmidt, "Discrete square root filtering: A

survey of current techniques," *IEEE Trans. Automat. Contr.*, vol. 16, no. 6, pp. 727–736, 1971.

[34] G. J. Bierman, *Factorization methods for discrete sequential estimation*. Courier Corporation, 2006.

[35] S. Habibi, "The smooth variable structure filter," *Proc. IEEE*, vol. 95, no. 5, pp. 1026–1059, 2007.

[36] S. A. Gadsden and S. R. Habibi, "A new robust filtering strategy for linear systems," *J. Dyn. Syst. Meas. Control*, vol. 135, no. 1, p. 14503, 2013.

[37] M. Al-Shabi, S. A. Gadsden, and S. R. Habibi, "Kalman filtering strategies utilizing the chattering effects of the smooth variable structure filter," *Signal Processing*, vol. 93, no. 2, pp. 420–431, 2013.

[38] S. Habibi, "The smooth variable structure filter," *Proc. IEEE*, vol. 95, no. 5, pp. 1026–1059, 2007.

[39] L. H. Koopmans, *The spectral analysis of time series*. Elsevier, 1995.

4. A Robust Model-Based Strategy for Real-time Fault Detection and Diagnosis in an Electro-Hydraulic Actuator Using Updated Interactive Multiple Model Smooth Variable Structure Filter

Ahsan Saeedzadeh*[1], Saeid Habibi[1], Marjan Alavi[2], Peyman Setoodeh[1]

[1] Department of Mechanical Engineering, McMaster University, Hamilton, ON, Canada

[2] W Booth School of Engineering Practice and Technology, McMaster University, Hamilton, ON, Canada

Published in Journal of Dynamic Systems, Measurement, and Control, 2023 1;145(10). DOI: 10.1115/1.4063206. This paper is republished here with permission.

Abstract

In industries where harsh environments and stringent safety requirements are prevalent, the widespread use of applications has made it essential to focus on Fault Detection and Diagnosis (FDD) in hydraulic actuators. To achieve this, Model-based FDD techniques are utilized, which employ estimation tools like observers and filters. However, for many applications, particularly in fluid power systems, observability, and parameter uncertainty pose constraints to extracting information and estimating parameters. To address these issues, an efficient form of Interactive Multiple Model (IMM), called Updated IMM (UIMM), is applied to an Electro-Hydrostatic Actuator (EHA) to detect and isolate persisting friction and leakage faults. The UIMM method progresses through a series of models that correspond to the fault condition's progression instead of considering all models at once (as is done in IMM). This

reduces the number of models running simultaneously, providing two significant benefits: enhanced computational efficiency and avoidance of combinatorial explosion. The Smooth Variable Structure Filter with Variable Boundary Layer (SVSF-VBL) is used for state and parameter estimation in conjunction with UIMM. SVSF-VBL is a reliable suboptimal estimation method that performs better than the Kalman Filter regarding uncertainties related to the system and modeling. The performance of the UIMM method is validated by the simulation of fault conditions for a typical EHA. A Fault Tolerable Control System (FTCS) has been designed to demonstrate the use of the proposed FDD strategy for fault management in a closed-loop system.

Keywords: Electro-Hydraulic Actuator, Fault Detection and Diagnosis, Smooth Variable Structure Filter, Updated Interactive Multiple Model.

4.1. Introduction

Emerging methodologies and technologies in areas such as artificial intelligence, sensors, signal processing, control systems, and real-time computation have paved the way for replacing traditional maintenance methods with automated approaches for fault management. Such approaches can be categorized into two main groups: Model-based Fault Detection and Diagnosis (FDD) and Signal-based FDD. Model-based FDD strategies typically require system models complemented by estimation strategies.

Regarding fluid power systems, since there is a rich literature on the modeling of such systems, model-based FDD has been a popular approach among researchers [6]. This paper proposes a novel model-based FDD algorithm for the Electro-Hydraulic

Actuator (EHA). The EHA includes a closed-loop circuit that controls a linear hydraulic actuator by adjusting the flow rate by changing the speed of a fixed displacement gear pump using an electric motor. This system is commonly used in aerospace as it is more efficient than the conventional servo-valve-controlled hydraulic systems, in terms of its average size and energy consumption. The focus of this study is on detecting leakage and friction, which are the most common faults in the EHA [6]–[10]. In fluid power systems, model-based FDD usually relies on three pillars:

- **Residual-based fault detection:** This approach, which is also known as the observer-based method, compares the predicted value of the output from an observer to the measured output in order to obtain a residual error. If the residual error components exceed the predefined thresholds, faults are detected, and then isolated through further analyses. The core element of this diagnostic system is an observer or a filter [7], [9], [10]. Diagnostic observers are mainly used for estimating the output rather than the state vector as opposed to those used in control. Moreover, open-loop configurations involved in diagnostic observers accentuate the adverse effects of modeling errors [11]. Regardless of the form of implementation, robustness is essential for a diagnostic observer and allows for reducing false alarms [9], [12]–[15]. When a fault occurs, observers, which are designed to be sensitive to that specific type of fault, will provide significant residuals, while residuals of other observers remain insignificant. Perfect fault isolation relies on decoupling observer residuals, which is not always feasible, because of restrictive conditions imposed by the number of faults to be isolated and the number of available sensors. To address this problem, approximate decoupling has been proposed

[11], [12], [16], which solves an optimization problem to enhance the effect of faults on the residuals while minimizing the effect of unknown inputs and uncertainties.

- **Parameter estimation:** It is usually part and parcel of residual analysis and provides useful information for fault diagnosis and quantification. In this regard, various methods have been proposed in the literature including Recursive Least Square (RLS) [17], [18], robust RLS [19], State Augmented Extended Kalman Filter (SAEKF) [20], [21], and Robust Estimation Algorithm (REA) based on SAEKF [22].
- **Adaptive multiple models:** Since observability is a common concern in most fluid power applications including the case study of this paper, adaptive strategies such as Interactive Multiple Model (IMM) estimations have been proposed to address this issue [23]–[26]. The main idea behind such a method is to use a finite number of models to represent different fault conditions. A finite number of filters are run in parallel based on these models, which provide the estimated state vector as well as its corresponding covariance and likelihood. The provided information allows for computing a mode probability for each filter as an indicator of the accuracy of the corresponding model. Then, based on the residuals provided by the models, a probability distribution is computed over the fault models, which is used for fault diagnosis. Multiple-model decision mechanisms can be categorized into two groups:
    - Static: The model is assumed to be fixed during the process, which may not be a realistic assumption in an FDD problem.

- Dynamic: It is assumed that switching can occur in the system over time, which can be modeled as a Markov process.

IMM can be viewed as the optimal dynamic multiple-model estimator [27]. Combinations of the IMM strategy with different filters have achieved excellent performance in FDD applications. These algorithms include the combination of IMM with Kalman Filter (IMM-KF) and variations of the Smooth Variable Structure Filter (SVSF) such as Smooth Variable Structure Filter with Variable Boundary Layer (IMM-SVSF-VBL) [28]. SVSF is a robust state estimation algorithm in the predictor-corrector form, which is based on the variable structure/sliding mode condition [29]. SVSF-VBL is the optimal version of SVSF, in which the width of the smoothing boundary layer is obtained by minimizing the trace of the estimation error covariance matrix [30]. The idea is to use the obtained optimal gain when the a priori estimation error is inside a time-varying smoothing boundary layer but apply a discontinuous corrective action if the error is going outside it.

In this paper, a computationally efficient variation of the IMM, referred to as Updated IMM (UIMM) which is applicable for irreversible faults, has been proposed to combine with robust SVSF-VBL filtering. The resulting FDD strategy, called UIMM-SVSF-VBL, combines the computational effectiveness and improved identifiability of the UIMM strategy with the robustness of SVSF filtering, making it very suited for real-time applications like closed-loop systems. A Fault Tolerant Control System (FTCS) is designed, employing UIMM-SVSF-VBL for state estimation and fault identification, in a closed-loop system. Assuming the occurring faults are persistent, the UIMM algorithm relies on adjusting the deployed models in

a way that each one reflects a single typical fault. In this way, computational efficiency can be improved by reducing the number of models which are used for state estimation at each cycle. Reducing the number of models allows this algorithm to effectively handle multiple faults and reduce false labeling which increases identifiability. In the UIMM, if the system detects a fault, model parameters will be updated for all filters, accordingly. For this purpose, the maximum mode probability among all faulty conditions is compared with the mode probability threshold for its corresponding fault. If it passes the threshold, the fault is detected, and the parameters of all the remaining models are updated considering the detected fault. Then for a fault-tolerant control system, the control law is updated based on the detected fault.

Here, the proposed FDD strategy for the EHA system is built on the following three elements:

- System models for healthy and faulty conditions of a typical EHA system.
- The SVSF-VBL estimation algorithm addresses model uncertainties.
- The UIMM strategy allows multiple models and estimation strategies to work in parallel.

The proposed FDD algorithm is validated via simulations.

The rest of the paper is organized as follows: In section 2, the EHA system is described, and its model is developed. Section 3 presents the SVSF-VBL estimation strategy, which includes one filter for each condition. In section 4, several SVSF-VBL filters are combined in a UIMM structure to complete the FDD strategy. Section 5

compares the results of the proposed FDD strategy with IMM-SVSF-VBL and IMM-KF. Concluding remarks are provided in the last section.

4.2. Electro-Hydraulic Actuator Model

The EHA is more compact and energy-efficient than conventional servo-valve-controlled hydraulic systems also known as Electro-Hydraulic Systems (EHS) [31], [32]. Open-loop hydraulic circuits in EHS require a large external hydraulic supply, leading to several drawbacks, including high energy consumption due to the pumps continuously running and the requirement of an extensive fluid distribution system with a reservoir that increases the weight of the system [33]. Additionally, expensive servo valves are needed for precision control [33]. In contrast, EHA employs a closed-loop circuit where the pump directly controls the position of the hydraulic actuator, resulting in a higher power-to-weight ratio and energy efficiency.

Most EHAs use a variable displacement piston pump, which runs continuously, leading to a slight decrease in energy efficiency and ripple effects that can negatively impact high-precision motion [32]. The EHA studied in this research varies the flow by changing the speed and direction of a fixed displacement gear pump, which produces less ripple since only one gear creates the pumping action at any time. This configuration also has submicron precision position control capability, as reported in the literature [32].

The following EHA model is obtained from data described in a prior work [28] on a prototype EHA developed at the CMHT laboratory. An inner circuit is used to prevent cavitation, which includes an accumulator and three check valves. The inner circuit also provides a conduit for the pump's case drain. A bi-directional relief valve

is installed for safety purposes. The schematic of a prototype EHA system is shown in Figure 2-9. The results presented in this paper are generated using a simulation model of this EHA system in MATLAB. The parameters used in this mathematical model were validated for this system using experimental data in [28].

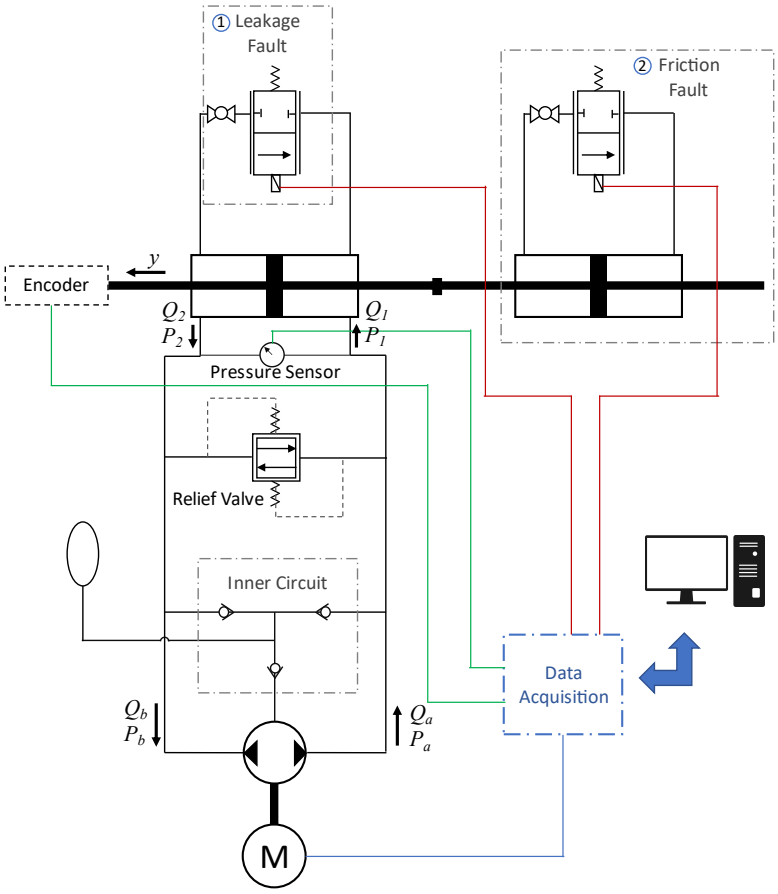

Figure 4-1. Schematic of the electro-hydraulic actuator system.

To introduce the leakage fault, a proportional valve is installed in parallel to the hydraulic cylinder, which is represented by changing the leakage coefficient in the simulation model for leakage fault. Another hydraulic circuit, including a proportional valve and a hydraulic cylinder, is deployed to add friction fault. This is simulated as a change in viscous friction coefficient in the friction fault model through

changing the valve orifice. Considering a control volume on the pump inlet and outlet, the pump flow rate can be calculated as follows:

$$Q_a = D_p\omega_p - L_p(P_a - P_b) - \frac{V_a}{\beta_e}\left(\frac{dP_a}{dt}\right), \tag{4.1}$$

$$Q_a = D_p\omega_p - L_p(P_a - P_b) + \frac{V_b}{\beta_e}\left(\frac{dP_b}{dt}\right), \tag{4.2}$$

where Q_a and Q_b are pump outlet and inlet flowrates, D_p is the pump displacement, P_a and P_b are pump outlet and inlet pressures, respectively, ω_p is the pump speed, L_p is the pump internal leakage coefficient, V_a and V_b denote the fluid volume in the control volume for chambers 1 and 2, respectively (including pump chamber and pipes), and β_e is the effective bulk modulus of the hydraulic fluid. Similarly, the flowrate of cylinder ports is obtained using the following equations:

$$Q_1 = A_c\dot{y} - \frac{V_0 - A_c y}{\beta_e}\left(\frac{dP_1}{dt}\right) - L_{in}(P_1 - P_2) + L_{out}(P_1) \tag{4.3}$$

$$Q_2 = A_c\dot{y} - \frac{V_0 - A_c y}{\beta_e}\left(\frac{dP_2}{dt}\right) + L_{in}(P_1 - P_2) - L_{out}(P_1) \tag{4.4}$$

In these equations, Q_1 and Q_2 are flowrate into and out of cylinder chambers, respectively, y is the cylinder position, A_c is the cylinder cross-section, V_0 is the actuator control volume for each side when placed in its reference central position, L_{in} and L_{out} are the internal and external leakage coefficients in the cylinder, and P_1 and P_2 are cylinder chamber pressures. The accumulator pressure is set to 40psi to prevent cavitation assuming that its associated dynamic effects are negligible [34]. Ignoring external leakage in the pipes and connections, $Q_1 = Q_a$ and $Q_2 = Q_b$, which leads to the following equation:

$$Q_1 + Q_2 = Q_a + Q_b, \tag{4.5}$$

Furthermore, assuming that pressure drops in the pipes are negligible, then $P_1 = P_a$ and $P_2 = P_b$. Let the leakage coefficient be defined as $L_t = L_p + L_{in} + \frac{L_{out}}{2}$ and the nominal actuator volume as $V_0 = V_a + A_c y = V_b - A_c y$. Assuming the actuator is unsaturated and the variance in external load is negligible, $\frac{dP_1}{dt} \approx -\frac{dP_2}{dt}$. Equations (4.1) to (4.5) lead to the following relation between the actuator position and pump speed:

$$D_p \omega_p = A\dot{y} + \frac{V_0}{\beta_e}\left(\frac{dP_1}{dt} - \frac{dP_2}{dt}\right) - L_t(P_1 - P_2). \tag{4.6}$$

According to Newton's second law, the relation between the cylinder position and the differential pressure in the linear actuator is obtained as:

$$(P_1 - P_2)A_c = M\ddot{y} + F_f, \tag{4.7}$$

where M denotes load mass and F_f is the actuator friction, which can be formulated as a second-order quadratic function related to the actuator velocity $\dot{y}$ as follows [33]:

$$F_f = a\dot{y} + (by^2 + c) + sgn(\dot{y}). \tag{4.8}$$

Taking dynamics into account and ignoring the nonlinear portion of the friction equation, the following third-order discrete-time state-space model is obtained for the EHA [34]:

$$\begin{cases} x_1(k+1) = x_1(k) + T_s x_2(k) + v_1(k) \\ x_2(k+1) = \left(1 - \frac{T_s a}{M}\right)x_2(k) + \frac{T_s A_c}{M}x_3(k) + v_2(k) \\ x_3(k+1) = \left(1 - \frac{T_s \beta_e L_t}{V_0}\right)x_3(k) + \frac{T_s \beta_e D_p}{V_0}u(k) - \frac{T_s \beta_e A_c}{V_0}x_2(k) + v_3(k) \end{cases} \tag{4.9}$$

$$\begin{cases} z_1(k) = x_1(k) + w_1(k) \\ z_2(k) = x_3(k) + w_2(k) \end{cases}$$

In this model, the state vector is defined as $\boldsymbol{x} = [y \quad \dot{y} \quad P_1 - P_2]$, measurement signals $z_1(k)$ and $z_2(k)$ are provided by an encoder and a differential pressure sensor, and the process and measurement noise are denoted by $\boldsymbol{v}(k)$ and $\boldsymbol{w}(k)$, respectively. Occurrence of a leakage or friction fault in the system leads to a change in the corresponding parameters L_t or a. The nominal values of the parameters were selected according to [34], which are presented in Table 3-1. Next section provides a brief account of the SVSF.

Table 4-1: The electro-hydraulic actuator parameters [24].

Physical Significance	Parameter	Value
Piston Area	A_c	1.52×10^{-3} m^2
Pump Displacement	Dp	5.57×10^{-7} m^3
Mass	M	7.38 kg
Bulk Modulus	β_e	2.07×10^{8} Pa
System Volume	V_0	1.08×10^{-3} m^3

4.3. Smooth Variable Structure Filter with Variable Boundary Layer

An uncertain linear system can be represented by the following state-space model:

$$\boldsymbol{x}(k+1) = \left(\widehat{\boldsymbol{A}}(k) + \boldsymbol{\Delta A}(k)\right)\boldsymbol{x}(k) + \left(\widehat{\boldsymbol{B}}(k) + \boldsymbol{\Delta B}(k)\right)\boldsymbol{u}(k) + \boldsymbol{v}(k), \quad (4.10)$$

$$\boldsymbol{z}(k) = \left(\widehat{\boldsymbol{C}}(k) + \boldsymbol{\Delta C}(k)\right)\boldsymbol{x}(k) + \boldsymbol{w}(k), \quad (4.11)$$

where $\widehat{\boldsymbol{A}}(k)$, $\widehat{\boldsymbol{B}}(k)$, and $\widehat{\boldsymbol{C}}(k)$ represent the nominal model, and $\boldsymbol{\Delta A}$, $\boldsymbol{\Delta B}$, and $\boldsymbol{\Delta C}$ denote the unknown uncertainties. It is assumed that the system is contaminated by white process noise $\boldsymbol{v}(k)$ and white measurement noise $\boldsymbol{w}(k)$ characterized by the

covariance matrices $\boldsymbol{Q}(k)$ and $\boldsymbol{R}(k)$, respectively. In the prediction stage of the SVSF algorithm, states and measurements are predicted according to the model as:

$$\hat{\boldsymbol{x}}(k+1|k) = \hat{\boldsymbol{A}}(k)\hat{\boldsymbol{x}}(k|k) + \hat{\boldsymbol{B}}(k)\boldsymbol{u}(k), \tag{4.12}$$

$$\hat{\boldsymbol{z}}(k+1|k) = \hat{\boldsymbol{C}}(k+1)\hat{\boldsymbol{x}}(k+1|k). \tag{4.13}$$

The corresponding error covariance matrix is obtained as:

$$\boldsymbol{P}(k+1|k) = \hat{\boldsymbol{A}}(k)\boldsymbol{P}(k|k)\hat{\boldsymbol{A}}(k)^{\intercal} + \boldsymbol{Q}(k). \tag{4.14}$$

The following a priori measurement error is computed as the difference between the actual measurements and their predicted values:

$$\boldsymbol{e_z}(k+1|k) = \boldsymbol{z}(k+1) - \hat{\boldsymbol{z}}(k+1|k). \tag{4.15}$$

The innovation covariance is obtained based on the a priori covariance matrix in Eqn. (4.14) as:

$$\boldsymbol{S}(k+1) = \hat{\boldsymbol{C}}(k+1)\boldsymbol{P}(k+1|k)\hat{\boldsymbol{C}}(k+1)^{\intercal} + \boldsymbol{R}(k+1). \tag{4.16}$$

Then, the variable boundary layer is updated using the innovation covariance as:

$$\begin{aligned}\boldsymbol{\psi_{VBL}}(k+1) = \big(&diag(|\boldsymbol{e_z}(k+1|k)|_{abs} \\ &+ \gamma|\boldsymbol{e_z}(k|k)|_{abs})^{-1}\hat{\boldsymbol{C}}(k)\boldsymbol{P}(k+1|k)\hat{\boldsymbol{C}}(k)^{\intercal}\boldsymbol{S}(k \\ &+ 1)^{-1}\big)^{-1},\end{aligned} \tag{4.17}$$

where $\boldsymbol{S}$ is the innovation covariance, $\boldsymbol{\psi}_{VBL}$ is the variable boundary layer, and γaffects the convergence rate with a value between 0 and 1. To update the filter gain, $\boldsymbol{\psi}_{VBL}$ is compared with $\boldsymbol{\psi}_{lim}$, which is obtained based on system uncertainties. If $\boldsymbol{\psi}_{VBL} \leq \boldsymbol{\psi}_{lim}$, the filter gain is computed as:

$$\boldsymbol{W}(k+1) = \boldsymbol{P}(k+1|k)\hat{\boldsymbol{C}}(k)^{\intercal}\boldsymbol{S}(k+1)^{-1}, \tag{4.18}$$

Otherwise, the filter gain is updated by a discontinuous corrective action as follows:

$$\boldsymbol{W}(k+1) = \widehat{\boldsymbol{C}}(k+1)^{+}\big(\boldsymbol{e_z}(k+1|k) + \gamma \boldsymbol{e_z}(k|k)\big) \odot sgn\big(\boldsymbol{e_z}(k+1|k)\big)\boldsymbol{e_z}(k+1|k)^{-1} \tag{4.19}$$

Using the filter gain and the a priori estimation, the a posteriori state estimate, measurement error, and covariance matrix are updated as follows:

$$\widehat{\boldsymbol{x}}(k+1|k+1) = \widehat{\boldsymbol{x}}(k+1|k) + \boldsymbol{W}(k+1)\boldsymbol{e_z}(k+1|k), \tag{4.20}$$

$$\boldsymbol{e_z}(k+1|k+1) = \boldsymbol{z}(k+1) - \widehat{\boldsymbol{C}}(k+1)\widehat{\boldsymbol{x}}(k+1|k+1), \tag{4.21}$$

$$\boldsymbol{P}(k+1|k+1) = \boldsymbol{P}(k+1|k) - \boldsymbol{W}(k+1)\boldsymbol{S}(k+1)\boldsymbol{W}(k+1)^{\intercal}. \tag{4.22}$$

The flowchart of the SVSF-VBL algorithm is shown in Figure 2-2. Since the velocity is not measured, the state variables of the state-space model in Eqn.(4.9) are rearranged as follows; $\boldsymbol{x_1}$ is the position of the actuator, $\boldsymbol{x_2}$ is the pressure difference, and $\boldsymbol{x_3}$ is velocity; to be consistence with SVSF for fewer measurement than state variables [29]. The corresponding matrices for the state-space model of the EHA system are obtained as follows:

$$\widehat{\boldsymbol{A}} = \begin{bmatrix} 1 & T_s & 0 \\ 0 & 1 - \dfrac{T_s\beta_e L_t}{V_0} & -\dfrac{T\beta_e A_c}{V_0} \\ 0 & \dfrac{T_s A}{M} & 1 - \dfrac{T_s a}{M} \end{bmatrix}, \qquad \widehat{\boldsymbol{B}} = \begin{bmatrix} 0 \\ \dfrac{T_s\beta_e D_p}{V_0} \\ 0 \end{bmatrix}, \tag{4.23}$$

$$\widehat{\boldsymbol{C}} = \begin{bmatrix} 1 & 0 & 0 \\ 0 & 1 & 0 \end{bmatrix}$$

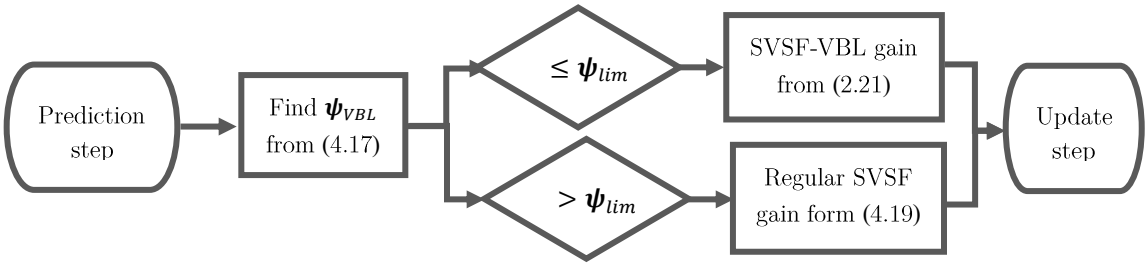

Figure 4-2. Smooth variable structure filter with variable boundary layer.

4.4. Updated Interactive Multiple Model Design

Different stages of the Updated Interactive Multiple Model (UIMM) strategy include Mixing probability calculation; Mixing stage; Likelihood calculation; Finding mode probabilities; Combined state and covariance estimation; and Fault detection and model update. They are summarized as follows [27]:

4.4.1. Mixing Probability Calculation.

First, the mixing probability is obtained as:

$$\mu_{i|j}(k-1|k-1) = \frac{P_{ij}\mu_i(k-1)}{\bar{c}_j}, \qquad i,j = 1,\dots,r, \tag{4.24}$$

$$\bar{c}_j = \sum_{i=1}^{r} p_{ij}\mu_i(k-1), \qquad j = 1, \dots, r, \tag{4.25}$$

where $\boldsymbol{\mu}$ is the mode probability, p_{ij} is the probability of switching from model i to model j, and r is the number of models.

4.4.2. Mixing Stage

Initial conditions for filters are obtained from the following equations:

$$\hat{\boldsymbol{x}}^{0j}(k-1|k-1) = \sum_{i=0}^{r} \hat{\boldsymbol{x}}^{i}(k-1|k-1)\mu_{i|j}(k-1|k-1), \quad j = 1,\dots,r, \tag{4.26}$$

$$\begin{aligned}\boldsymbol{P}^{0j}(k-1|k-1) = \textstyle\sum_{i=1}^{r}\Big(&\mu_{i|j}(k-1|k-1)\boldsymbol{P}^{i}(k-1|k-1) + \\ &\big[\hat{\boldsymbol{x}}^{i}(k-1|k-1) - \hat{\boldsymbol{x}}^{0j}(k-1|k-1)\big].\big[\hat{\boldsymbol{x}}^{i}(k-1|k-1) - \\ &\hat{\boldsymbol{x}}^{0j}(k-1|k-1)\big]^{\mathrm{T}}\Big),\ j = 1,\dots,r,\end{aligned} \tag{4.27}$$

Where $\boldsymbol{x}^{0j}$ states and $\boldsymbol{P}^{0j}$ is the covariance of the filter j obtained based on mixing probabilities from the previous step.

4.4.3. Likelihood Calculation

As shown in Figure 4-3, The state estimates and their respective covariance matrices are computed by feeding the filters with the measurements and the initial conditions from the preceding step. Subsequently, the likelihood function for each filter is derived as follows:

$$\Lambda_j = \mathcal{N}\{\boldsymbol{z}(k); \hat{\boldsymbol{z}}^j[k|\, k-1; \hat{\boldsymbol{x}}^{0j}(k-1|\, k-1)], \boldsymbol{S}^j[k; \boldsymbol{P}^{0j}(k-1|k-1)]\}, \quad j = 1, \dots, r, \tag{4.28}$$

Where Λ_j is the likelihood of filter j and $\mathcal{N}$ is the normal distribution.

4.4.4. Finding Mode Probabilities

Mode probability of each model is determined by utilizing the likelihood function derived from the previous step:

$$\mu_i(k) = \frac{\Lambda_j(k)\bar{c}_j}{\sum_{j=1}^{r}\Lambda_j(k)\bar{c}_j}, \qquad j = 1, \dots, r, \tag{4.29}$$

Where μ_i is the mode probability of filter i which indicates the probability of model i to be the true model and is used for detecting faults in the system.

4.4.5. Combined State and Covariance Estimation

During this step, the estimated states and their corresponding covariance are updated and prepared for use in the subsequent cycle as follows:

$$\hat{x}(k|k) = \sum_{j=1}^{r} \mu_j(k)\hat{x}^j(k|k), \tag{4.30}$$

$$\boldsymbol{P}(k|k) = \sum_{j=1}^{r}\Big\{\mu_j(k)\widehat{\boldsymbol{P}}^j(k|k) + \big[\hat{\boldsymbol{x}}^j(k|k) - \hat{\boldsymbol{x}}(k|k)\big] \cdot \big[\hat{\boldsymbol{x}}^j(k|k) - \hat{\boldsymbol{x}}(k|k)\big]^{\mathrm{T}}\Big\}, \tag{4.31}$$

Where $\widehat{\boldsymbol{x}}$ are estimated states and $\widehat{\boldsymbol{P}}$ is the estimated covariance of the system which is used for the next cycle.

4.4.6. Fault Detection and Model Update.

This section is added to the UIMM strategy to focus on a subset of models (instead of all possible models in the IMM structure) based on the system condition. In this step, the mode probability in Eqn.(4.28) is used to find out if there is a specific fault in the system. For this purpose, the maximum mode probability is compared against the threshold for the fault associated with the corresponding model, $\mu_{threshold}$, as follows:

$$\mu_f(k) = \max_i \mu_i(k), \tag{4.32}$$

$$\begin{cases} \text{If } \mu_f \geq \mu_{threshold}, & \text{fault f occurred} \\ \text{If } \mu_f < \mu_{threshold}, & \text{no fault} \end{cases} \tag{4.33}$$

If a fault is detected in the system, the filter models are updated accordingly. Due to noise and uncertainty in the system, the mode probability usually spikes even when there is not any fault in the system. To avoid false alarms, the moving average of mode probability $\mu_i(k)$ is used. The flowchart of the UIMM for one cycle is presented in Figure 4-3.

The primary benefit of the UIMM approach over IMM is its notable reduction in the number of parallel filters, as illustrated in Table 2-1. In the UIMM strategy, only individual fault models are included in the filter bank, whereas the IMM strategy considers all potential combinations of faults within the system, leading to an exponential increase in the number of required models. This reduction in the number

of filters enhances computational efficiency and mitigates the risk of combinatorial explosion.

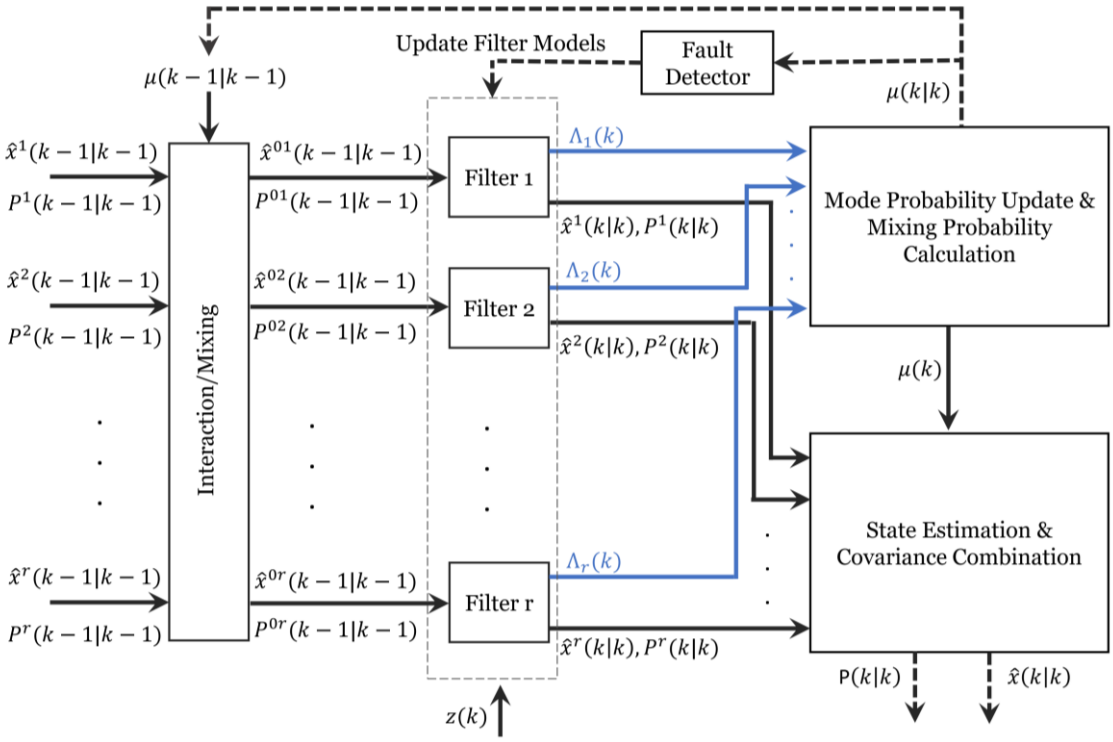

Figure 4-3. The UIMM flowchart for one cycle.

Table 4-2: Comparing the number of filters in IMM and UIMM algorithms.

Number of Faults	**1**	**2**	**3**	**4**	**n**
Number of Filters in IMM	2	4	8	16	2^n
Number of Filters in UIMM	2	3	4	5	n+1

4.5. Results and Discussion

Within this section, the application of the UIMM-SVSF-VBL strategy is employed to detect and isolate faults related to leakage and friction in the EHA system. The outcomes of this strategy are then compared to those obtained from the

IMM-SVSF-VBL and IMM-KF approaches. The leakage and friction coefficients are changed based on Table 4-3 to simulate the faults. The nominal values for leakage and friction coefficient of a healthy system have been determined based on the parameters reported in [24]. To incorporate leakage, a tiny hole with a diameter of less than 5mm has been assumed across the cylinder chamber. The friction coefficients for friction faults have also been acquired from [19]. To assess the robustness of the system, a 20% mismatch in bulk modulus ($\beta_{\text{True}} = 1.2\beta_{\text{Model}}$) and a 5% mismatch in pump displacement and system mass ($D_{p\text{True}} = 0.95D_{p\text{Model}}$ and $M_{\text{True}} = 1.05M_{\text{Model}}$) are considered.

Table 4-3. The conditions for different faults.

Condition	Leakage Coefficient L_t	Friction Coefficient a
Normal	$4.8 \times 10^{-12} \frac{m^3}{s.pa}$	$2144\, N.s/m$
Leakage Fault	$2 \times 10^{-9} \frac{m^3}{s.pa}$	$2144\, N.s/m$
Friction Fault	$4.8 \times 10^{-12} \frac{m^3}{s.pa}$	$7440\, N.s/m$
Minor Leakage	$10^{-9} \frac{m^3}{s.pa}$	$2144\, N.s/m$
Minor Friction	$4.8 \times 10^{-12} \frac{m^3}{s.pa}$	$3000\, N.s/m$

Three scenarios were investigated in this study: open-loop with major faults, open-loop with minor faults (to demonstrate the superior performance of the UIMM-SVSF-VBL strategy compared to IMM-SVSF-VBL in identifying minor faults) and closed-loop systems for real-time control applications. The following sequence of events was simulated to replicate fault conditions in all of these scenarios:

1. The system begins in a healthy state at the start of the simulation.
2. At $t = 1$s, a leakage fault is introduced.
3. At $t = 2$s, the friction fault is also applied.

This sequence of events was used consistently across all three cases. Table 4-4 illustrates the parameters employed for each FDD strategy. The state vector elements are defined as follows: $\boldsymbol{x_1}$ represents the actuator position, $\boldsymbol{x_2}$ denotes the pressure difference across chambers, and $\boldsymbol{x_3}$ signifies the load velocity. In order to ensure a fair comparison, the same parameters were utilized for all strategies. To enhance the robustness of the Kalman filter against parameter mismatch, an artificial process noise was introduced for the IMM-KF strategy [35]. This was achieved by incorporating a larger process noise ($\boldsymbol{Q}$) for the IMM-KF with the introduced fake noise. The parameters employed in the UIMM strategy differ from those in IMM due to the utilization of a reduced number of filters in the filter bank.

Table 4-4. Parameters used for each FDD strategy.

Parameter	**UIMM-SVSF-VBL**	**IMM-SVSF-VBL**	**IMM-KF**	**IMM-KF with introduced artificial noise**
Measurement Noise ($\boldsymbol{R}$)	$\begin{bmatrix} 10^{-10} & 0 \\ 0 & 10^{3} \end{bmatrix}$	$\begin{bmatrix} 10^{-10} & 0 \\ 0 & 10^{3} \end{bmatrix}$	$\begin{bmatrix} 10^{-10} & 0 \\ 0 & 10^{3} \end{bmatrix}$	$\begin{bmatrix} 10^{-10} & 0 \\ 0 & 10^{3} \end{bmatrix}$
Process Noise ($\boldsymbol{Q}$)	$\begin{bmatrix} 10^{-12} & 0 & 0 \\ 0 & 10^{2} & 0 \\ 0 & 0 & 10^{-10} \end{bmatrix}$	$\begin{bmatrix} 10^{-12} & 0 & 0 \\ 0 & 10^{2} & 0 \\ 0 & 0 & 10^{-10} \end{bmatrix}$	$\begin{bmatrix} 10^{-12} & 0 & 0 \\ 0 & 10^{2} & 0 \\ 0 & 0 & 10^{-10} \end{bmatrix}$	$\begin{bmatrix} 10^{-12} & 0 & 0 \\ 0 & 10^{2} & 0 \\ 0 & 0 & 10^{-10} \end{bmatrix}$
Initial Error Covariance	$\begin{bmatrix} 10^{-6} & 0 & 0 \\ 0 & 10^{6} & 0 \\ 0 & 0 & 10^{-4} \end{bmatrix}$	$\begin{bmatrix} 10^{-6} & 0 & 0 \\ 0 & 10^{6} & 0 \\ 0 & 0 & 10^{-4} \end{bmatrix}$	$\begin{bmatrix} 10^{-6} & 0 & 0 \\ 0 & 10^{6} & 0 \\ 0 & 0 & 10^{-4} \end{bmatrix}$	$\begin{bmatrix} 10^{-6} & 0 & 0 \\ 0 & 10^{6} & 0 \\ 0 & 0 & 10^{-4} \end{bmatrix}$
Initial State Estimate ($\boldsymbol{x}(0\|0)$)	$\begin{bmatrix} 0 \\ 0 \\ 0 \end{bmatrix}$	$\begin{bmatrix} 0 \\ 0 \\ 0 \end{bmatrix}$	$\begin{bmatrix} 0 \\ 0 \\ 0 \end{bmatrix}$	$\begin{bmatrix} 0 \\ 0 \\ 0 \end{bmatrix}$
Initial Mode Probability ($\boldsymbol{\mu}(0)$)	$\begin{bmatrix} 0.5 \\ 0.25 \\ 0.25 \end{bmatrix}$	$\begin{bmatrix} 0.4 \\ 0.2 \\ 0.2 \\ 0.2 \end{bmatrix}$	$\begin{bmatrix} 0.4 \\ 0.2 \\ 0.2 \\ 0.2 \end{bmatrix}$	$\begin{bmatrix} 0.4 \\ 0.2 \\ 0.2 \\ 0.2 \end{bmatrix}$

Transition Matrix ($\boldsymbol{P}_{ij}$)	$\begin{bmatrix} 0.98 & 0.01 & 0.01 \\ 0.01 & 0.98 & 0.01 \\ 0.01 & 0.01 & 0.98 \end{bmatrix}$	$\begin{bmatrix} 0.97 & 0.01 & 0.01 & 0.01 \\ 0.01 & 0.97 & 0.01 & 0.01 \\ 0.01 & 0.01 & 0.97 & 0.01 \\ 0.01 & 0.01 & 0.01 & 0.97 \end{bmatrix}$	$\begin{bmatrix} 0.97 & 0.01 & 0.01 & 0.01 \\ 0.01 & 0.97 & 0.01 & 0.01 \\ 0.01 & 0.01 & 0.97 & 0.01 \\ 0.01 & 0.01 & 0.01 & 0.97 \end{bmatrix}$	$\begin{bmatrix} 0.97 & 0.01 & 0.01 & 0.01 \\ 0.01 & 0.97 & 0.01 & 0.01 \\ 0.01 & 0.01 & 0.97 & 0.01 \\ 0.01 & 0.01 & 0.01 & 0.97 \end{bmatrix}$
Boundary Layer ($\boldsymbol{\psi}_{\text{lim}}$)	$\begin{bmatrix} 10^{-3} \\ 10 \end{bmatrix}$	$\begin{bmatrix} 10^{-3} \\ 10 \end{bmatrix}$	-	-

4.5.1. Case 1: Open-Loop System with Major Faults

In the present section, the performance of the UIMM-SVSF-VBL strategy in comparison to IMM-SVSF-VBL and IMM-KF with and without the inclusion of artificial noise is studied. The evaluation is conducted on an open-loop system featuring major leakage and friction faults from Table 4-3, employing the previously defined sequence of events. The outcomes presented in Table 4-5 and Figure 4-4 demonstrate that the proposed strategy effectively identifies both leakage and friction faults and exhibits superior performance in state estimation.

IMM-SVSF-VBL can effectively detect and isolate the faults, but the presence of a larger bank of filters results in more intense spikes in the mode probability signals compared to those observed in UIMM-SVSF-VBL (Figure 4-4b).

IMM-KF is unable to detect both the leakage and friction faults, resulting in a significant estimation error for the velocity when no measurements are available due to model mismatch (Figure 4-4c). To address this issue, the process noise covariance $\boldsymbol{Q}$ is increased by introducing artificial white noise to accommodate a higher level of system uncertainty caused by the model mismatch. Despite the improved performance achieved by incorporating the artificial process noise, IMM-KF still fails

to identify the friction fault, as depicted in Figure 4-4d. Given the unsatisfactory performance of IMM-KF without the inclusion of artificial noise, it is not included for comparison in the subsequent sections.

Table 4-5. Comparing FDD results for different approaches.

State	IMM-SVSF-VBL Normalized RMSE	UIMM-SVSF-VBL Normalized RMSE	IMM-KF with artificial noise Normalized RMSE	IMM-KF Normalized RMSE
Position	$1.4355e-04$	$1.3611e-04$	$2.0268e-04$	0.0018
Velocity	0.0385	0.0365	0.0556	0.4021
Pressure	$1.2605e-04$	$1.2605e-04$	$9.4810e-04$	$1.2985e-04$
Leakage Detection	Pass	Pass	Pass	Pass
Friction Detection	Pass	Pass	Pass	Pass

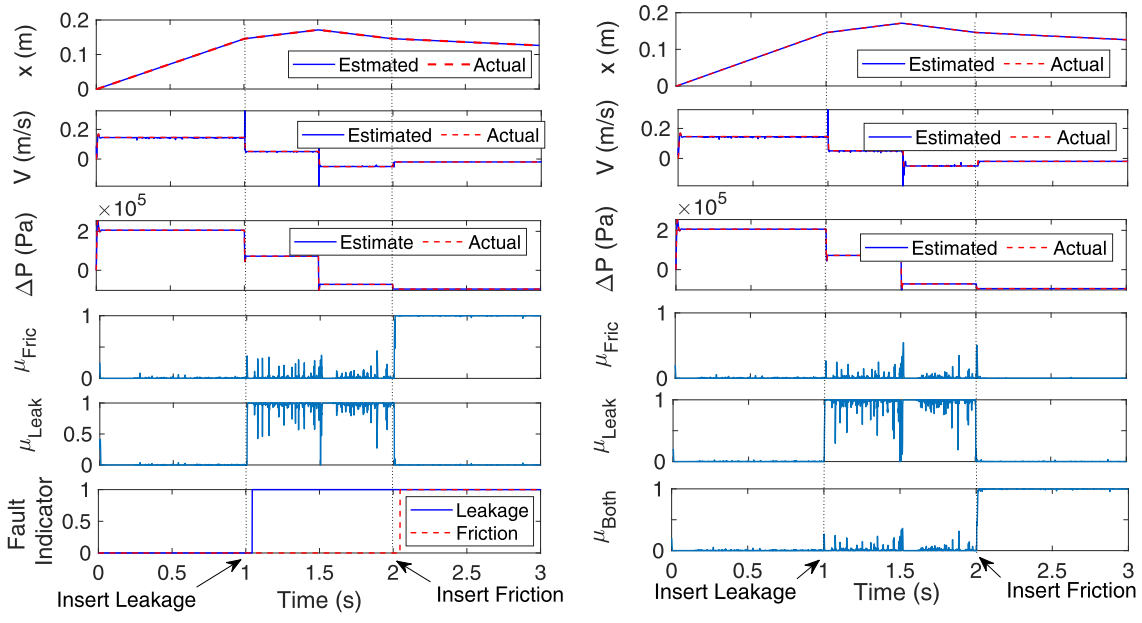

a) UIMM-SVSF-VBL b) IMM-SVSF-VBL

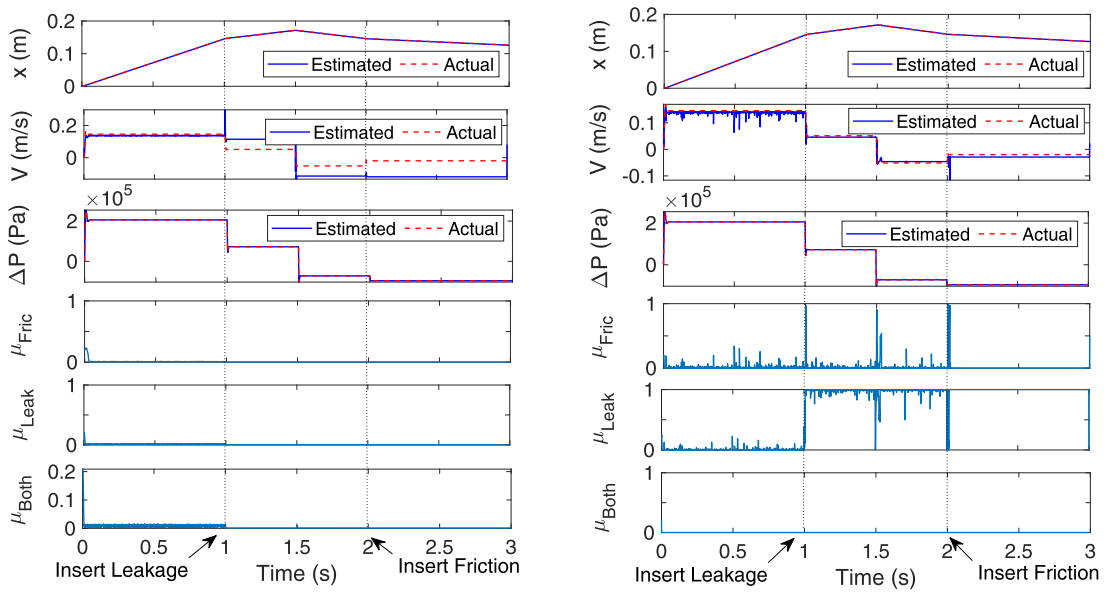

c) IMM-KF d) IMM-KF with added artificial noise

Figure 4-4. Fault detection and diagnosis for the open-loop system with major faults.

4.5.2. Case 2: Open-Loop System with Minor Faults

In the current section, the performance of the UIMM-SVSF-VBL strategy in comparison to IMM-SVSF-VBL and IMM-KF with artificial noise is investigated. The assessment is carried out on an open-loop system that exhibits minor leakage and friction faults, as indicated in Table 4-3. The evaluation is performed using the predetermined sequence of events. In scenarios where faults are minor, the distinctions between the models are not substantial, leading to increased severity of the combinatorial effect within the IMM algorithm.

The outcomes presented in Figure 4-5 and Table 4-6 reveal that both IMM-SVSF-VBL and IMM-KF were unsuccessful in isolating the faults, whereas UIMM-SVSF-VBL effectively detected and isolated the faults. As depicted in Figure 4-5b IMM-SVSF-VBL exhibits insufficient performance in accurately detecting the minor leakage fault, resulting in frequent model switching. Also, IMM-KF fails to identify

the minor friction fault and triggers a false friction alarm even when the system is in a healthy state (Figure 4-5c).

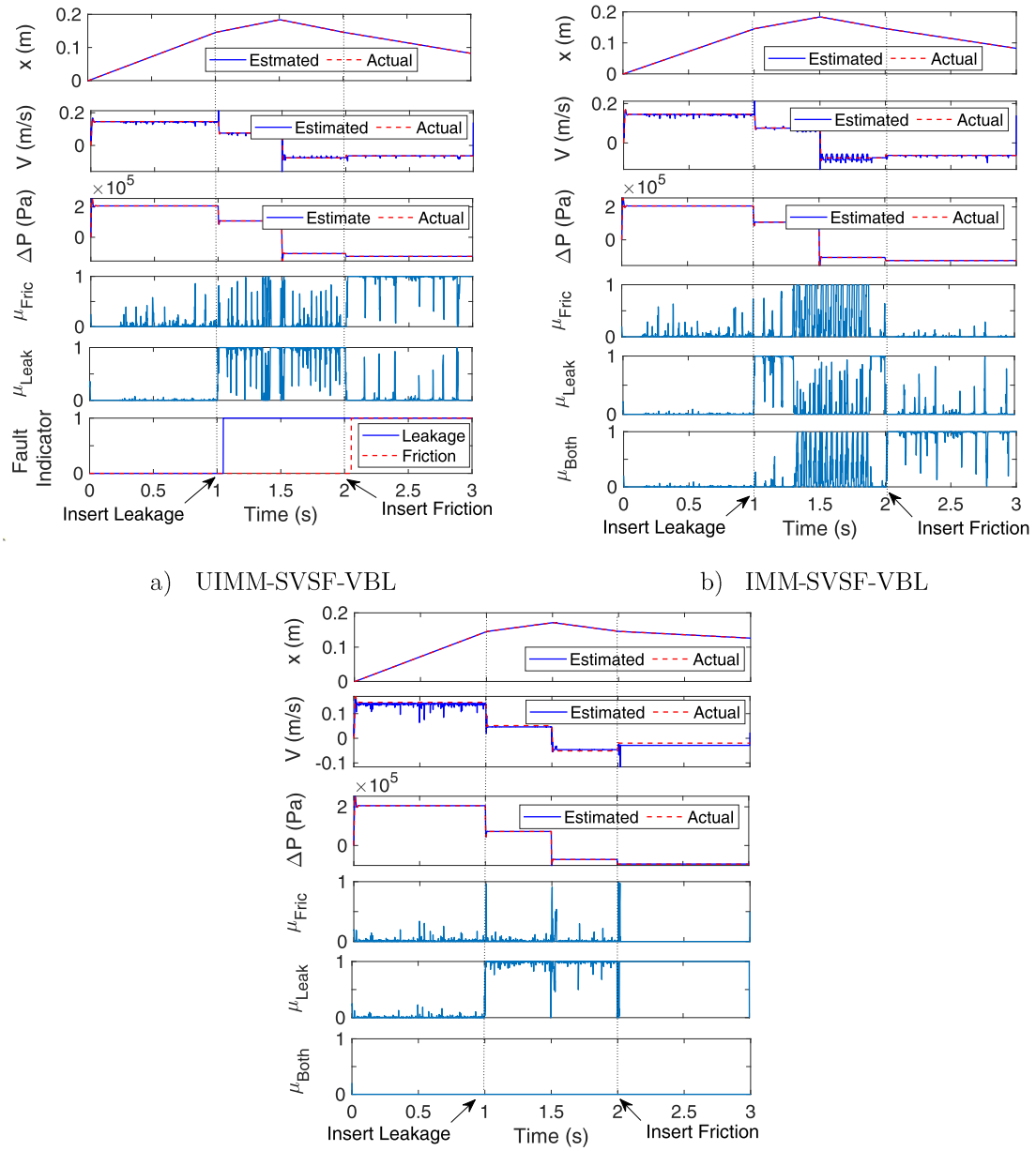

a) UIMM-SVSF-VBL

b) IMM-SVSF-VBL

c) IMM-KF with added artificial noise

Figure 4-5. Fault detection and diagnosis for the open-loop system with minor faults.

Table 4-6. Comparing FDD results for different approaches.

State	IMM-SVSF-VBL Normalized RMSE	UIMM-SVSF-VBL Normalized RMSE	IMM-KF with artificial noise Normalized RMSE
Position	$2.0200e-04$	$1.5863e-04$	$2.4970e-04$
Velocity	0.0518	0.0440	0.0673
Pressure	$1.2605e-04$	$1.2605e-04$	$7.3394e-04$
Leakage Detection	Fail	Pass	Pass
Friction Detection	Pass	Pass	Fail

4.5.3. Case 3: Open-Loop System with Proportional-Derivative Controller

In the context of a closed-loop system, UIMM-SVSF-VBL can be applied to provide state feedback for the controller while simultaneously detecting faults through the utilization of mode probability, as depicted in Figure 2-8. In this section, a proportional-derivative (PD) controller has been designed to control the position of the EHA using feedback estimates obtained from UIMM-SVSF-VBL. The obtained results have been compared to those obtained from IMM-SVSF-VBL and IMM-KF, as illustrated in Figure 4-7 and Table 4-7.

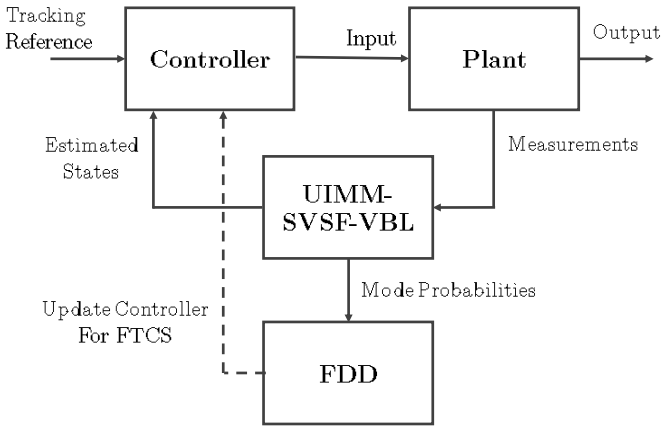

Figure 4-6. Flowchart of the UIMM-SVSF-VBL application in closed-loop system for real-time FDD and control.

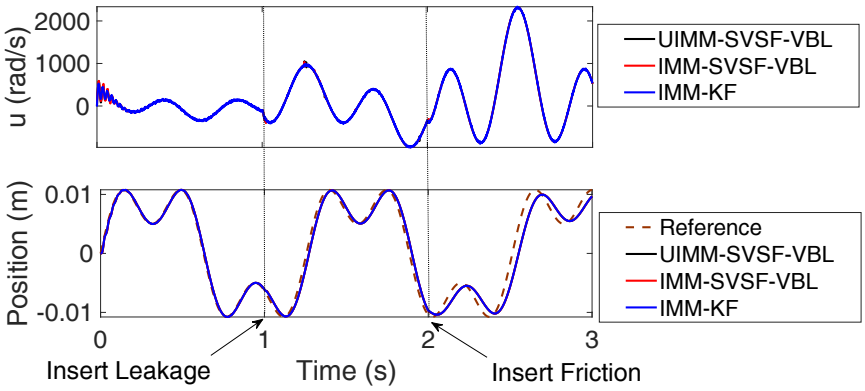

Figure 4-7. Position control of the EHA using PD controller.

Table 4-7. Comparing FDD results for different approaches.

State	IMM-SVSF-VBL Normalized RMSE	UIMM-SVSF-VBL Normalized RMSE	IMM-KF with artificial noise Normalized RMSE
Tracking Error	0.1230	0.1229	0.1225
Position	0.0032	0.0027	0.0018
Velocity	0.0632	0.0376	0.7663
Pressure	$1.8174e-04$	$1.8173e-04$	$5.7716e-05$
Leakage Detection	Pass	Pass	Fail
Friction Detection	Pass	Pass	Fail

As shown the controller's performance remains consistent across all three cases due to the adoption of a highly precise position sensor with a minimal covariance error of 10^{-10} (The incremental encoder employed in the EHA reported at [28] exhibits a high accuracy of $\pm 5\mu m$). Consequently, the filters assign considerable weight to the measurement signal, leading to the nearly identical estimated positions employed by the PD controller across all three scenarios. Table 4-7 and Figure 4-8 demonstrate the successful detection of leakage and friction faults by UIMM-SVSF-VBL and IMM-SVSF-VBL, whereas IMM-KF fails to identify either fault. In the

event of leakage and friction occurring within the system (following $t = 1s$ in Figure 4-7), the tracking error increases because the PD gains are tuned based on the healthy condition. In response to this concern, the forthcoming section presents the development of a Fault-Tolerant Control System (FTCS) utilizing the UIMM-SVSF-VBL strategy.

4.5.4. Design of A Fault-Tolerant Control System

The real-time detection and diagnosis of faults play a pivotal role in the advancement of Fault Tolerant Control Systems (FTCS), which are crucial for ensuring the reliability and robustness of various industrial processes. It enhances system performance by employing an adaptive controller that dynamically adjusts the gains in response to system faults. Figure 4-10 compares an FTCS equipped with an adaptive controller and a PD controller, using the UIMM-SVSF-VBL. The Results show that the adaptive controller effectively maintains proper reference signal tracking even in the presence of faults.

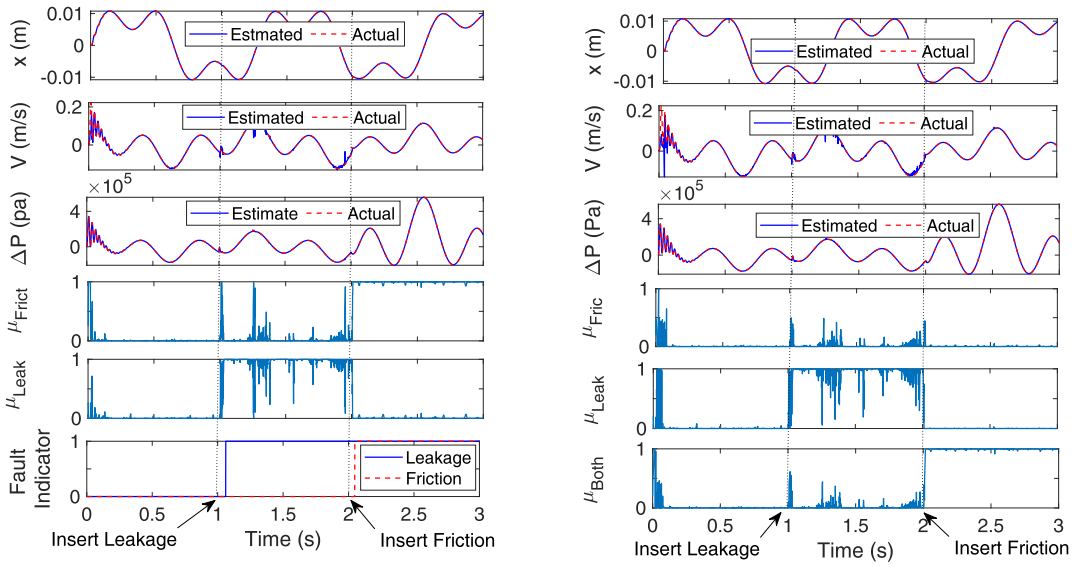

a) UIMM-SVSF-VBL b) IMM-SVSF-VBL

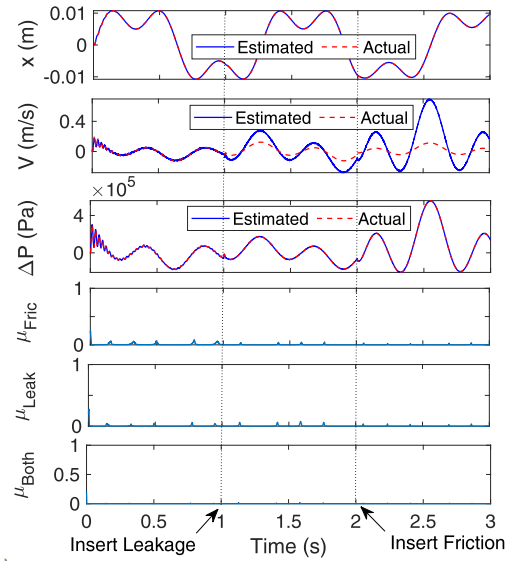

c) IMM-KF with added artificial noise

Figure 4-8. Fault detection and diagnosis for the closed-loop system with PD controller.

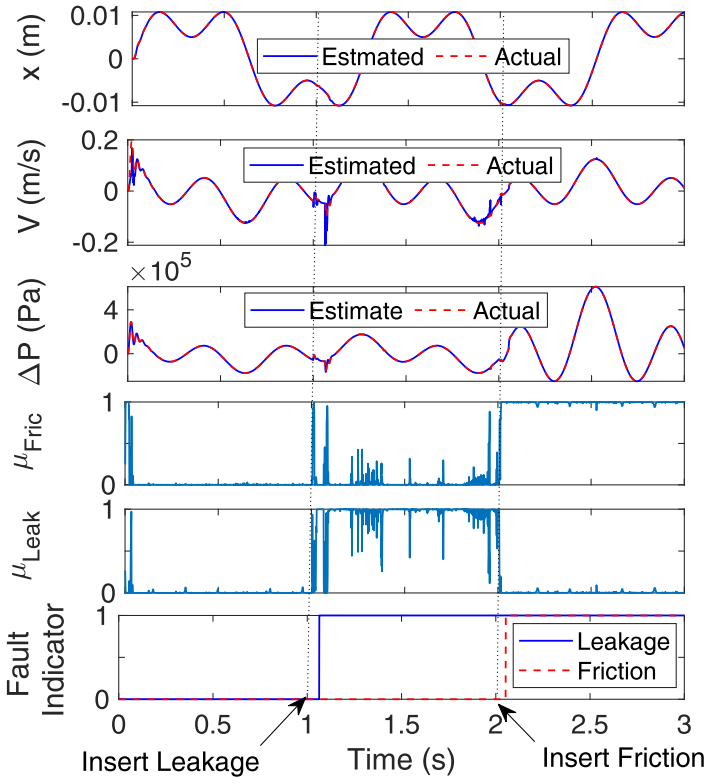

Figure 4-9. Fault detection and diagnosis in a fault-tolerant position control system using UIMM-SVSF-VBL.

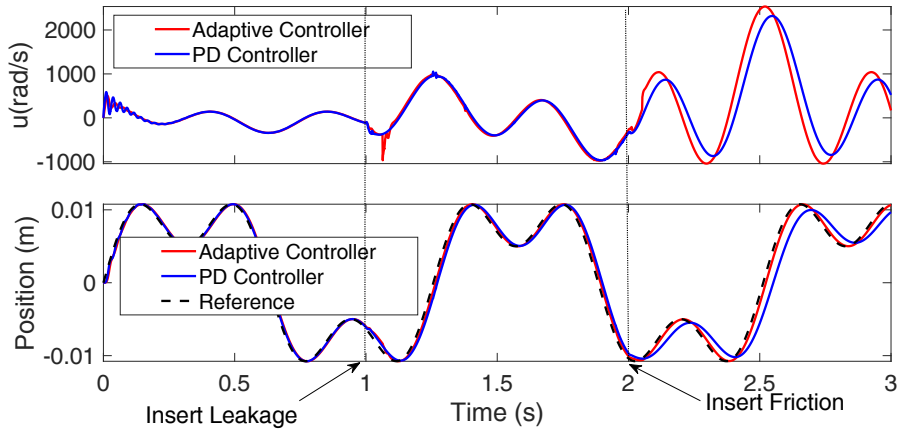

Figure 4-10. Comparing the PD controller and FTCS with adaptive controller for the EHA system using UIMM-VBL-SVSF.

4.6. Conclusions

This research paper introduces the UIMM-SVSF algorithm as a novel approach for the detection and isolation of leakage and friction faults in a typical EHA system. The proposed algorithm improves performance by significantly reducing the number of required running models. This reduction not only enhances computational efficiency but also mitigates the combinatorial effect. Results show that UIMM-SVSF has a better performance compared to IMM-SVSF and IMM-KF. Furthermore, both the IMM-SVSF and the IMM-KF suffer from a combinatorial effect, especially for minor faults. In the case of model parameter mismatch, the IMM-KF requires added artificial process noise to accommodate modeling uncertainties at the cost of compromising its performance. It is important to note that investigation is limited to leakage and friction faults, which are prevalent in hydraulic systems. Expansion of the fault condition set calls for increasing the number of models, which in turn, increases the computational complexity. In this regard, the proposed UIMM-SVSF

algorithm will be the method of choice due to its computational efficiency, especially for real-time applications such as fault-tolerable control systems.

4.7. References

[1] V. Venkatasubramanian, R. Rengaswamy, K. Yin, and S. N. Kavuri, "A review of process fault detection and diagnosis part I: Quantitative model-based methods," *Comput. Chem. Eng.*, vol. 27, no. 3, pp. 293–311, 2003.

[2] F. Gustafsson and F. Gustafsson, *Adaptive filtering and change detection*, vol. 1. Wiley New York, 2000.

[3] I. Hwang, S. Kim, Y. Kim, and C. E. Seah, "A survey of fault detection, isolation, and reconfiguration methods," *IEEE Trans. Control Syst. Technol.*, vol. 18, no. 3, pp. 636–653, 2009.

[4] G. Pang, C. Shen, L. Cao, and A. Van Den Hengel, "Deep learning for anomaly detection: A review," *ACM Comput. Surv.*, vol. 54, no. 2, pp. 1–38, 2021.

[5] V. Chandola, A. Banerjee, and V. Kumar, "Anomaly detection: A survey," *ACM Comput. Surv.*, vol. 41, no. 3, pp. 1–58, 2009.

[6] R. Isermann, *Fault-diagnosis systems: an introduction from fault detection to fault tolerance*. Springer Science & Business Media, 2005.

[7] L. An and N. Sepehri, "Hydraulic actuator leakage fault detection using extended Kalman filter," *Int. J. Fluid Power*, vol. 6, no. 1, pp. 41–51, 2005.

[8] H. Khan, S. C. Abou, and N. Sepehri, "Nonlinear observer-based fault detection technique for electro-hydraulic servo-positioning systems," *Mechatronics*, vol. 15, no. 9, pp. 1037–1059, 2005.

[9] Z. Shi, F. Gu, B. Lennox, and A. D. Ball, "The development of an adaptive threshold for model-based fault detection of a nonlinear electro-hydraulic system," *Control Eng. Pract.*, vol. 13, no. 11, pp. 1357–1367, 2005.

[10] Y. Chinniah, R. Burton, and S. Habibi, "Failure monitoring in a high performance hydrostatic actuation system using the extended Kalman filter," *Mechatronics*, vol. 16, no. 10, pp. 643–653, 2006.

[11] P. M. Frank and X. Ding, "Survey of robust residual generation and evaluation methods in observer-based fault detection systems," *J. Process Control*, vol. 7, no. 6, pp. 403–424, 1997.

[12] P. M. Frank, "Robust model-based fault detection in dynamic systems," *IFAC Proc. Vol.*, vol. 25, no. 4, pp. 1–13, 1992.

[13] P. M. Frank, "Enhancement of robustness in observer-based fault detection," *Int. J. Control*, vol. 59, no. 4, pp. 955–981, 1994.

[14] A. Emami-Naeini, M. M. Akhter, and S. M. Rock, "Effect of model uncertainty on failure detection: the threshold selector," *IEEE Trans. Automat. Contr.*, vol. 33, no. 12, pp. 1106–1115, 1988.

[15] P. M. Frank and X. Ding, "Frequency domain approach to optimally robust residual generation and evaluation for model-based fault diagnosis," *Automatica*, vol. 30, no. 5, pp. 789–804, 1994.

[16] X.-C. Lou, A. S. Willsky, and G. C. Verghese, "Optimally robust redundancy relations for failure detection in uncertain systems," *Automatica*, vol. 22, no. 3, pp. 333–344, 1986.

[17] R. Song and N. Sepehri, "Fault detection and isolation in fluid power systems using a parametric estimation method," in *IEEE CCECE2002. Canadian Conference on Electrical and Computer Engineering. Conference Proceedings (Cat. No. 02CH37373)*, 2002, vol. 1, pp. 144–149.

[18] D. Soudbakhsh and A. M. Annaswamy, "PROGNOSTICS AND HEALTH MONITORING OF ELECTRO-HYDRAULIC SYSTEMS," in *Proceedings of the ASME 2017 Dynamic Systems and Control Conference*, 2017, pp. 1–6.

[19] S. Gayaka and B. Yao, *Fault Detection, Identification and Accommodation for an Electro-hydraulic System: An Adaptive Robust Approach*, vol. 41, no. 2. IFAC, 2008.

[20] M. Ringkowski and O. Sawodny, "Model-Based Fault-Detection of a Hydraulic Switching Valve," in *2019 American Control Conference (ACC)*, 2019, pp. 4460–4465.

[21] M. F. Asmussen, H. C. Pedersen, L. Lilleengen, A. Larsen, and T. Farsakoglou, "Investigating Fault Detection and Diagnosis in a Hydraulic

Pitch System Using a State Augmented EKF-Approach," in *Fluid Power Systems Technology*, 2019, vol. 59339, p. V001T01A030.

[22] V. Stojanovic and D. Prsic, "Robust identification for fault detection in the presence of non-Gaussian noises: application to hydraulic servo drives," *NONLINEAR Dyn.*, 2020.

[23] S. Kim, J. Choi, and Y. Kim, "Fault detection and diagnosis of aircraft actuators using fuzzy-tuning IMM filter," *IEEE Trans. Aerosp. Electron. Syst.*, vol. 44, no. 3, pp. 940–952, 2008.

[24] S. A. Gadsden, Y. Song, and S. R. Habibi, "Novel model-based estimators for the purposes of fault detection and diagnosis," *IEEE/ASME Trans. Mechatronics*, vol. 18, no. 4, pp. 1237–1249, 2013.

[25] H. H. Afshari, S. A. Gadsden, and S. R. Habibi, "Robust fault diagnosis of an electro-hydrostatic actuator using the novel dynamic second-order SVSF and IMM strategy," *Int. J. Fluid Power*, vol. 15, no. 3, pp. 181–196, 2014.

[26] Q. Zhang, "Stochastic hybrid system actuator fault diagnosis by adaptive estimation," *IFAC-PapersOnLine*, vol. 48, no. 21, pp. 150–155, 2015.

[27] Y. Bar-Shalom, X. R. Li, and T. Kirubarajan, *Estimation with applications to tracking and navigation: theory algorithms and software*. John Wiley & Sons, 2004.

[28] S. A. Gadsden, Y. Song, and S. R. Habibi, "Novel model-based estimators for the purposes of fault detection and diagnosis," *IEEE/ASME Trans. Mechatronics*, vol. 18, no. 4, pp. 1237–1249, 2013.

[29] S. Habibi, "The smooth variable structure filter," *Proc. IEEE*, vol. 95, no. 5, pp. 1026–1059, 2007.

[30] S. A. Gadsden, M. El Sayed, and S. R. Habibi, "Derivation of an optimal boundary layer width for the smooth variable structure filter," in *Proceedings of the 2011 American Control Conference*, 2011, pp. 4922–4927.

[31] A. Saeedzadeh, A. Tivay, M. Zareinejad, S. M. Rezaei, A. Rahimi, and K. Baghestan, "Energy-efficient hydraulic actuator position tracking using hydraulic system operation modes," *Proc. Inst. Mech. Eng. Part E J. Process Mech. Eng.*, vol. 232, no. 1, pp. 49–64, 2018.

[32] S. Habibi, R. Burton, and E. Sampson, "High precision hydrostatic actuation systems for micro-and nanomanipulation of heavy loads," 2006.

[33] E. Sampson, S. Habibi, R. Burton, and Y. Chinniah, "Effect of controller in reducing steady-state error due to flow and force disturbances in the electrohydraulic actuator system," *Int. J. fluid power*, vol. 5, no. 2, pp. 57–66, 2004.

[34] Y. U. Song, "Electro-Hydrostatic Actuator Fault Detection and Diagnosis," McMaster University, 2013.

[35] M. Athans and C.-B. Chang, "Adaptive estimation and parameter identification using multiple model estimation algorithm," 1976.

5. Adaptive Estimation Using Interacting Multiple Model with Moving Window

Ahsan Saeedzadeh*[1], Peyman Setoodeh[1], Saeid Habibi[1], Marjan Alavi[2]

[1] Department of Mechanical Engineering, McMaster University, Hamilton, ON, Canada

[2] W Booth School of Engineering Practice and Technology, McMaster University, Hamilton, ON, Canada

Abstract

State estimation is paramount in control, monitoring, and fault management across various domains. Uncertainty in model parameters and changing system dynamics pose significant challenges to accurate state estimation. This paper proposes a novel adaptive estimation strategy called Moving Window Interacting Multiple Model (MWIMM). Using a moving window improves identifiability and computational efficiency of the multiple model algorithms by focusing on a subset of possible models, rather than considering all models at each stage. MWIMM enables the estimation of gradual changes in the system, making it valuable for fault intensity and Remaining Useful Life (RUL) estimation. The paper provides an overview of adaptive estimation strategies, presents the formulation of MWIMM for fault intensity and RUL estimation, and investigates the parameter estimation problem. Results are compared with those of augmented state Extended Kalman Filter (EKF) estimation, and it is shown that the proposed MWIMM approach offers a promising alternative for effectively handling extensive parameter uncertainty and accommodating gradual changes in system parameters.

Keywords: Adaptive Estimation, Moving Window IMM, Fault Diagnosis, RUL Estimation.

5.1. Introduction

State estimation is an essential step in various fields, including control, monitoring, and fault management [1]. However, system states may be partially observable or even unobservable. In addition to the challenges posed by the unknown states, another important barrier in state estimation is the uncertainty within the model parameters. Since these parameters are often not precisely known, the estimation process is inherently unpredictable and imprecise. Moreover, system dynamics gradually change over time due to ageing. It is also possible that a system undergoes abrupt changes, which include switching in the entire system dynamics. Hybrid models are deployed to capture this phenomenon. In such cases, estimating the model parameters alongside the states becomes particularly valuable, as it aids in detecting faults and predicting their future behavior as well as allowing for proactive maintenance and management.

State estimation accuracy heavily depends on the prior knowledge of model parameters. When parameters are precisely known, which is unrealistic in most applications, the Kalman Filter (KF) offers optimal state estimation for linear systems assuming zero-mean Gaussian noise [1]. Furthermore, in the presence of small parameter uncertainties, the impact of parametric mismatch is typically insignificant compared to the process noise, enabling the KF to maintain a satisfactory performance [2]. However, for scenarios involving moderate parameter uncertainty, alternative approaches become necessary. One approach involves introducing artificial

white noise by increasing specific elements of the process noise covariance matrix, Q, within the KF algorithm [2]. Another technique adaptively adjusts the process noise covariance matrix by monitoring residuals within the KF [3]. Alternatively, a robust estimation strategy such as the Smooth Variable Structure Filter (SVSF) with Variable Boundary Layer (SVSF-VBL) optimizes estimation error while considering parametric uncertainty through deploying a switching gain [4].

In the presence of significant parametric uncertainty, the traditional approach of increasing process noise and treating it as equivalent to white noise within the KF becomes inadequate. In this case, the effect of parametric uncertainties becomes significant and cannot be considered as added white noise [2]. Although SVSF can guarantee boundedness of estimation error in the presence of large uncertainties, it requires a large corrective gain, which leads to chattering [5]. While the mean error may decrease rapidly due to this significant gain, the excessive control action, can result in a large Root Mean Square Error (RMSE) for SVSF [6]. As an alternative, particle filters are known nonlinear filtering techniques suitable for more general systems characterized by unknown uncertainties and non-Gaussian probability density functions (PDFs) [7]. However, their performance is contingent on the number of particles employed and they require very high computational power. An infinite number of particles would be necessary for the estimation error to converge to zero in an ideal setting [8].

Joint state and parameter estimation offers an alternative approach for dealing with extensive parametric uncertainties and for accommodating gradual changes in model parameters. However, this method presents challenges due to its reliance on

nonlinear filtering and calls for solving complex nonlinear Partial Differential Equations (PDEs) to obtain the optimal solution. The augmented state Extended Kalman Filter (EKF) provides a suboptimal solution [9], which is susceptible to bias estimation and divergence for several reasons [10], [11]. Firstly, the augmented states lack meaningful dynamics, making it challenging to intuitively select the artificially introduced noise based on engineering guesses [2]. Secondly, discriminative training methods for determining the process noise covariance matrix depend on measured states, and including augmented states can negatively impact the training process [3], [12]. Additionally, validity of linearization used in the EKF becomes compromised in the presence of significant parametric uncertainty. Moreover, incorporating augmented states can render the system unobservable [9].

Alternatively, adaptive estimation strategies offer a different viewpoint that tackles significant uncertainties and enables the estimation of abrupt changes in the system that is a possible occurrence in hybrid systems and fault detection scenarios. In this paper, a novel adaptive estimation strategy is developed based on the Interacting Multiple Model (IMM) method. The new algorithm called Moving Window Interacting Multiple Model (MWIMM) offers the following advantages:

- It is capable of estimating gradual changes in system parameters, making it valuable for fault prognosis and Remaining Useful Life (RUL) estimation problems. This is achieved through utilizing parameter bins.
- It improves computational efficiency and avoids computational explosion, which are two common problems associated with MMAE algorithms. This is

accomplished by narrowing down the search space to a specific window rather than considering all potential models at each stage.

- It relaxes the assumed irreversible condition used in Updated IMM (UIMM) algorithm [13], thus extending its application to a wider range of problem domains.

The paper follows the subsequent structure: Section 2 presents an overview of adaptive estimation strategies. In Section 3, the formulation of MWIMM for fault intensity and remaining useful life estimation is presented. Section 4 investigates the application of the proposed MWIMM in a comprehensive parameter estimation problem, comparing the results with parameter estimation using augmented state extended Kalman filter. Section 5 explores the influence of three crucial factors—identifiability, optimality, and system excitation—on the performance of the multiple model adaptive estimation strategy in general and the proposed method specifically. It is demonstrated through a case study that for a Multiple Model Adaptive Estimation (MMAE) strategy, observability of all models in the filter bank does not guarantee identifiability. Finally, the paper concludes with summarizing remarks in the last section.

5.2. Background: Adaptive Estimation Strategy

Adaptive estimation using multiple models for hypothesis testing, known as Multiple Model Adaptive Estimation (MMAE), proves to be a valuable tool for handling large parameter uncertainty and hybrid systems characterized by different system models with distinct parameter sets [2]. MMAE assumes that engineering knowledge can serve as prior information about the hybrid models and the feasible range of

parameters. This approach enables the estimation of system states while providing an algorithm to identify changing parameters or the true underlying model. MMAE finds extensive applications in real-time problems, including autonomous vehicles [14], target tracking [15], fault diagnosis [16], [17], and fault-tolerant control systems [13], [18]. The multiple model estimation procedure involves three main steps: generating individual state estimates that correspond to a given parameter vector, evolving the hypothesis probability, and combining the individual estimates.

In the realm of MMAE, two distinct approaches can be observed: static and dynamic. Static MMAE assumes the exclusive usage of a single model throughout the entire process, without any transitions or jumps occurring. Consequently, it is unsuitable for time-variant systems characterized by changing parameters or instances where the system switches between different models. On the other hand, dynamic MMAE is specifically designed for time-varying systems and proves to be well-suited for online fault diagnosis or target tracing applications [1]. Notably, within the realm of dynamic MMAE, three widely recognized strategies are General Pseudo-Bayesian estimator of first order (GPB1), General Pseudo-Bayesian estimator of second order (GPB2) and Interacting Multiple Model (IMM). Among these, IMM gained interest due to its reported computational efficiency while maintaining a performance comparable to that of GPB2 [1]. As a result, IMM emerges as a promising choice for dynamic MMAE applications. Hence, the proposed method in this study is built on IMM.

In this research, a novel strategy known as the Mowing Window Interacting Multiple Model (MWIMM) is proposed as an enhanced and computationally efficient

version of the IMM approach, demonstrating improved performance in identifiability. MWIMM demonstrates relevance in scenarios where models exhibit varying degrees of chronological order, such as aging or fault intensity analysis. Furthermore, it proves valuable in addressing parameter estimation challenges in time-varying systems characterized by gradual parameter changes. It can be considered as a general format of Updated IMM (UIMM), relaxing the irreversible assumption, thereby widening its applicability to a broader range of problems [19].

5.3. Moving Window Interactive Multiple Model for Fault Intensity and Remaining Useful Life Estimation

The novel Moving Window Interactive Multiple Model (MWIMM) strategy is proposed and is well-suited for addressing problems characterized by a gradual progression of degradation, such as estimating a system's Remaining Useful Life (RUL) and measuring fault intensity. Assessment of RUL involves evaluating the level of degradation in a system and estimating its remaining operational lifespan, with the estimation of battery State of Health (SoH) being a prominent example. Precise fault intensity measurement is a fundamental pillar in prognostics and condition monitoring applications. Taking account of the inherent chronological order involved in these issues, MWIMM strategy can effectively estimate RUL and quantify fault intensity, incorporating supplementary temporal information to enhance computational efficiency, and improve identifiability compared to IMM strategy. Consider a general linear system that is subject to switching as described below:

$$\boldsymbol{x}(k) = \boldsymbol{A}\big(M(k)\big)\boldsymbol{x}(k-1) + \boldsymbol{B}\big(M(k)\big)\boldsymbol{u}(k) + \boldsymbol{v}\big(k-1, M(k)\big), \tag{5.1}$$

$$\boldsymbol{z}(k) = \boldsymbol{C}\big(M(k)\big)\boldsymbol{x}(k) + \boldsymbol{D}\big(M(k)\big)\boldsymbol{u}(k) + \boldsymbol{w}\big(k, M(k)\big). \tag{5.2}$$

In this context, $\boldsymbol{x}(k)$ and $\boldsymbol{z}(k)$ are state and measurement vectors respectively, $M(k)$ represents the true model at time k, while $\boldsymbol{A}\big(M(k)\big)$, $\boldsymbol{B}\big(M(k)\big)$, $\boldsymbol{C}\big(M(k)\big)$, and $\boldsymbol{D}\big(M(k)\big)$ refer to the system matrices associated with model $M(k)$. Additionally, $\boldsymbol{v}\big(k-1, M(k)\big)$ and $\boldsymbol{w}\big(k, M(k)\big)$ represent the process and measurement noise corresponding to model $M(k)$, respectively. These systems are also known as jump-linear systems, assuming that the mode jump process exhibits left continuity [1]. This means that the influence of the new model initiates from time k onwards. The vector $\boldsymbol{x}(k)$, which takes on continuous values, and the discrete variable $M(k)$ are sometimes denoted as the base state and modal state, respectively [1].

The model at time k is assumed to be among the N possible fault severity levels as:

$$M(k) \in \left\{M_{FL[i]}\right\}_{i=0}^{N-1}, \tag{5.3}$$

where the subscript $FL[i]$ stands for fault intensity level of "i". A larger "i" means the model has a more severe fault (i.e., the model $M_{FL[0]}$ corresponds to a healthy system or zero fault intensity level, and model $M_{FL[i]}$ has the fault intensity level of "i"). Similarly for RUL estimation, $M(k)$ is assumed to be among the N possible RUL levels as:

$$M(k) \in \left\{M_{RUL[i]}\right\}_{i=0}^{N-1}. \tag{5.4}$$

Here, the index "i" serves as an indicator of the system's level of degradation. For instance, the model $M_{RUL[0]}$ corresponds to zero degradation or the maximum RUL, while the model $M_{RUL[i]}$ represents the RUL level associated with the degradation level "i" of the system. In a general formulation applicable to all level-based model

sets, such as fault intensity level sets or RUL level sets, equations (2.24) and (5.4) can be expressed as follows:

$$M(k) \in \{M_{L[i]}\}_{i=0}^{N-1}. \tag{5.5}$$

In this context, $M_{L[i]}$ represents the model corresponding to level "i". Assuming that the model switching follows a Markov process with a known mode transition, a common assumption in MMAE strategies leads to the following [1]:

$$p_{ij} \triangleq P\{M(k) = M_{L[j]} | M(k-1) = M_{L[i]}\}. \tag{5.6}$$

The mode transition probabilities, represented by p_{ij}, are constant over time and independent of the base state. To account for the inherent temporal information associated with the chronological order, it is possible to build the transition matrix assuming that the transition probability increases when the model levels are in close proximity, as illustrated in equation (5.7):

$$|i - j_1| < |i - j_2| \rightarrow p_{ij_1} > p_{ij_2}. \tag{5.7}$$

In contrast to the IMM strategy, the MWIMM approach utilizes a filter bank that includes only neighboring models of the matched model, incorporating information aligned with the chronological order. Consequently, the number of filters operating in parallel depends on the chosen size of the moving window that defines the neighborhood. As illustrated in Figure 2-9, when a model transition occurs, signifying a change in the matched model, the moving window adjusts accordingly. Regarding the initial condition, it is reasonable to assume that the system is in a healthy state (level zero) at the commencement of the process. However, the proposed algorithm can start from any other initial condition.

Remark 1: *In cases where the true model is not included within the model bank contained in the window employed by the MWIMM approach, an automatic adjustment takes place. Such cases can occur due to incorrect initial conditions or a significant and abrupt change during the process that pushes the model outside the window. The adjustment process involves initial convergence towards the "nearest" model [1], followed by the subsequent sliding of the window's position.* ■

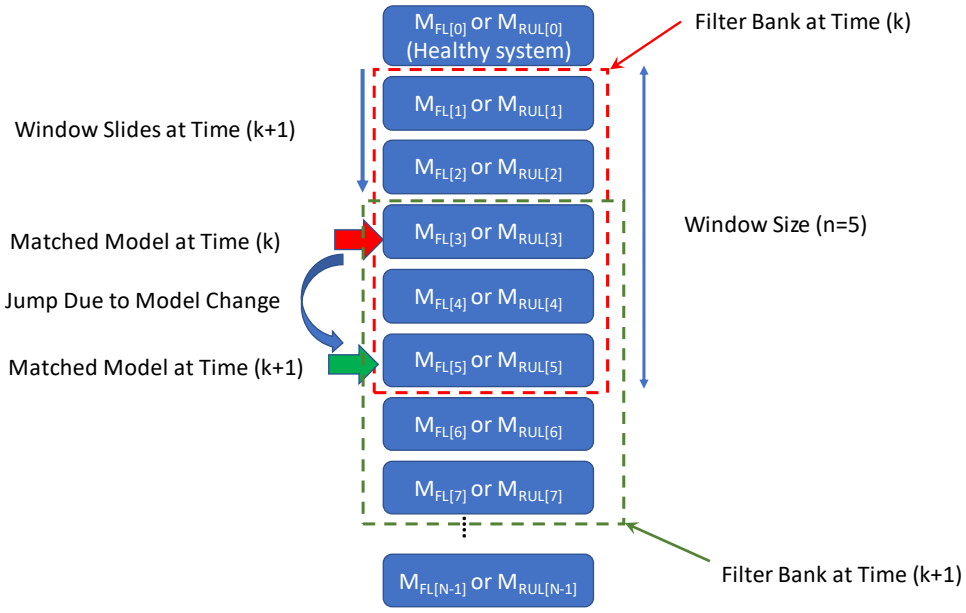

Figure 5-1. Flowchart illustrating the MWIM approach for estimating RUL and addressing fault intensity issues.

Remark 2: *In general, it is advisable to opt for an odd-sized window in the MWIMM framework, with the matched model positioned at the center. This choice helps prevent any bias towards switching to higher or lower levels. However, depending on the application, it is permissible to employ a skewed window that tilts towards a specific direction. For instance, in the case of RUL*

estimation, where switching consistently occurs in the direction of lower RUL due to the nature of aging, the MWIMM design can incorporate a skewed window that promotes switching predominantly in that specific direction ■

Remark 3*: The applicability of the MWIMM strategy extends to nonlinear systems by employing linearization techniques, following the same underlying principles utilized in IMM strategy [1].* ■

Remark 4: *The computational efficiency of the MWIMM approach is enhanced by reducing the number of running filters, number of combinations and number of probability calculations in comparison to the IMM strategy. This improvement is demonstrated in Table 5-1, where "n" represents the size of the moving window and "N" denotes the total number of models. The same strategy can be applied to GPB1 and GPB2 estimators using targeted moving windows, known as MWGPB1 and MWGPB2 respectively, in Table 5-1, resulting in improved computational efficiency.*

Table 5-1: A Comparative Analysis of Computational Requirements among Various MMAE Strategies.

Adaptive Estimation Strategy	**Number of Combinations**	**Number of Filters**	**Number of Probability Calculations**
IMM [1]	$N+1$	N	N^2+N
MWIMM	$n+1$	n	$n2+n$
GPB1 [1]	1	N	N
MWGPB1	1	n	n
GPB2 [1]	$N+1$	N^2	N^2+N
MWGPB2	$n+1$	n^2	n^2+n

■

Based on Remark 1, it can be inferred that selecting a window of size $n = 3$ with the matched model in the center is generally adequate since the MWIMM strategy adjusts the window position over time to encompass the true model. However, in situations where the model levels are closely spaced, resulting from selecting small bin levels, and the system undergoes rapid changes, the sliding window may lag behind and fail to converge to include the true model in a timely manner. Increasing the window size addresses this issue by sacrificing computational efficiency (as shown in Table 5-1), but it facilitates the inclusion of the true model within the sliding window and expedites convergence. Further elaboration on these issues will be provided in the subsequent section, which discusses the selection of MWIMM parameters for parameter estimation problems.

5.4. Moving Window Interactive Multiple Model for Parameter Identification

The MWIMM strategy can be applied in a general context for parameter identification tasks when system parameters are unknown and potentially subject to time variations. Consider a general linear system as follows, with parameter $\theta(k)$ being unknown and time-varying:

$$\boldsymbol{x}(k) = \boldsymbol{A}\big(\theta(k)\big)\boldsymbol{x}(k-1) + \boldsymbol{B}\big(\theta(k)\big)\boldsymbol{u}(k) + \boldsymbol{Q}\big(\theta(k)\big)v(k-1), \tag{5.8}$$

$$\boldsymbol{z}(k) = \boldsymbol{C}\big(\theta(k)\big)\boldsymbol{x}(k) + \boldsymbol{D}\big(\theta(k)\big)\boldsymbol{u}(k) + \boldsymbol{R}\big(\theta(k)\big)\boldsymbol{w}(k), \tag{5.9}$$

where $\boldsymbol{A}\big(\theta(k)\big)$, $\boldsymbol{B}\big(\theta(k)\big)$, $\boldsymbol{C}\big(\theta(k)\big)$, and $\boldsymbol{D}\big(\theta(k)\big)$ represent system matrices, $\boldsymbol{Q}\big(\theta(k)\big)$ and $\boldsymbol{R}\big(\theta(k)\big)$ denote the matrices associated with process noise and measurement noise, respectively, as functions of $\theta(k)$. Without loss of generality $\theta(k)$ is assumed to be bounded as follows:

$$\beta_1 \leq \theta(k) \leq \beta_2. \tag{5.10}$$

Then, the set of models can be created based on discretizing the value of $\theta(k)$ to N bins as:

$$\theta_i \triangleq \beta_1 + \frac{(2i+1)}{2N}(\beta_2 - \beta_1) \quad where\ i \in \{0,1,\dots,N-1\}, \tag{5.11}$$

$$M(k) \in \{M_{L[\theta_i]}\}_{i=0}^{N-1}, \tag{5.12}$$

where θ_i represents the central value of the ith bin, and $M_{L[\theta_i]}$ corresponds to the model associated with parameter θ_i, which can be derived based on equations (5.8) and (5.9). The total number of models (N) depends on the chosen bin size for θ_i. Thus, identification of parameter θ entails determining the model $M(k)$ in equation (5.12), which can be solved using the MWIMM strategy. Opting for a smaller bin size enhances the resolution for identification of θ; however, this leads to closely spaced $M_{L[\theta_i]}$ models, posing a greater challenge for MWIMM in terms of identification. Figure 5-2 illustrates the application of MWIMM in a parameter identification context for estimating a time-varying parameter. This figure highlights the importance of two additional parameters: the window size and the updating time for the MWIMM sliding window. Remark 1 suggests that a window size of $n = 3$, with the matched model positioned in the center, is generally sufficient. However, for improved performance, the window size can be determined by considering the confidence interval of the Probability Density Function (PDF), if such information is available (as depicted in Figure 5-2). The impact of the updating time and bin size will be extensively investigated in the following section through several case studies.

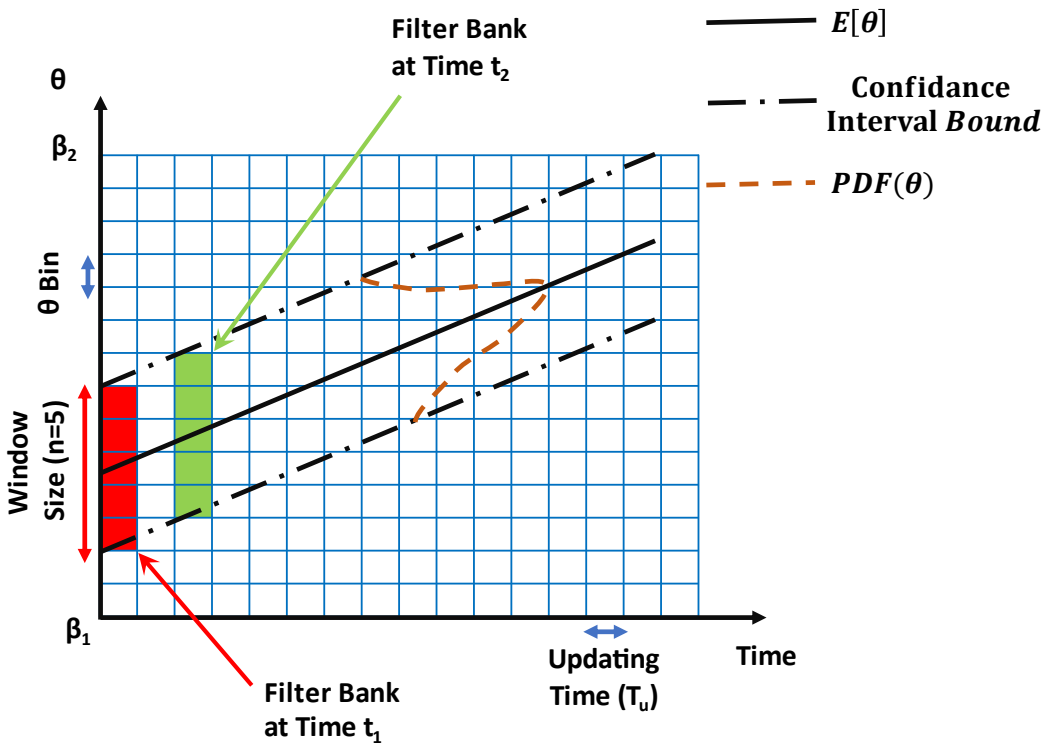

Figure 5-2. *Parameter identification using the MWIMM strategy.*

Remark 5: *If the probability distribution function of the parameter to be identified ($\boldsymbol{\theta}$) is available, the transition matrix for the MWIMM strategy can be formed accordingly.* ■

Remark 6: *The aforementioned approach can also be applied for identification of multiple parameters by utilizing a parameter vector ($\boldsymbol{\theta}$), whereby the number of models grows exponentially with respect to the number of parameters to be identified.* ■

5.4.1. Case Study: Second Order System Parameter identification

This section utilizes the MWIMM strategy with the Kalman Filter as the underlying filter (referred to as MWIMM-KF) to estimate the natural frequency of a second-order system. Assuming that only the first state has been measured, the state-space model (5.13) represents a generic second-order system with parameters such as

damping ratio ζ, natural frequency ω_0, measurement noise $\boldsymbol{w}(k)$, and process noise $\boldsymbol{v}(k)$:

$$\begin{cases} x_1(k+1) = x_1(k) + T_s x_2(k) + v_1(k) \\ x_2(k+1) = -T_s\omega_0^2 x_1(k) + (1 - 2T_s\zeta\omega_0)x_2(k) + T_s b u(k) + v_2(k)' \\ z(k) = x_1(k) + w(k). \end{cases} \quad (5.13)$$

here T_s denotes the time-step and u is the system input. Let us assume that parameters of the system are specified as follows: $\zeta = 0.1$, $b = 100$, uncorrelated process noise $v_1(k) \sim \mathcal{N}(0, 10^{-12})$ and $v_2(k) \sim \mathcal{N}(0, 10^{-6})$, and measurement noise $w(k) \sim \mathcal{N}(0, 10^{-10})$. Given that the system behavior changes gradually over time due to variations in the natural frequency, the MWIMM strategy can be employed to estimate the natural frequency.

In this approach, a window size of three is chosen, limiting the consideration to three models in the filter bank at each instant. To ensure a high resolution, the bin size for the natural frequency is set to 0.05 Hz. The sampling time used in the filter is 0.002s, while the updating time bin for the sliding window (T_u) is 0.1s. The transition matrix P_{ij}, initial mode probability $\mu(0)$, and mode probability threshold for sliding $\mu_{Threshold}$, are determined as follows:

$$\boldsymbol{P}_{ij} = \begin{bmatrix} 0.9 & 0.05 & 0.05 \\ 0.05 & 0.9 & 0.05 \\ 0.05 & 0.05 & 0.9 \end{bmatrix}, \quad \boldsymbol{\mu}(0) = \begin{bmatrix} 0.25 \\ 0.5 \\ 0.25 \end{bmatrix}, \quad \mu_{Threshold} = 0.5. \quad (5.14)$$

The threshold for the mode probability in the sliding window reflects the sliding window's sensitivity to model transitions. A higher threshold value makes the MWIMM window reluctant to sliding, thereby minimizing false transitions caused by noise. However, it also reduces the sensitivity of the estimation to parameter changes.

In this case study, a threshold of 0.5 is chosen to ensure that sliding occurs only when the new "matched model" has the highest probability among the model banks. The minimum threshold can be set as the maximum mode probability at each time step to establish a reference level.

The covariance matrices used for the Kalman filter are derived from the measurement and process noises in the following manner:

$$\boldsymbol{Q} = \begin{bmatrix} 10^{-12} & 0 \\ 0 & 10^{-6} \end{bmatrix}, \qquad \boldsymbol{R} = 10^{-10}, \qquad \boldsymbol{P}(0|0) = \begin{bmatrix} 1 & 0 \\ 0 & 1 \end{bmatrix}. \tag{5.15}$$

The results illustrated in Figure 6-1 show the MWIMM-KF's effective estimation of both states, while successfully identifying the gradual change in the natural frequency. With a chosen window size of three ($n = 3$), Figure 6-1.a displays three mode probabilities: “Model Low”, “Model Mid”, and “Model Up”, corresponding to models with lower, middle, and higher natural frequencies within the window.

When the mode probability of “Model Up” surpasses the others (t between 25s and 125s), it signifies an increasing natural frequency, prompting an upward slide of the MWIMM window. Conversely, when the mode probability of “Model Low” exceeds the others (from $t = 175s$ to $t = 275s$), it indicates a decreasing natural frequency, causing the window to slide downward. Finally, when the mode probability of “Model Mid” outweighs the others ($t \leq 25s$ or $125s \leq t \leq 175s$ or $275s \leq t$), it signifies a constant natural frequency, resulting in the window to remain stationary. In Figure 6-1.b, the estimated natural frequency exhibits step levels with a resolution of 0.05 Hz, derived from the chosen frequency bin in the MWIMM models.

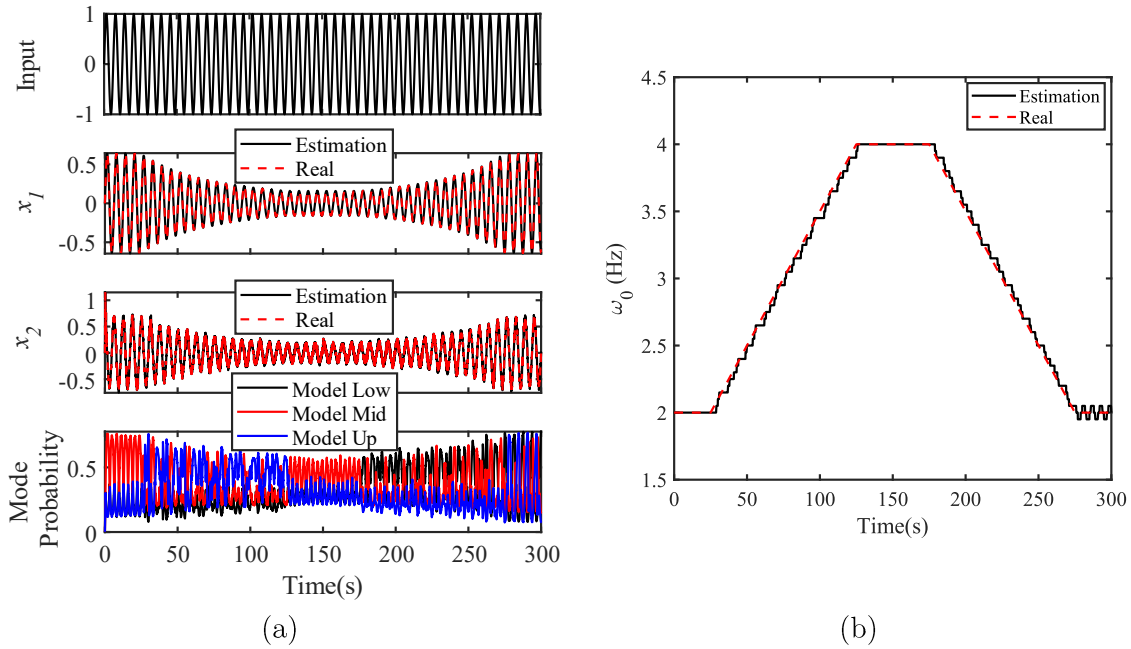

Figure 5-3. *Using MWIMM-KF for estimating the time-varying parameter of a second-order system: (a) State estimation; (b) Parameter identification.*

Effect of Bin Size and Updating Time

The choice of bin size within the MWIMM strategy significantly impacts the process of parameter estimation by influencing both the accuracy and convergence of the estimation. A smaller bin size enhances the resolution of the estimated parameter, allowing for finer details to be captured. However, when a parameter undergoes rapid changes, MWIMM with a small bin size will slide the window of filter bank slower than the rate of parameter change and will fail to converge to the true value in a timely manner. This issue is shown in Figure 5-4, where Bin1 demonstrates a scenario in which the MWIMM strategy lacks sufficient time to effectively track the gradual change in the target parameter. To address this challenge, one potential solution is to increase the window size ($n > 3$), allowing for a larger interval to be covered in each update. Nevertheless, this approach necessitates running more filters in parallel,

leading to increased computational demand and a higher risk of combinatorial explosion [13]. Additionally, employing a small bin size diminishes the difference between the models in the filter bank, and potentially further escalates the risk of combinatorial explosion.

In Figure 5-5, the natural frequency estimation of the previously introduced second-order system is performed using different bin sizes under the exact same conditions. It is evident that larger bin sizes, such as 0.4 Hz and 0.2 Hz, lead to a deterioration in the resolution of the parameter estimation. On the other hand, employing a very small bin size of 0.02 Hz causes the MWIMM strategy to lag behind and ultimately fail in accurately estimating the natural frequency.

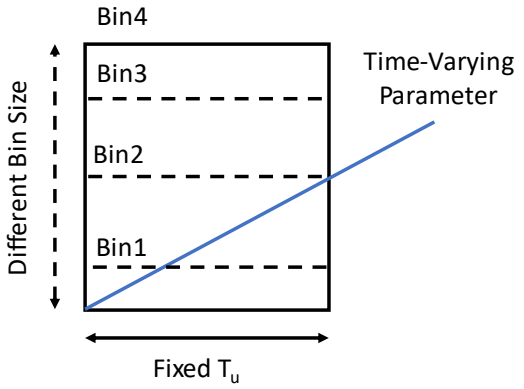

Figure 5-4. *Schematic depiction of the effect of the rate of change of a parameter on determining an appropriate bin size.*

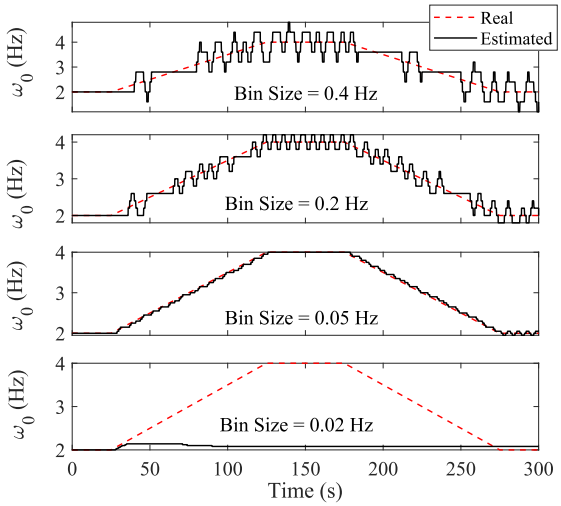

Figure 5-5. *Estimating natural frequency for different bin size.*

These observations highlight the trade-off involved in selecting an appropriate bin size in MWIMM. A balance must be struck between achieving higher resolution and ensuring timely convergence to the true parameter value. The choice of bin size should be tailored to the specific characteristics of the parameter being estimated and the dynamics of the system under investigation.

Employing a longer updating time in the MWIMM increases the amount of measurement data available for estimating the correct model, thereby reducing the likelihood of false switching, and yielding smoother parameter estimation results. However, when the rate of change of the parameter is high, MWIMM with a longer updating time, as demonstrated in Figure 5-6 for updating T_{u3} and T_{u4}, tends to lag behind. In Figure 5-7, estimation of the natural frequency is conducted for the previously introduced second-order system using various updating times while maintaining a fixed bin size of 0.05Hz, as utilized previously. As depicted in this figure, a smaller updating time of 0.01s results in higher fluctuations in the estimated natural frequency, as expected. Conversely, larger updating times such as 1s and 2s cause the MWIMM to be unable to keep pace with the rapid rate of change in the natural frequency.

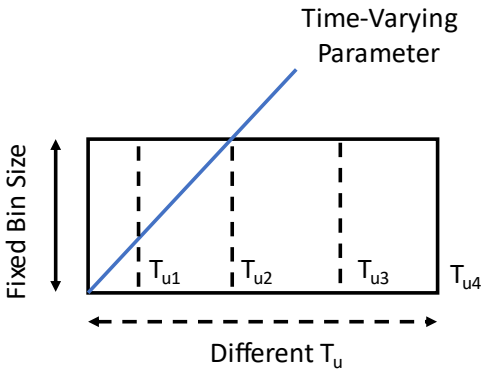

Figure 5-6. *Schematic depiction of the effect of the rate of change of a parameter on determining an appropriate updating time.*

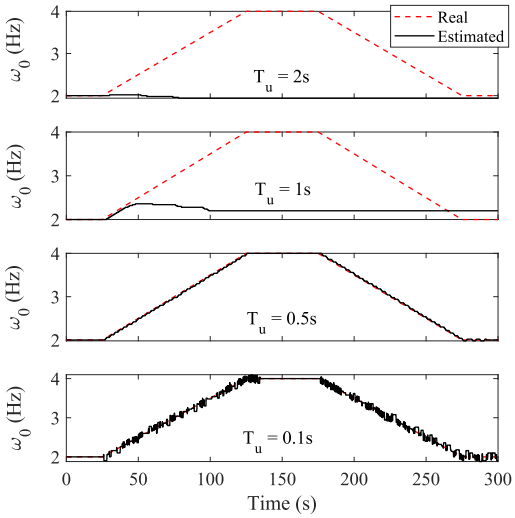

Figure 5-7. *Estimating natural frequency for different updating time.*

Identifying Both Natural Frequency and Damping Ratio

One alternative approach for estimating the natural frequency involves utilizing joint state and parameter estimation. This technique considers the natural frequency as an augmented state within the system and employs a nonlinear filter, such as the Extended Kalman Filter (EKF), to estimate it alongside other states, as long as the system maintains observability. However, it is important to note that this method provides a suboptimal solution, and the accuracy of the linearization is compromised when there is significant uncertainty in the parameters. By considering the natural frequency as an augmented state in the system described in (5.13), it is possible to prove observability of the system using Lie derivative. Consequently, the natural frequency can be estimated using the EKF estimation method. In this section, the EKF-based MWIMM method (MWIMM-EKF) is applied to identify the damping ratio and the natural frequency of a second-order system, thereby demonstrating the applicability of the MWIMM approach for nonlinear systems as well.

Regarding the natural frequency as an augmented state, we can reformulate the model in equation (5.13) as follows:

$$\begin{cases} x_1(k+1) = x_1(k) + T_s x_2(k) + v_1(k) \\ x_2(k+1) = -T_s x_3^2(k) x_1(k) + \big(1 - 2T_s \zeta x_3(k)\big) x_2(k) + T_s b u(k) + v_2(k), \\ x_3(k+1) = x_3(k) + v_3(k) \end{cases} \tag{5.16}$$
$$z(k) = x_1(k) + w(k).$$

State variable x_3, which represents the natural frequency, incorporates artificial noise $v_3(k) \sim \mathcal{N}(0, 10^{-6})$. The MWIMM employs the same parameters as described in equation (5.14). However, here, the set of considered models is formed according to discretization of damping ratio, and model validation is performed using the estimated value of the damping ratio at each time step. To ensure accurate resolution,

a bin size of 0.05 is chosen for the damping ratio. Moreover, when considering the augmented state vector, covariance matrices of the EKF are updated as follows:

$$\boldsymbol{Q} = \begin{bmatrix} 10^{-12} & 0 & 0 \\ 0 & 10^{-6} & 0 \\ 0 & 0 & 10^{-6} \end{bmatrix},\ \boldsymbol{R} = 10^{-10},\ \boldsymbol{P}(0|0) = \begin{bmatrix} 1 & 0 & 0 \\ 0 & 1 & 0 \\ 0 & 0 & 1 \end{bmatrix}. \tag{5.17}$$

Form equation (5.16), the measurement function can be obtained as $h(x) = x_1$. The observability matrix can then be computed utilizing Lie derivatives in the following manner:

$$\boldsymbol{\mathcal{O}}(x,u) = \begin{bmatrix} dL_f^0 h(x) \\ dL_f^1 h(x) \\ \cdots \\ dL_f^{n-1} h(x) \end{bmatrix} = \begin{bmatrix} 1 & 0 & 0 \\ 0 & 1 & 0 \\ x_3^2 & 2\zeta x_3 & 2\zeta x_2 + 2x_3 x_1 \end{bmatrix}. \tag{5.18}$$

Here, $dL_f^n h$ represents the nth order Lie derivative of the measurement function h with respect to the system model f, and $\mathcal{O}$ represents the observability matrix. The observability matrix is full rank as long as $2\xi x_2 + 2x_3 x_1$ is not equal to zero. It means that the system is observable. The only scenario for the system to be unobservable is when both states x_1 and x_2 are zero (trivial solution for any linear system) which is very rare, and can be ignored. Figure 5-8 demonstrates that the MWIMM-EKF accurately estimates natural frequency, damping ratio, and system states, including scenarios with both constant and unknown damping ratios (Figure 5-8.a) as well as time-varying damping ratios (Figure 5-8.b).

For comparative analysis, in this section, the augmented state EKF is employed to estimate both natural frequency and damping ratio along with other states. Therefore, equation (5.13) can be reformulated as follows:

$$\begin{cases} x_1(k+1) = x_1(k) + T_s x_2(k) + v_1(k) \\ x_2(k+1) = -T_s x_3^2(k) x_1(k) + \big(1 - 2T_s x_4(k) x_3(k)\big) x_2(k) + T_s b u(k) + v_2(k) \\ x_3(k+1) = x_3(k) + v_3(k) \\ x_4(k+1) = x_4(k) + v_4(k) \end{cases}, \tag{5.19}$$
$$z(k) = x_1(k) + w(k),$$

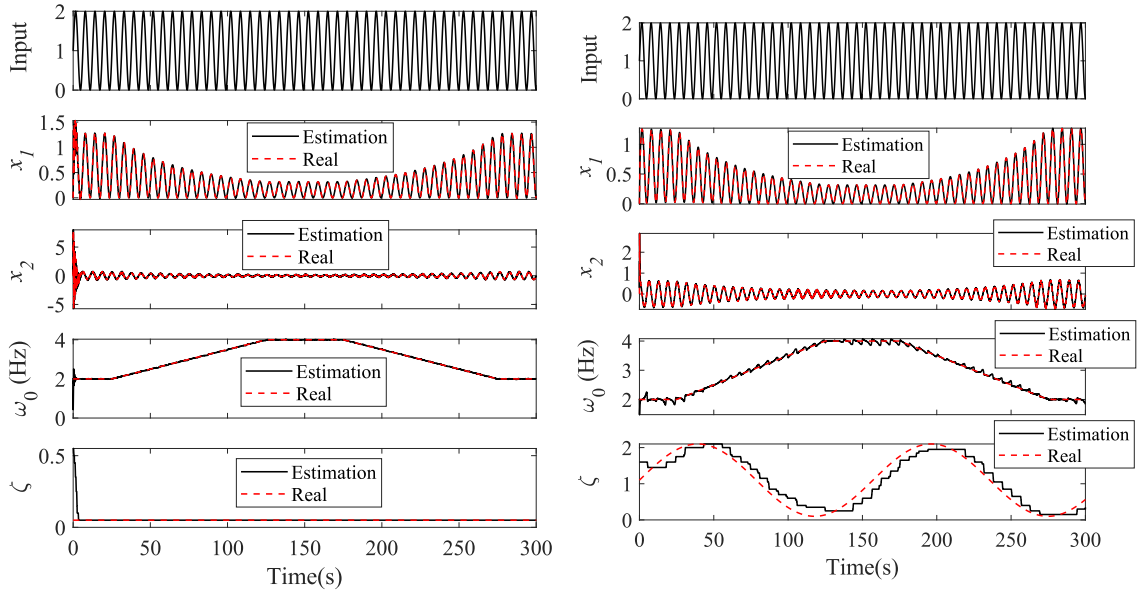

Figure 5-8. *Estimating natural frequency and damping ratio using MWIMM-EKF: (a) Constant unknown damping ratio; (b) Time-varying damping ratio.*

where x_3 is natural frequency and x_4 is damping ratio. In order to ensure a fair comparison, all conditions in this section are assumed to be identical to those in the previous section. However, there is one distinction regarding the artificial noise v_4 corresponding to damping ratio x_4. Obtaining this artificial noise for the augmented state EKF is not straightforward due to the lack of information about dynamics of the augmented states. Consequently, it becomes challenging to intuitively select the noise based on engineering guesswork [2], and employing discriminative training methods is ineffective for determining the process noise for all four states using only one measurement x_1.

Assuming that damping ratio can fluctuate with standard deviation of 0.01, an added artificial noise is assumed with the normal distribution of $v_4(k) \sim \mathcal{N}(0, 10^{-4})$. Covariance matrices of the EKF are then derived as follows:

$$\boldsymbol{Q} = \begin{bmatrix} 10^{-12} & 0 & 0 & 0 \\ 0 & 10^{-6} & 0 & 0 \\ 0 & 0 & 10^{-6} & 0 \\ 0 & 0 & 0 & 10^{-4} \end{bmatrix},\ \boldsymbol{R} = 10^{-10},\ \boldsymbol{P}(0|0) = \begin{bmatrix} 1 & 0 & 0 & 0 \\ 0 & 1 & 0 & 0 \\ 0 & 0 & 1 & 0 \\ 0 & 0 & 0 & 1 \end{bmatrix}. \quad (5.20)$$

The observability matrix can then be computed using Lie derivatives as:

$$\begin{aligned} \boldsymbol{\mathcal{O}}(x,u) &= \begin{bmatrix} dL_f^0 h(x) \\ dL_f^1 h(x) \\ \dots \\ dL_f^{n-1} h(x) \end{bmatrix} \\ &= \begin{bmatrix} 1 & 0 & 0 & 0 \\ 0 & 1 & 0 & 0 \\ x_3^2 & 2x_4x_3 & 2x_3x_1 + 2x_2x_4 & 2x_2x_3 \\ 2x_3^3x_4 & 4x_3^2x_4^2 + x_3^2 & 8x_3x_4^2x_2 + 6x_3^2x_4x_1 + 2x_2x_3 + 2bx_4u & 8x_4x_3^2x_2 + 2x_3^3x_1 + 2bx_3u \end{bmatrix}. \end{aligned} \quad (5.21)$$

As shown, it is not necessarily guaranteed that the observability matrix to be full rank, indicating that in general, observability cannot be proven. Figure 5-9 illustrates that the augmented state EKF fails to estimate both constant and time-varying damping ratio.

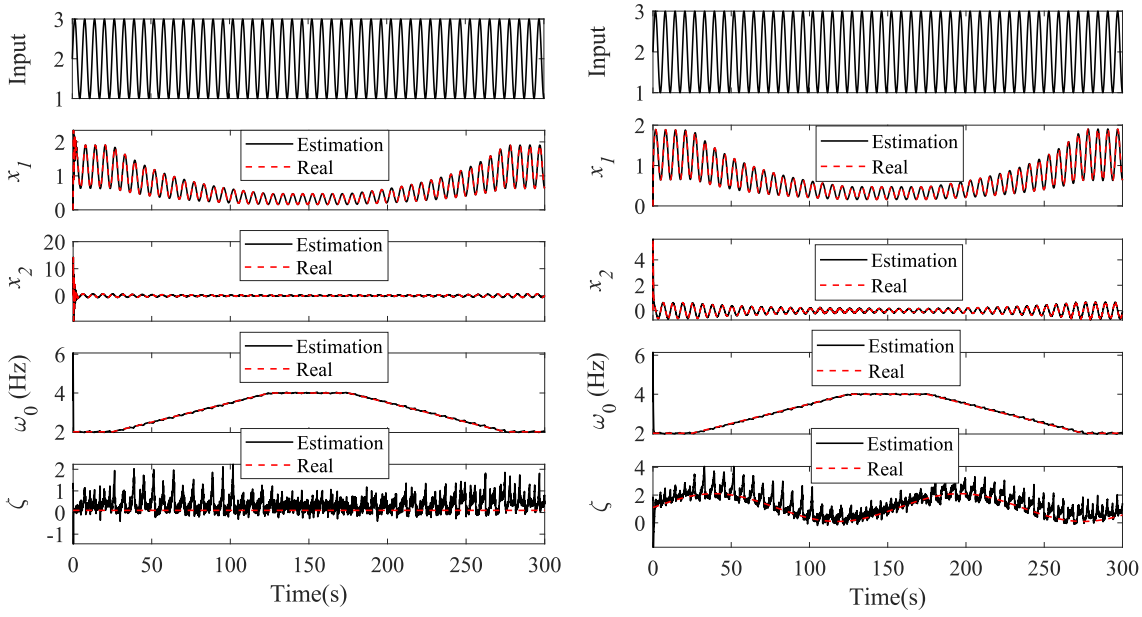

Figure 5-9. *Estimating natural frequency and damping ratio using Augmented state EKF: (a) Constant unknown damping ratio; (b) Time-varying damping ratio.*

5.5. Discussion And Future Directions

To comprehensively investigate the performance of the Multiple-Model Adaptive Estimation (MMAE) strategy, particularly the Moving Window IMM (MWIMM) proposed in this paper, it is essential to carefully examine three key factors. These factors play a crucial role in understanding the efficacy of these strategies:

1. **Identifiability:** This factor evaluates the ability of the MMAE strategy to accurately identify the true model among the bank of possible models. It is important to note that even if all the models within the bank are observable, identifiability cannot be guaranteed. The absence of identifiability indicates the singularity of the Fisher information matrix, and vice versa [20]. In such cases, it becomes necessary to incorporate prior information by imposing constraints on the model or consider reparameterization of the model as potential solutions.
2. **Optimality:** Theoretically speaking, optimality can be guaranteed only in the case of static MMAE, where the system has time-invariant parameters [2]. For dynamic multiple-model adaptive estimation strategies such as Interacting Multiple Models (IMM) and MWIMM, which deal with systems with time-varying parameters, only suboptimal solutions can be obtained.
3. **System Excitation:** To accurately estimate time-varying parameters, the system under study needs to be excited. This excitation is necessary for convergence towards the true model. Therefore, to maintain observability, careful consideration should be given to the level of system excitation, especially for nonlinear systems.

Understanding these factors can significantly contribute to the development and evaluation of effective estimation strategies in various applications. In the following section, an illustrative example is presented to show the identifiability challenge encountered in dynamic multiple model adaptive estimation.

Consider a second-order system, exemplified by a mass-spring-damper configuration, which is derived by an external force F as:

$$\begin{cases} x_1(k+1) = x_1(k) + T_s x_2(k) + v_1(k) \\ x_2(k+1) = -T_s\omega_0^2 x_1(k) + (1 - 2T_s\zeta\omega_0)x_2(k) + T_s bu(k) + v_2(k) - T_s F' \\ z(k) = x_2(k) + w(k). \end{cases} \tag{5.22}$$

Using the previously mentioned parameter values, including a natural frequency of 2Hz, a damping ratio of 0.1, a value of b equivalent to 100, uncorrelated process noise $v_1(k) \sim \mathcal{N}(0, 10^{-12})$, and $v_2(k) \sim \mathcal{N}(0, 10^{-6})$. Now considering the availability of velocity measurement for the second state, subject to measurement noise $w(k) \sim \mathcal{N}(0, 10^{-8})$. Additionally, assume the external force F to possess three distinct levels, namely low (50N), mid (500N), and high (2000N). System observability is assessed as follows:

$$\begin{aligned} \boldsymbol{C} = [0 \quad 1],\ \boldsymbol{A} = \begin{bmatrix} 0 & 1 \\ -\omega_0^2 & -2\zeta\omega_0 \end{bmatrix} \Rightarrow \boldsymbol{\mathcal{O}} = \begin{bmatrix} \boldsymbol{C} \\ \boldsymbol{CA} \end{bmatrix} = \begin{bmatrix} 0 & 1 \\ -\omega_0^2 & -2\zeta\omega_0 \end{bmatrix} \\ \Longrightarrow full\ rank. \end{aligned} \tag{5.23}$$

The observability matrix with full rank indicates that the system is observable, allowing for unique determination of states x_1 and x_2. Nevertheless, as demonstrated in the following illustration, the external force cannot be estimated as an augmented state using the KF due to the system's lack of observability.

$$\begin{cases} x_1(k+1) = x_1(k) + T_s x_2(k) + v_1(k) \\ x_2(k+1) = -T_s\omega_0^2 x_1(k) + (1 - 2T_s\zeta\omega_0)x_2(k) - T_s x_3(k) + T_s bu(k) + v_2(k), \\ x_3(k+1) = x_3(k) + v_3(k) \\ z(k) = x_2(k) + w(k)\,. \end{cases} \tag{5.24}$$

In equation (5.24), the augmented state $\boldsymbol{x_3}$ represents the external force. To perform observability test, the observability matrix can be derived as follows:

$$\begin{aligned} \boldsymbol{C} = [0 \quad 1 \quad 0], \quad \boldsymbol{A} = \begin{bmatrix} 0 & 1 & 0 \\ -\omega_0^2 & -2\zeta\omega_0 & -1 \\ 0 & 0 & 0 \end{bmatrix} \Rightarrow \boldsymbol{\mathcal{O}} = \begin{bmatrix} \boldsymbol{C} \\ \boldsymbol{CA} \\ \boldsymbol{CA}^2 \end{bmatrix} \\ = \begin{bmatrix} 0 & 1 & 0 \\ -\omega_0^2 & -2\zeta\omega_0 & -1 \\ 2\zeta\omega_0^3 & (4\zeta^2-1)\omega_0^2 & 2\zeta\omega_0 \end{bmatrix} \Longrightarrow Rank(\boldsymbol{\mathcal{O}}) = 2 \\ \Rightarrow \boldsymbol{\mathcal{O}}\ is\ not\ full\ rank. \end{aligned} \tag{5.25}$$

According to Equation (5.25), it is evident that the system lacks observability, thereby preventing the estimation of the external force using the augmented KF. In order to address this issue, an alternative approach is IMM-KF. This method involves incorporating models for low, mid, and high external forces, and leveraging the mode probability to determine the true model at each time step, thereby enabling the identification of the external force. To assess the effectiveness of this approach, a series of events is considered as a simulation scenario:

1. For the initial 10 seconds, the external force is set to a low level ($\boldsymbol{F = 50N}$).
2. From 10 seconds to 20 seconds, the external force transitions to a mid-level ($\boldsymbol{F = 500N}$).
3. Finally, for the last 10 seconds, the external force switches to a high level ($\boldsymbol{F = 2000N}$).

Figure 5-10.a demonstrates that the IMM-KF fails to accurately estimate the state $\boldsymbol{x_1}$ and cannot correctly identify the external force, despite each model in the filter bank being individually observable based on Equation (5.25). However, as depicted in Figure 5-10.b and Figure 5-10.c, the IMM-KF can successfully estimate the states and identify the external force accurately when either the measurement for state $\boldsymbol{x_1}$ or both states are available. Overall, Figure 5-10 illustrates that the IMM-

KF achieves the best performance when measurements for both states are available, which is intuitively reasonable.

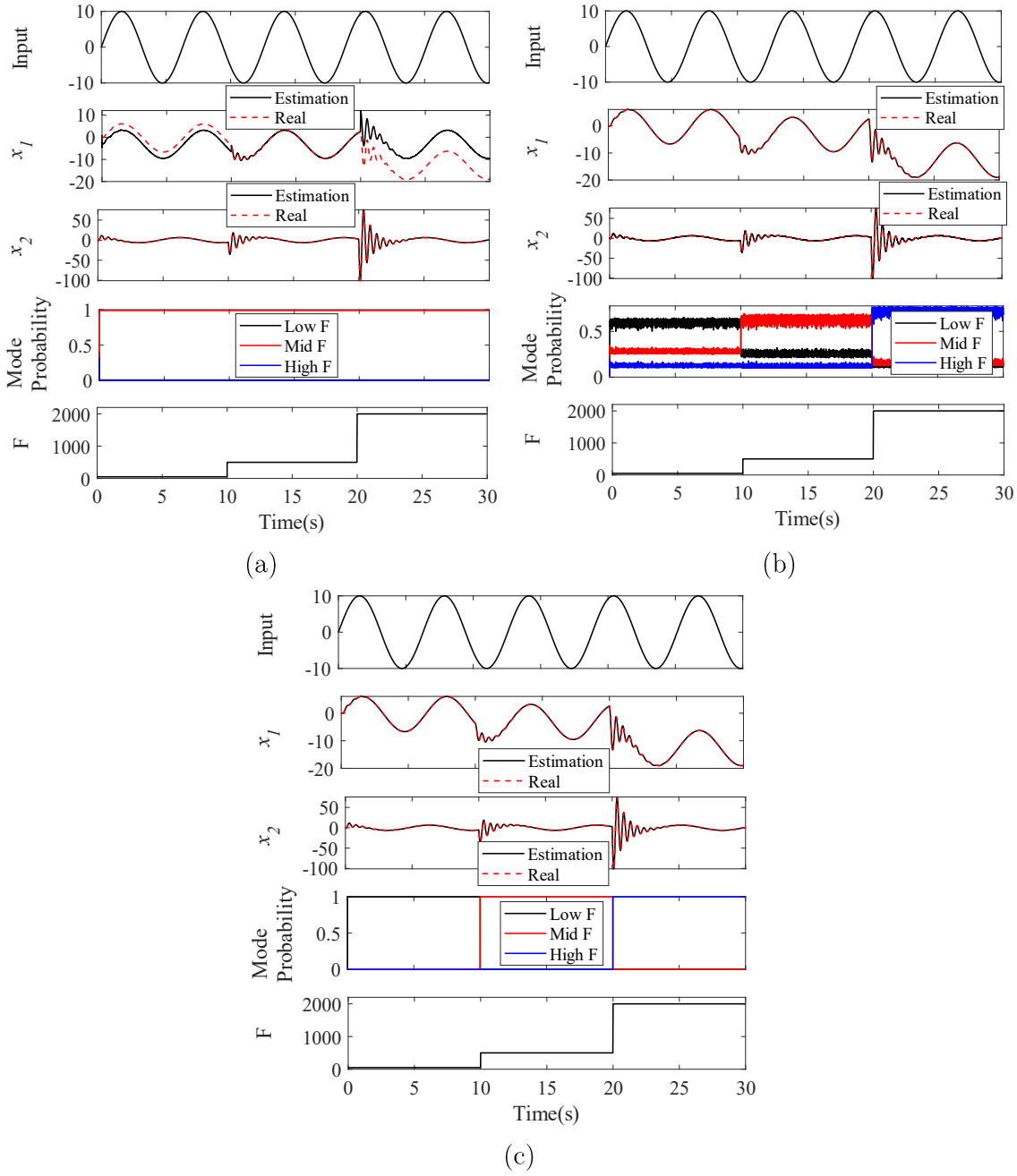

Figure 5-10. *Identifying the external force for a second order system using IMM-KF: (a) Measurement feedback from* x_2*; (b) Measurement feedback from* x_1*; (c) Measurement feedback from both states.*

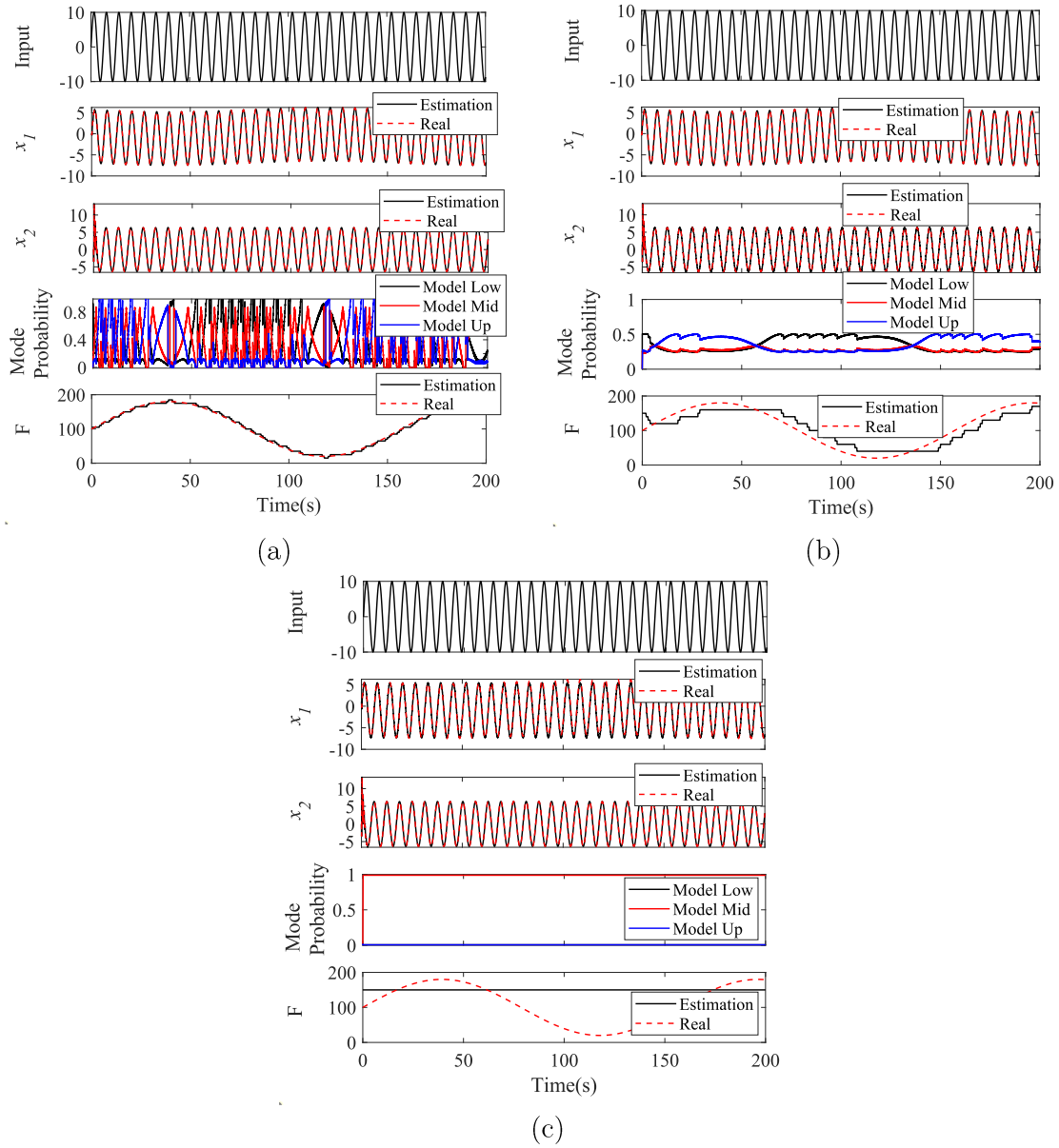

Figure 5-11. *Identifying the time-varying external force for a second order system using MWIMM-KF: (a) Measurement feedback from* $\boldsymbol{x_2}$*; (b) Measurement feedback from* $\boldsymbol{x_1}$*; (c) Measurement feedback from both states.*

Consequently, MWIMM is unable to accurately estimate the time-varying external force in cases where only the $\boldsymbol{x_2}$ measurement is available, as depicted in Figure 5-11. However, the external force estimation is achievable when either the $\boldsymbol{x_1}$

measurement or both state measurements are available. Additionally, it is evident that the performance of MWIMM improves significantly when both states are measured, as the system exhibits a higher degree of observability.

A viable approach to address the identifiability concern in this scenario involves utilizing a robust filter, such as the Smooth Variable Structure Filter (SVSF), in lieu of the Kalman filter to account for model mismatch. An IMM-SVSF-VBL, equipped with a small boundary layer for the measured state and a large boundary layer for the unmeasured state, can effectively detect sudden changes in the external force by including additional information as follows:

- By setting a small boundary layer threshold for the measured state $\boldsymbol{x_2}$, the IMM-SVSF-VBL is capable of recognizing changes in the system model, triggering the corrective action of the SVSF.
- Conversely, a large boundary layer threshold for the unmeasured state $\boldsymbol{x_1}$ implies that the system relies on the filter bank models to estimate the unmeasured state $\boldsymbol{x_1}$, avoiding from correcting the a priori estimations of the filters based on new measurements. Consequently, the incorrect models maintain a substantial a priori error, helping the IMM to find the most relevant model.

As depicted in Figure 5-12.a, unlike IMM-KF, IMM-SVSF-VBL successfully identifies sudden changes in the level of the external force. However, as demonstrated in Figure 5-12.b, it still struggles to identify the external force level when it changes gradually. In such cases, the slow deviation of the a priori error does not cross the boundary layer, giving the incorrect filter (representing a low external force model

here) sufficient time to adjust the gain, to maintain a small a priori error and prevent the IMM from switching. This limitation stems from the fact that the impact of a changing external force is akin to the displacement of a spring (x_1), and the filter cannot distinguish between the two solely based on the system's velocity measurement. This is due to the unobservability of the augmented state as shown in Equation (5.25).

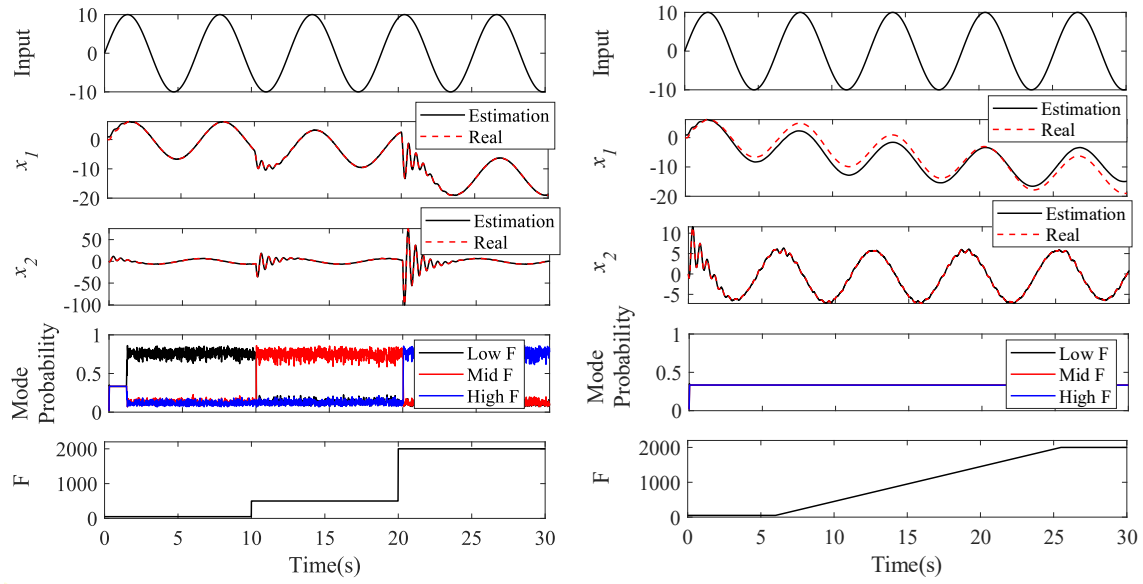

Figure 5-12. External load level identification in a second-order system form velocity measurement using IMM-SVSF-VBL: (a) Sudden change in the external load level; (b) Gradual change in the external load level.

5.6. Conclusion

In this study, a novel adaptive estimation strategy called Mowing Window Interacting Multiple Model (MWIMM) has been introduced to address the challenges of state estimation in the presence of uncertain model parameters and changing system dynamics. Focusing on a subset of possible models at each stage instead of considering all models, MWIMM improves identifiability and computational efficiency by

effectively narrowing down the search space for the true model. This approach enables the estimation of gradual changes in the system, making it particularly valuable for estimation of fault intensity and remaining useful life.

Parameter estimation problem was investigated, comparing the results obtained by the proposed method and the augmented state extended Kalman filter. The results demonstrated that the proposed MWIMM approach presents a promising alternative for effectively handling extensive parameter uncertainty and accommodating gradual changes in system parameters.

Instead of merging, an alternative for decreasing the number of regime sequences in MMAE algorithms involves employing pruning. Pruning entails the removal of low probability branches (i.e., regime sequence) from MMAE tree, in contrast to the merging approach used in IMM. While merging algorithms such as IMM filters are widely employed in estimation tasks like target tracking, a pruning algorithm like Multiple Model Pruning (MMP) [21] is more relevant for detecting changes in fault detection problems. In these scenarios, accurately identifying changes in the system's behavior is more important than estimating the system state. An entirely distinct approach to reduce the complexity and improve the performance of MMAE algorithms in addressing fault detection problems involves the adoption of the MMP algorithm. Future research can explore pruning techniques and compare their performance with merging approaches employed in this paper, such as IMM and MWIMM, for fault detection and diagnosis problems.

5.7. References

[1] Y. Bar-Shalom, X. R. Li, and T. Kirubarajan, *Estimation with applications to tracking and navigation: theory algorithms and software*. John Wiley & Sons, 2004.

[2] M. Athans and C.-B. Chang, "Adaptive estimation and parameter identification using multiple model estimation algorithm," 1976.

[3] M. Karasalo and X. Hu, "An optimization approach to adaptive Kalman filtering," *Automatica*, vol. 47, no. 8, pp. 1785–1793, 2011.

[4] S. A. Gadsden, S. Habibi, and T. Kirubarajan, "Kalman and smooth variable structure filters for robust estimation," *IEEE Trans. Aerosp. Electron. Syst.*, vol. 50, no. 2, pp. 1038–1050, 2014.

[5] S. Habibi, "The smooth variable structure filter," *Proc. IEEE*, vol. 95, no. 5, pp. 1026–1059, 2007.

[6] M. Al-Shabi, S. A. Gadsden, and S. R. Habibi, "Kalman filtering strategies utilizing the chattering effects of the smooth variable structure filter," *Signal Processing*, vol. 93, no. 2, pp. 420–431, 2013.

[7] P. Setoodeh, S. Habibi, and S. Haykin, *Nonlinear Filters: Theory and Applications*. John Wiley & Sons, 2022.

[8] D. Simon, *Optimal state estimation: Kalman, H infinity, and nonlinear approaches*. John Wiley & Sons, 2006.

[9] M. S. Grewal and A. P. Andrews, *Kalman filtering: Theory and Practice with MATLAB*. John Wiley & Sons, 2014.

[10] L. Ljung, "Asymptotic behavior of the extended Kalman filter as a parameter estimator for linear systems," *IEEE Trans. Automat. Contr.*, vol. 24, no. 1, pp. 36–50, 1979.

[11] L. Nelson and E. Stear, "The simultaneous on-line estimation of parameters and states in linear systems," *IEEE Trans. Automat. Contr.*, vol. 21, no. 1, pp. 94–98, 1976.

[12] P. Abbeel, A. Coates, M. Montemerlo, A. Y. Ng, and S. Thrun, "Discriminative training of kalman filters.," in *Robotics: Science and systems*,

2005, vol. 2, p. 1.

[13] A. Saeedzadeh, S. Habibi, M. Alavi, and P. Setoodeh, "A Robust Model-Based Strategy for Real-Time Fault Detection and Diagnosis in an Electro-Hydraulic Actuator Using Updated Interactive Multiple Model Smooth Variable Structure Filter," *J. Dyn. Syst. Meas. Control*, pp. 1–32, 2023.

[14] Y. Lu, H. Ma, E. Smart, and H. Yu, "Real-time performance-focused localization techniques for autonomous vehicle: A review," *IEEE Trans. Intell. Transp. Syst.*, 2021.

[15] T. Kirubarajan, Y. Bar-Shalom, K. R. Pattipati, and I. Kadar, "Ground target tracking with variable structure IMM estimator," *IEEE Trans. Aerosp. Electron. Syst.*, vol. 36, no. 1, pp. 26–46, 2000.

[16] M. Efe and D. P. Atherton, "The IMM approach to the fault detection problem," *IFAC Proc. Vol.*, vol. 30, no. 11, pp. 603–608, 1997.

[17] S. A. Gadsden, Y. Song, and S. R. Habibi, "Novel model-based estimators for the purposes of fault detection and diagnosis," *IEEE/ASME Trans. Mechatronics*, vol. 18, no. 4, pp. 1237–1249, 2013.

[18] Y. Zhang and J. Jiang, "Integrated active fault-tolerant control using IMM approach," *IEEE Trans. Aerosp. Electron. Syst.*, vol. 37, no. 4, pp. 1221–1235, 2001.

[19] A. Saeedzadeh, S. R. Habibi, and M. Alavi, "A Robust FDD Approach for an EHA Using the Chattering in Mode Probability of the IMM-SVSF."

[20] H. Bozdogan, "Model selection and Akaike's information criterion (AIC): The general theory and its analytical extensions," *Psychometrika*, vol. 52, no. 3, pp. 345–370, 1987.

[21] F. Gustafsson and F. Gustafsson, *Adaptive filtering and change detection*, vol. 1. Wiley New York, 2000.

6. Concluding Remarks

This chapter outlines the main research contributions and outcomes discussed in this thesis. Moreover, it provides recommendations for future works aimed at expanding and furthering the current research.

6.1. Summary of Research

This thesis considers the application of model-based methodologies to enhance fault diagnosis, introducing creative estimation strategies aimed at improving the diagnostic procedure. The core of this research centers on the application of stochastic filtering methods, with a particular focus on the Kalman Filter (KF) to manage challenges posed by process and measurement noise and robust filtering methods using Smooth Variable Structure Filters (SVSF) to effectively tackle uncertainties encountered in the fault diagnosis problems. The proposed algorithms aim to enhance computational efficiency, address fault discretization, and present robust fault detection strategies.

In addition to the innovation vector, which plays a role in filtering algorithms to adjust the predicted state vector based on the most recent estimation, the Smooth Variable Structure Filter (SVSF) has an additional set of indicators: the chattering signals associated with various state variables. Chapter 3 explored the concept of utilizing these chattering signals for the purpose of fault detection and identifying model mismatches. Within this chapter, mathematical expressions were formulated to describe the chattering signal of the SVSF in scenarios involving both full-state and partial-state measurements. The analysis extended to investigating the spectrogram of the chattering signal to extract temporal and spectral information.

Building upon the concept of Monte Carlo simulation and considering the characteristics of process and measurement noise, the expected value of the power spectrum of the chattering signal was determined and examined under normal operating conditions.

In Chapter 3, thresholds were established based on an analysis of power spectrum of the chattering of the SVSF filter for identifying faults. The threshold selection process was based on a careful balance between minimizing the risk of false alarms and ensuring that no significant system events leading to changes, such as faults, are overlooked. The strategy for determining this threshold took into account the probability distribution of the power spectrum of the chattering signal. A confidence interval was derived from this distribution, facilitating fault detection using a single realization of the event sequence, which is particularly suitable for real-time applications. Moreover, to retrieve temporal information regarding a fault, an analysis of the chattering signal using the short-time Fourier transform was conducted. The effectiveness of this proposed method in terms of fault detection and identification was demonstrated through the evaluation of various scenarios involving a typical second-order system and an electro-hydraulic actuator.

Employing a bank of filters within a Multiple Model Adaptive Estimation (MMAE) structure is a well-established model-based Fault Detection and Diagnosis (FDD) strategy known for addressing identifiability challenges. The parallel structure of these filters allows for swift adaptation, ensuring accurate state estimation in the event of a fault. Nevertheless, this approach suffers from two formidable obstacles: high computational demands and the assumption of fault parameters as discrete values from a finite set. Chapter 4 introduced the Updated Interactive Multiple Model

(UIMM) framework to address the computational intensity issue. By considering the irreversible nature of faults, the UIMM-SVSF algorithm demonstrated superior computational efficiency and reduced false alarm rates compared to the traditional IMM strategy. In chapter three the UIMM-SVSF was applied to diagnose leakage and friction faults in an Electro-Hydraulic Actuator (EHA), where it significantly outperformed IMM-SVSF and IMM-KF. The computational efficiency of UIMM-SVSF positions it as an ideal choice for real-time applications, particularly for Fault-Tolerant Control Systems (FTCS).

Expanding on this topic, Chapter 5 introduced an innovative strategy referred to as the 'Moving Window Interacting Multiple Model' (MWIMM). MWIMM is considered as an improved and computationally efficient variant of the IMM approach with enhanced performance in terms of identifiability. This enhancement is achieved by narrowing the search space to a specific window, instead of evaluating all potential models. MWIMM can be viewed as a broader adaptation of the Updated IMM (UIMM) concept, as it relaxes the assumption of irreversibility, thereby broadening its applicability to a wider spectrum of problems. MWIMM proves its relevance in situations where models exhibit varying degrees of temporal progression, such as scenarios involving aging or the analysis of fault intensity. Additionally, it demonstrates its utility in addressing challenges related to parameter estimation within dynamic systems characterized by gradual parameter variations.

6.2. Recommendations for Future Research

For a comprehensive evaluation of the Multiple-Model Adaptive Estimation (MMAE) strategy, specifically the Moving Window IMM (MWIMM) as proposed in Chapter 5, it is imperative to delve into three pivotal factors: Identifiability,

Optimality, and System Excitation. These factors constitute fundamental elements in assessing the effectiveness of these strategies which only briefly studied in chapter 5. Future research directions could explore the impact of these factors on the performance of the multiple model adaptive estimation strategy.

Another area worthy of further exploration is the robustness of the MWIMM algorithm. The Kalman filter utilized in the MWIMM algorithm, as discussed in Chapter 5, assumes that the process and measurement noise of the system adhere to zero-mean and Gaussian distributions. Consequently, any bias or uncertainty present in the system can impact the performance of this strategy, and in extreme cases, it may lead to instability in the Kalman filter. Consider the system studied in chapter 5, as shown in equation (5.13). Let's assume the system behavior changes gradually over time due to variations in the damping ratio. Then the MWIMM-KF strategy can be employed to estimate the damping ratio. To study the robustness of this approach, different levels of bias or uncertainty has been introduced to the natural frequency of the system. These scenarios are outlined below, and the results of the MWIMM-KF are presented in Figure 6-1.

1. System with out bias or uncertainty: In this situation, the MWIMM-KF exhibits excellent performance as expected.
2. System with small bias or uncertainty (1% additive uncertainty): Despite a slight increase in estimation error compared to the scenario without bias, KF effectively manages to estimate states because the bias or uncertainty falls within the range of process noise.
3. System with medium bias or uncertainty (10% additive uncertainty): In this scenario, MWIMM-KF fails to estimate the damping ratio as the bias or

uncertainty exceeds the range of process noise. Therefore, none of the models in the MWIMM window capable of representing the system's behavior. MWIMM-KF tries to resolve this issue by switching to negative damping to adjust for the bias in natural frequency which only makes the problem even worse.

4. System with large bias or uncertainty (50% additive uncertainty): In this scenario, MWIMM-KF becomes unstable in less than 2 seconds.

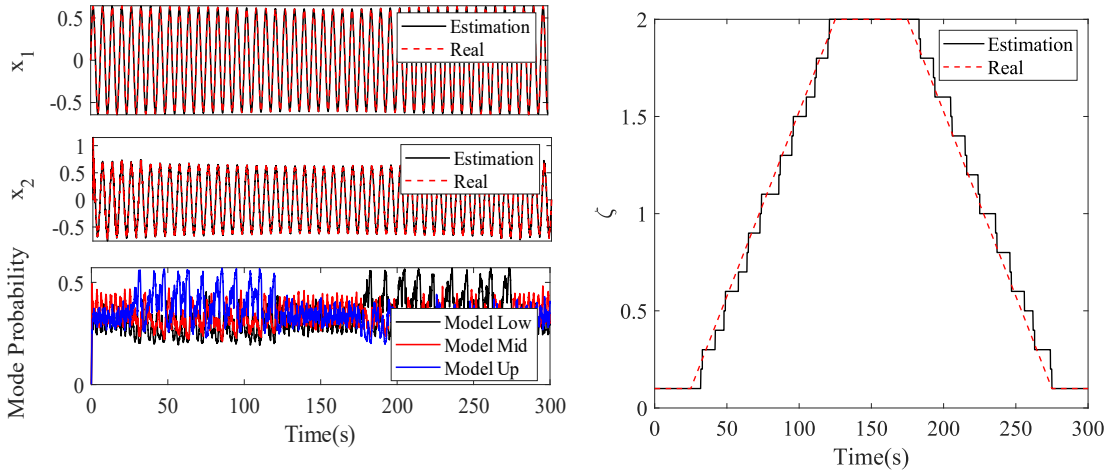

(a)

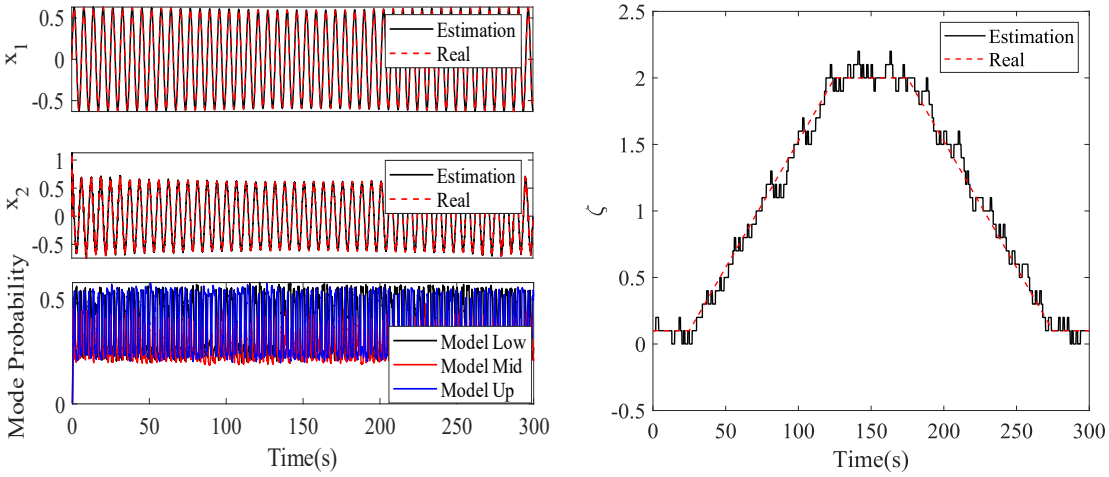

(b)

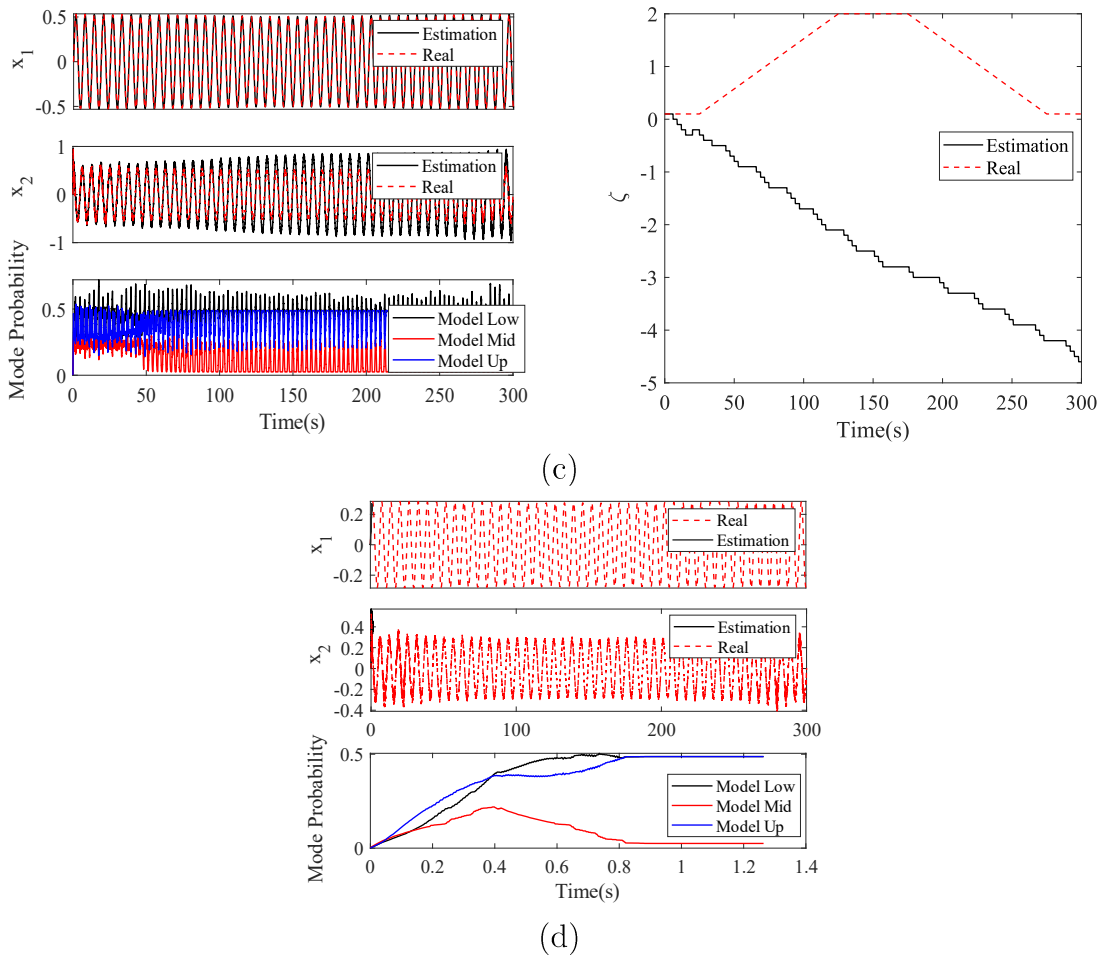

Figure 6-1. *Using MWIMM-KF for estimating the time-varying parameter of a second-order system with different level of bias or uncertainty: (a) No bias; (b) Small bias (1%); (c) Medium bias (10%); (d) Large bias (50%).*

One approach to improve robustness is to use robust filtering strategy such as SVSF-VBL, instead of Kalman filter. The results for the same conditions using MWIMM-SVSF are illustrated in Figure 6-2. The results also compared with MWIMM-KF in Table 6-1. In the scenario without bias, both KF and SVSF-VBL exhibit similar performance as expected. Note that employing a very small Fixed Boundary Layer (FBL) may compromise the performance of SVSF-VBL, as it relies on the fixed bound instead of the optimized bound obtained from system noise most of the time.

In the case of small bias SVSF estimation error is slightly larger than KF, because corrective actions from FBL occurring more frequently with a larger a priori error from uncertainty. Enhancing SVSF performance can be achieved by increasing FBL, but this comes at the expense of a larger error boundary.

For medium and large bias, MWIMM-SVSF fails to estimate damping ratio. However, it ensures stability and boundedness of the estimation error. This is because, when the prior error exceeds the fixed boundary layer, SVSF loses confidence in the model and relies on corrective actions from the fixed boundary layer. As a result, the estimation error of the damping ratio levels off.

Table 6-1: Comparing MWIMM-KF with MWIMM-SVSF for different bias level.

Estimation Error No Bias	**MWIMM-KF Normalized RMSE**	**MWIMM-SVSF Normalized RMSE**
x_1	7.6419e-04	7.6419e-04
x_2	0.0056	0.0056
ζ	0.0311	0.0311
Estimation Error small Bias/uncertainty (1%)	**MWIMM-KF Normalized RMSE**	**MWIMM-SVSF Normalized RMSE**
x_1	7.6399e-04	7.6387e-04
x_2	0.0087	0.0345
ζ	0.0368	0.0376
Estimation Error medium Bias/uncertainty (10%)	**MWIMM-KF Normalized RMSE**	**MWIMM-SVSF Normalized RMSE**
x_1	5.8131e-04	7.6335e-04
x_2	0.2035	0.5365
ζ	37.3749	27.2272
Estimation Error large Bias/uncertainty (50%)	**MWIMM-KF Normalized RMSE**	**MWIMM-SVSF Normalized RMSE**
x_1	unstable	7.7567e-04
x_2	unstable	0.6884
ζ	unstable	22.8583

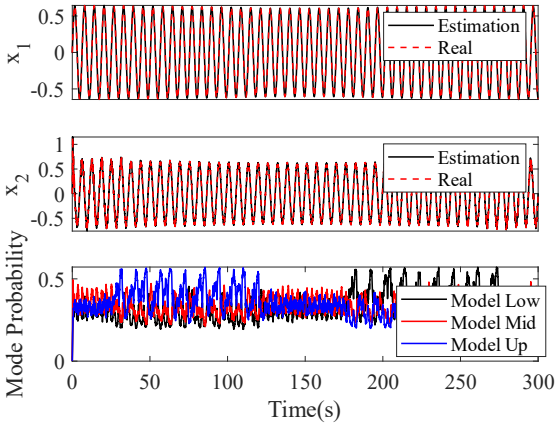
x1
x2
Mode Probability
Estimation
Real
Model Low
Model Mid
Model Up
Time(s)

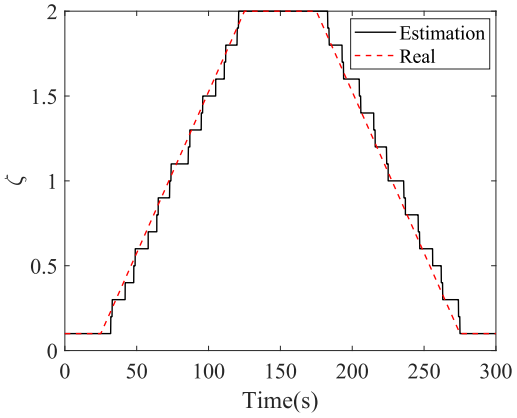
ζ
Estimation
Real
Time(s)

(a)

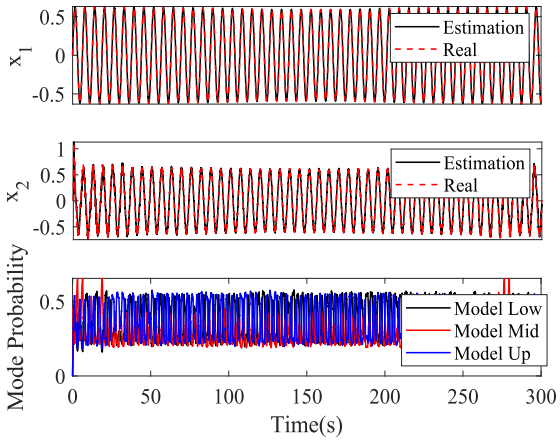
x1
x2
Mode Probability
Estimation
Real
Model Low
Model Mid
Model Up
Time(s)

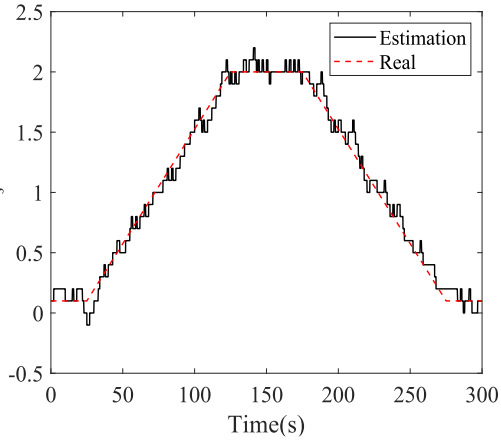
ζ
Estimation
Real
Time(s)

(b)

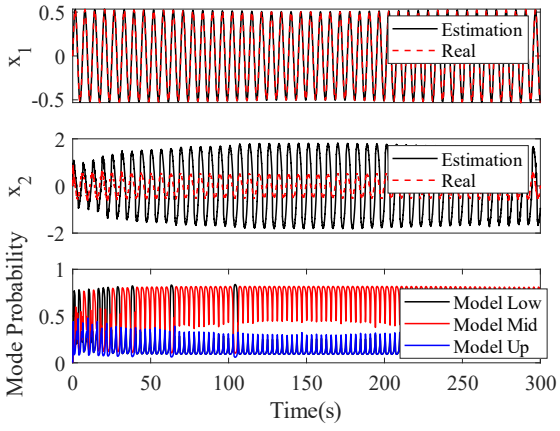
x1
x2
Mode Probability
Estimation
Real
Model Low
Model Mid
Model Up
Time(s)

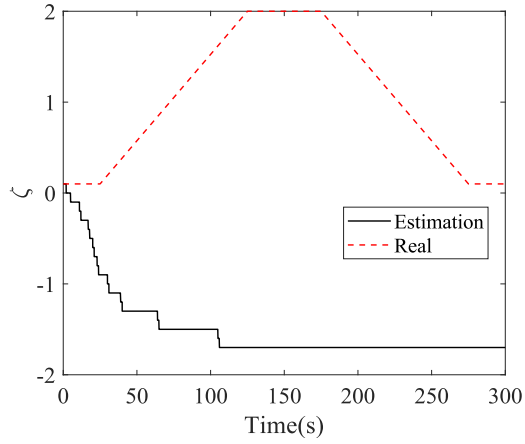
ζ
Estimation
Real
Time(s)

(c)

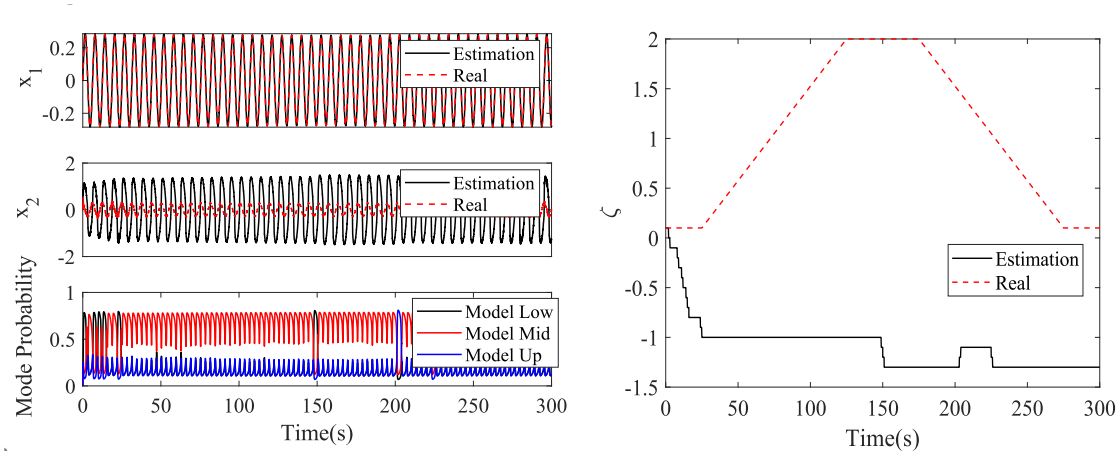

(d)

Figure 6-2. *Using MWIMM-SVSF for estimating the time-varying parameter of a second-order system with different level of bias or uncertainty: (a) No bias; (b) Small bias (1%); (c) Medium bias (10%); (d) Large bias (50%).*

As shown, although MWIMM-SVSF ensures the stability and boundedness of the estimation error, neither of these approaches effectively captures the states and unknown parameters (e.g. damping ratio) under conditions of medium and large uncertainty. This outcome is expected, given that when uncertainty significantly outweighs the differences between model hypotheses, the comparison becomes irrelevant for identifying the true model. A more in-depth exploration of this issue could be pursued in the future, developing a robust estimation strategy based on the variable structure system concept, as demonstrated here. This could involve a comprehensive analysis of parameters such as bin size, window size, and process noise (Q) to enhance performance, and potentially delving into other robust strategies.

Instead of merging, as seen in the IMM strategy, an alternative for decreasing the number of regime sequences in MMAE algorithms involves employing pruning.

Pruning entails the removal of low probability branches (i.e., regime sequence) from MMAE tree, in contrast to the merging approach used in IMM. While merging algorithms such as IMM filters are widely employed in estimation tasks like target tracking, a pruning algorithm like Multiple Model Pruning (MMP) [5] is more relevant for detecting changes in fault detection problems. In these scenarios, accurately identifying changes in the system's behavior is more important than estimating the system state. The MMP algorithm has three main steps [5]:

1. Recursively compute the conditional filter for a bank of M sequences.
2. After the measurement update at time k, retain only the M/S most probable branches and prune the rest.
3. At time $k+1$, allow the M/S considered branches to split into $S.M/S = M$ branches and update their *a posteriori* probabilities.

An entirely distinct approach to reduce the complexity and improve the performance of MMAE algorithms in addressing fault detection problems involves the adoption of the MMP algorithm. Future research can explore pruning techniques and compare their performance with merging approaches employed in this thesis, such as IMM, UIMM, and MWIMM, for fault detection and diagnosis problems.

Examining the stability of the proposed MMAE algorithms within real-time closed-loop applications for the attainment of a fault-tolerant control system is an area that merits further exploration. The literature has previously addressed a comparable issue known as stability for Multiple Model Adaptive Control (MMAC) [96]–[98]. The central questions addressed in these studies are determining robustness guarantees [96] and finding ways to steer clear of a conservative design [97]. The

methodologies outlined in existing literature for ensuring robustness rely on nonlinear input-output stability theory, which involves the nonlinear gap metric [96], [98]. A similar methodology could potentially be applied to investigate the stability and robustness of the proposed algorithms in this thesis, particularly in the context of their utilization within a fault-tolerant control framework.

The fusion of data-driven techniques with the model-based approaches provided in this thesis holds immense potential. It was demonstrated in Chapter 3 through spectral analysis of the chattering phenomenon in filter-based SVSF estimations for fault diagnosis. This approach can be extended to incorporate other data-driven methodologies, including the integration of machine learning techniques. Future investigations may delve into hybrid systems that combine the strengths of both model-based and data-driven methodologies, providing comprehensive solutions for Fault Detection and Diagnosis (FDD) challenges. Such research topics have gained substantial momentum in recent years, often referred to as "physics-informed machine learning methods" [99]. The underlying premise is that while comprehensive models can be established for systems under normal conditions based on their physics, the development of explicit models to capture the effects of various potential faults is often difficult. Consequently, the integration of model-based methods with machine learning techniques can prove highly advantageous in addressing complex fault detection problems.

References

[1] V. Venkatasubramanian, R. Rengaswamy, K. Yin, and S. N. Kavuri, "A review of process fault detection and diagnosis part I: Quantitative model-

based methods," *Comput. Chem. Eng.*, vol. 27, no. 3, pp. 293–311, 2003.

[2] R. Isermann and P. Balle, "Trends in the application of model-based fault detection and diagnosis of technical processes," *Control Eng. Pract.*, vol. 5, no. 5, pp. 709–719, 1997.

[3] R. Isermann and R. Isermann, "Terminology in fault detection and diagnosis," *Combust. Engine Diagnosis Model. Cond. Monit. Gasol. Diesel Engines their Components*, pp. 295–297, 2017.

[4] S. Habibi, "The smooth variable structure filter," *Proc. IEEE*, vol. 95, no. 5, pp. 1026–1059, 2007.

[5] F. Gustafsson and F. Gustafsson, *Adaptive filtering and change detection*, vol. 1. Wiley New York, 2000.

[6] I. Hwang, S. Kim, Y. Kim, and C. E. Seah, "A survey of fault detection, isolation, and reconfiguration methods," *IEEE Trans. Control Syst. Technol.*, vol. 18, no. 3, pp. 636–653, 2009.

[7] G. Pang, C. Shen, L. Cao, and A. Van Den Hengel, "Deep learning for anomaly detection: A review," *ACM Comput. Surv.*, vol. 54, no. 2, pp. 1–38, 2021.

[8] V. Chandola, A. Banerjee, and V. Kumar, "Anomaly detection: A survey," *ACM Comput. Surv.*, vol. 41, no. 3, pp. 1–58, 2009.

[9] R. Isermann, *Fault-diagnosis systems: an introduction from fault detection to*

fault tolerance. Springer Science & Business Media, 2005.

[10] V. Venkatasubramanian, R. Rengaswamy, and S. N. Kavuri, "A review of process fault detection and diagnosis: Part II: Qualitative models and search strategies," *Comput. Chem. Eng.*, vol. 27, no. 3, pp. 313–326, 2003.

[11] V. Venkatasubramanian, R. Rengaswamy, K. Yin, and S. N. Kavuri, "A review of fault detection and diagnosis. Part III: Process history based methods," *Comput. Chem. Eng.*, vol. 27, pp. 327–346, 2003.

[12] P. M. Frank and X. Ding, "Survey of robust residual generation and evaluation methods in observer-based fault detection systems," *J. Process Control*, vol. 7, no. 6, pp. 403–424, 1997.

[13] P. M. Frank and J. Wunnenberg, "Robust fault diagnosis using unknown input observer schemes," *Fault diagnosis Dyn. Syst.*, pp. 47–97, 1989.

[14] X.-C. Lou, A. S. Willsky, and G. C. Verghese, "Optimally robust redundancy relations for failure detection in uncertain systems," *Automatica*, vol. 22, no. 3, pp. 333–344, 1986.

[15] M. Athans and C.-B. Chang, "Adaptive estimation and parameter identification using multiple model estimation algorithm," 1976.

[16] S. A. Gadsden, Y. Song, and S. R. Habibi, "Novel model-based estimators for the purposes of fault detection and diagnosis," *IEEE/ASME Trans. Mechatronics*, vol. 18, no. 4, pp. 1237–1249, 2013.

[17] B. Ristic, S. Arulampalam, and N. Gordon, *Beyond the Kalman filter: Particle filters for tracking applications*. Artech house, 2003.

[18] J. S. Liu and R. Chen, "Sequential Monte Carlo methods for dynamic systems," *J. Am. Stat. Assoc.*, vol. 93, no. 443, pp. 1032–1044, 1998.

[19] A. Saeedzadeh, S. Habibi, and M. Alavi, "A Model-Based FDD Approach for an EHA Using Updated Interactive Multiple Model SVSF," in *Fluid Power Systems Technology*, 2021, vol. 85239, p. V001T01A006.

[20] E. S. Page, "Continuous inspection schemes," *Biometrika*, vol. 41, no. 1/2, pp. 100–115, 1954.

[21] G. Lorden, "Procedures for reacting to a change in distribution," *Ann. Math. Stat.*, pp. 1897–1908, 1971.

[22] I. V Nikiforov, "A generalized change detection problem," *IEEE Trans. Inf. theory*, vol. 41, no. 1, pp. 171–187, 1995.

[23] A. Willsky and H. Jones, "A generalized likelihood ratio approach to the detection and estimation of jumps in linear systems," *IEEE Trans. Automat. Contr.*, vol. 21, no. 1, pp. 108–112, 1976.

[24] M. Basseville and A. Benveniste, "Desgin and comparative study of some sequential jump detection algorithms for digital signals," *IEEE Trans. Acoust.*, vol. 31, no. 3, pp. 521–535, 1983.

[25] P. Li and V. Kadirkamanathan, "Particle filtering based likelihood ratio

approach to fault diagnosis in nonlinear stochastic systems," *IEEE Trans. Syst. Man, Cybern. Part C (Applications Rev.*, vol. 31, no. 3, pp. 337–343, 2001.

[26] M. Basseville and A. Benveniste, *Detection of abrupt changes in signals and dynamical systems*. Springer, 1986.

[27] S. Wang, S. Habibi, and R. Burton, "Sliding mode control for an electrohydraulic actuator system with discontinuous non-linear friction," *Proc. Inst. Mech. Eng. part I J. Syst. Control Eng.*, vol. 222, no. 8, pp. 799–815, 2008.

[28] M. Bodson and J. E. Groszkiewicz, "Multivariable adaptive algorithms for reconfigurable flight control," *IEEE Trans. Control Syst. Technol.*, vol. 5, no. 2, pp. 217–229, 1997.

[29] S. Ganguli, G. Papageorgiou, S. Glavaski, and M. Elgersma, "Piloted Simulation of Fault, Detection, Isolation, and Reconfiguration Algorithms for a Civil Transport Aircraft," in *AIAA Guidance, Navigation, and Control Conference and Exhibit*, 2005, p. 5936.

[30] S. Ganguli, G. Papageorgiou, and S. Glavaski, "Aircraft fault detection, isolation and reconfiguration in the presence of measurement errors," in *AIAA Guidance, Navigation, and Control Conference and Exhibit*, 2006, p. 6551.

[31] K.-S. Kim, K.-J. Lee, and Y. Kim, "Reconfigurable flight control system

design using direct adaptive method," *J. Guid. Control. Dyn.*, vol. 26, no. 4, pp. 543–550, 2003.

[32] D. Zhang and Z. Gao, "Fault tolerant control using reinforcement learning and particle swarm optimization," *IEEE Access*, vol. 8, pp. 168802–168811, 2020.

[33] I. Ahmed, M. Quiñones-Grueiro, and G. Biswas, "Fault-tolerant control of degrading systems with on-policy reinforcement learning," *IFAC-PapersOnLine*, vol. 53, no. 2, pp. 13733–13738, 2020.

[34] C. Deng, D. Yue, W.-W. Che, and X. Xie, "Cooperative fault-tolerant control for a class of nonlinear MASs by resilient learning approach," *IEEE Trans. Neural Networks Learn. Syst.*, 2022.

[35] P. M. Frank, "Robust model-based fault detection in dynamic systems," *IFAC Proc. Vol.*, vol. 25, no. 4, pp. 1–13, 1992.

[36] P. M. Frank, "Enhancement of robustness in observer-based fault detection," *Int. J. Control*, vol. 59, no. 4, pp. 955–981, 1994.

[37] A. Emami-Naeini, M. M. Akhter, and S. M. Rock, "Effect of model uncertainty on failure detection: the threshold selector," *IEEE Trans. Automat. Contr.*, vol. 33, no. 12, pp. 1106–1115, 1988.

[38] R. J. Patton and J. Chen, "Robust fault detection using eigenstructure assignment: A tutorial consideration and some new results," in *Proceedings of the 30th IEEE Conference on Decision and Control*, 1991, vol. 3, pp.

2242–2247.

[39] R. J. Patton and J. Chen, "On eigenstructure assignment for robust fault diagnosis," *Int. J. Robust Nonlinear Control IFAC-Affiliated J.*, vol. 10, no. 14, pp. 1193–1208, 2000.

[40] R. V. Beard, "Failure accomodation in linear systems through self-reorganization.," Massachusetts Institute of Technology, 1971.

[41] H. L. Jones, "Failure detection in linear systems.," Massachusetts Institute of Technology, 1973.

[42] M.-A. Massoumnia, "A geometric approach to the synthesis of failure detection filters," *IEEE Trans. Automat. Contr.*, vol. 31, no. 9, pp. 839–846, 1986.

[43] K. Watanabe and D. M. Himmelblau, "Instrument fault detection in systems with uncertainties," *Int. J. Syst. Sci.*, vol. 13, no. 2, pp. 137–158, 1982.

[44] J. Wünnenberg and P. M. Frank, "Sensor fault detection via robust observers," in *System Fault Diagnostics, Reliability and Related Knowledge-Based Approaches: Volume 1 Fault Diagnostics and Reliability Proceedings of the First European Workshop on Fault Diagnostics, Reliability and Related Knowledge-Based Approaches, Island of Rhodes,* 1987, pp. 147–160.

[45] J. Chen, R. J. Patton, and H.-Y. Zhang, "Design of unknown input observers and robust fault detection filters," *Int. J. Control*, vol. 63, no. 1, pp. 85–105, 1996.

[46] F. Amato and M. Mattei, "Design of full order unknown input observers with H/sub/spl infin//performance," in *Proceedings of the International Conference on Control Applications*, 2002, vol. 1, pp. 74–75.

[47] E. Chow and A. Willsky, "Analytical redundancy and the design of robust failure detection systems," *IEEE Trans. Automat. Contr.*, vol. 29, no. 7, pp. 603–614, 1984.

[48] H. Ye, G. Wang, and S. X. Ding, "A new parity space approach for fault detection based on stationary wavelet transform," *IEEE Trans. Automat. Contr.*, vol. 49, no. 2, pp. 281–287, 2004.

[49] X. Ding, L. Guo, and T. Jeinsch, "A characterization of parity space and its application to robust fault detection," *IEEE Trans. Automat. Contr.*, vol. 44, no. 2, pp. 337–343, 1999.

[50] J. Stoustrup and H. H. Niemann, "Fault estimation—a standard problem approach," *Int. J. Robust Nonlinear Control IFAC-Affiliated J.*, vol. 12, no. 8, pp. 649–673, 2002.

[51] T. Song and E. G. Collins Jr, "Robust H estimation with application to robust fault detection," *J. Guid. Control. Dyn.*, vol. 23, no. 6, pp. 1067–1071, 2000.

[52] E. G. Collins, W. M. Haddad, V.-S. Chellaboina, and T. Song, "Robustness analysis in the delta-domain using fixed-structure multipliers," in *Proceedings of the 36th IEEE Conference on Decision and Control*, 1997,

vol. 4, pp. 3286–3291.

[53] A. A. Stoorvogel, H. H. Niemann, A. Saberi, and P. Sannuti, "Optimal fault signal estimation," *Int. J. Robust Nonlinear Control IFAC-Affiliated J.*, vol. 12, no. 8, pp. 697–727, 2002.

[54] H. Wang and J. Lam, "Robust fault detection for uncertain discrete-time systems," *J. Guid. Control. Dyn.*, vol. 25, no. 2, pp. 291–301, 2002.

[55] R. H. Chen and J. L. Speyer, "A generalized least-squares fault detection filter," *Int. J. Adapt. Control Signal Process.*, vol. 14, no. 7, pp. 747–757, 2000.

[56] R. H. Chen, D. L. Mingori, and J. L. Speyer, "Optimal stochastic fault detection filter," *Automatica*, vol. 39, no. 3, pp. 377–390, 2003.

[57] E. A. Wan and R. Van Der Merwe, "The unscented Kalman filter for nonlinear estimation," in *Proceedings of the IEEE 2000 Adaptive Systems for Signal Processing, Communications, and Control Symposium (Cat. No. 00EX373)*, 2000, pp. 153–158.

[58] M. Al-Shabi, S. A. Gadsden, and S. R. Habibi, "Kalman filtering strategies utilizing the chattering effects of the smooth variable structure filter," *Signal Processing*, vol. 93, no. 2, pp. 420–431, 2013.

[59] L. Ortega, J. Vilà-Valls, E. Chaumette, G. Pagès, and F. Vincent, "Robust Tracking under Measurement Model Mismatch via Linearly Constrained Extended Kalman Filtering," in *2020 59th IEEE Conference on Decision and*

Control (CDC), 2020, pp. 2924–2929.

[60] P. Kaminski, A. Bryson, and S. Schmidt, "Discrete square root filtering: A survey of current techniques," *IEEE Trans. Automat. Contr.*, vol. 16, no. 6, pp. 727–736, 1971.

[61] G. J. Bierman, *Factorization methods for discrete sequential estimation*. Courier Corporation, 2006.

[62] D. Simon, *Optimal state estimation: Kalman, H infinity, and nonlinear approaches*. John Wiley & Sons, 2006.

[63] S. R. Habibi and R. Burton, "The variable structure filter," *J. Dyn. Syst. Meas. Control. Trans. ASME*, vol. 125, no. 3, pp. 287–293, 2003.

[64] S. Habibi, "The smooth variable structure filter," *Proc. IEEE*, vol. 95, no. 5, pp. 1026–1059, 2007.

[65] D. Magill, "Optimal adaptive estimation of sampled stochastic processes," *IEEE Trans. Automat. Contr.*, vol. 10, no. 4, pp. 434–439, 1965.

[66] Y. Bar-Shalom, X. R. Li, and T. Kirubarajan, *Estimation with applications to tracking and navigation: theory algorithms and software*. John Wiley & Sons, 2004.

[67] A. Saeedzadeh, S. Habibi, M. Alavi, and P. Setoodeh, "A Robust Model-Based Strategy for Real-Time Fault Detection and Diagnosis in an Electro-Hydraulic Actuator Using Updated Interactive Multiple Model Smooth

Variable Structure Filter," *J. Dyn. Syst. Meas. Control*, pp. 1–32, 2023.

[68] S. A. Gadsden, Y. Song, and S. R. Habibi, "Novel model-based estimators for the purposes of fault detection and diagnosis," *IEEE/ASME Trans. Mechatronics*, vol. 18, no. 4, pp. 1237–1249, 2013.

[69] T. E. Menke and P. S. Maybeck, "Multiple model adaptive estimation applied to the VISTA F-16 flight control system with actuator and sensor failures," in *Proceedings of the IEEE 1992 National Aerospace and Electronics Conference@ m_NAECON 1992*, 1992, pp. 441–448.

[70] T. E. Menke and P. S. Maybeck, "Sensor/actuator failure detection in the Vista F-16 by multiple model adaptive estimation," *IEEE Trans. Aerosp. Electron. Syst.*, vol. 31, no. 4, pp. 1218–1229, 1995.

[71] S. Kim, J. Choi, and Y. Kim, "Fault detection and diagnosis of aircraft actuators using fuzzy-tuning IMM filter," *IEEE Trans. Aerosp. Electron. Syst.*, vol. 44, no. 3, pp. 940–952, 2008.

[72] A. Doucet, N. J. Gordon, and V. Krishnamurthy, "Particle filters for state estimation of jump Markov linear systems," *IEEE Trans. signal Process.*, vol. 49, no. 3, pp. 613–624, 2001.

[73] H. A. P. Blom and E. A. Bloem, "Exact Bayesian and particle filtering of stochastic hybrid systems," *IEEE Trans. Aerosp. Electron. Syst.*, vol. 43, no. 1, pp. 55–70, 2007.

[74] S. Narasimhan and G. Biswas, "Model-based diagnosis of hybrid systems,"

IEEE Trans. Syst. man, Cybern. A Syst. humans, vol. 37, no. 3, pp. 348–361, 2007.

[75] H.-R. Wang and H.-J. Gao, "Robust fault detection for uncertain time-delay systems with Markovian jump parameters," in *2007 International Conference on Machine Learning and Cybernetics*, 2007, vol. 2, pp. 1066–1071.

[76] F. Zhao, X. Koutsoukos, H. Haussecker, J. Reich, and P. Cheung, "Monitoring and fault diagnosis of hybrid systems," *IEEE Trans. Syst. Man, Cybern. Part B*, vol. 35, no. 6, pp. 1225–1240, 2005.

[77] M. Zhong, H. Ye, P. Shi, and G. Wang, "Fault detection for Markovian jump systems," *IEE Proceedings-Control Theory Appl.*, vol. 152, no. 4, pp. 397–402, 2005.

[78] P. Zhang, S. X. Ding, G. Z. Wang, and D. H. Zhou, "Fault detection of linear discrete-time periodic systems," *IEEE Trans. Automat. Contr.*, vol. 50, no. 2, pp. 239–244, 2005.

[79] P. Baroni, G. Lamperti, P. Pogliano, and M. Zanella, "Diagnosis of a class of distributed discrete-event systems," *IEEE Trans. Syst. Man, Cybern. A Syst. Humans*, vol. 30, no. 6, pp. 731–752, 2000.

[80] R. Isermann, "Process fault detection based on modeling and estimation methods—A survey," *automatica*, vol. 20, no. 4, pp. 387–404, 1984.

[81] S. Simani, C. Fantuzzi, R. J. Patton, S. Simani, C. Fantuzzi, and R. J. Patton, *Model-based fault diagnosis techniques*. Springer, 2003.

[82] R. Isermann, "Supervision, fault-detection and fault-diagnosis methods—an introduction," *Control Eng. Pract.*, vol. 5, no. 5, pp. 639–652, 1997.

[83] H. Khan, S. C. Abou, and N. Sepehri, "Nonlinear observer-based fault detection technique for electro-hydraulic servo-positioning systems," *Mechatronics*, vol. 15, no. 9, pp. 1037–1059, 2005.

[84] Y. Chinniah, R. Burton, and S. Habibi, "Failure monitoring in a high performance hydrostatic actuation system using the extended Kalman filter," *Mechatronics*, vol. 16, no. 10, pp. 643–653, 2006.

[85] H. H. Afshari, S. A. Gadsden, and S. R. Habibi, "Robust fault diagnosis of an electro-hydrostatic actuator using the novel dynamic second-order SVSF and IMM strategy," *Int. J. Fluid Power*, vol. 15, no. 3, pp. 181–196, 2014.

[86] Y. U. Song, "Electro-Hydrostatic Actuator Fault Detection and Diagnosis," McMaster University, 2013.

[87] M. Ringkowski and O. Sawodny, "Model-Based Fault-Detection of a Hydraulic Switching Valve," in *2019 American Control Conference (ACC)*, 2019, pp. 4460–4465.

[88] M. F. Asmussen, H. C. Pedersen, L. Lilleengen, A. Larsen, and T. Farsakoglou, "Investigating Fault Detection and Diagnosis in a Hydraulic Pitch System Using a State Augmented EKF-Approach," in *Fluid Power Systems Technology*, 2019, vol. 59339, p. V001T01A030.

[89] M. S. Grewal and A. P. Andrews, *Kalman filtering: Theory and Practice*

with MATLAB. John Wiley & Sons, 2014.

[90] M. Karasalo and X. Hu, "An optimization approach to adaptive Kalman filtering," *Automatica*, vol. 47, no. 8, pp. 1785–1793, 2011.

[91] P. Abbeel, A. Coates, M. Montemerlo, A. Y. Ng, and S. Thrun, "Discriminative training of kalman filters.," in *Robotics: Science and systems*, 2005, vol. 2, p. 1.

[92] M. Basseville, A. Benveniste, M. Goursat, and L. Mevel, "Subspace-based algorithms for structural identification, damage detection, and sensor data fusion," *EURASIP J. Adv. Signal Process.*, vol. 2007, pp. 1–13, 2006.

[93] M. Basseville, A. Benveniste, M. Goursat, L. Hermans, L. Mevel, and H. der Auweraer, "Output-only subspace-based structural identification: from theory to industrial testing practice," *J. Dyn. Syst. Meas. Control. Asme*, vol. 123, no. 4, 2001.

[94] P. Van Overschee and B. De Moor, *Subspace identification for linear systems: Theory—Implementation—Applications*. Springer Science & Business Media, 2012.

[95] A. Saeedzadeh, P. Setoodeh, M. Alavi, and S. Habibi, "Information Extraction Using Spectral Analysis of the Chattering of the Smooth Variable Structure Filter," *IEEE Access*, 2023.

[96] M. French and D. Buchstaller, "Robust stability for multiple model adaptive control: part I-the framework," *IEEE Trans. Automat. Contr.*, vol. 61, no. 3,

pp. 677–692, 2016.

[97] D. Buchstaller and M. French, "Robust stability for multiple model adaptive control: Part II—Gain bounds," *IEEE Trans. Automat. Contr.*, vol. 61, no. 3, pp. 693–708, 2015.

[98] M. French, "Adaptive control and robustness in the gap metric," *IEEE Trans. Automat. Contr.*, vol. 53, no. 2, pp. 461–478, 2008.

[99] G. E. Karniadakis, I. G. Kevrekidis, L. Lu, P. Perdikaris, S. Wang, and L. Yang, "Physics-informed machine learning," *Nat. Rev. Phys.*, vol. 3, no. 6, pp. 422–440, 2021.